

# SCIAMACHY L0-1c Processor ATBD

## Algorithm Theoretical Baseline Document for Processor V.8

Issue 6



---

<b>prepared</b>	<b>Institute</b>	<b>Date</b>	<b>Signature</b>
-----------------	------------------	-------------	------------------

S. Slijkhuis/G. Lichtenberg	DLR-IMF	May 7, 2014	
-----------------------------	---------	-------------	--

**checked**

SQWG

---

**copies to**

---

SQWG

ESA

---

# Contents

<b>1. Introduction</b>	<b>8</b>
1.1. Overview of the SCIAMACHY mission	8
1.2. Purpose and scope	8
1.3. Document Overview	8
1.4. Document Status and History	9
1.5. Abbreviations and Acronyms	10
1.6. Applicable Documents	12
<b>2. SCIAMACHY Background Information and Algorithms Overview</b>	<b>13</b>
2.1. Introduction to mission and data processing	13
2.1.1. Processing Requirements	13
2.1.2. Inheritance: relation to the GOME Data Processor	13
2.2. SCIAMACHY Instrument Characteristics	14
2.2.1. Instrument Hardware	14
2.2.2. Instrument Operation and Data Packet structure	15
2.2.3. Instrument Calibration requirements for Level 0 to 1c processing	17
2.3. The generic calibration equation	17
2.4. Determination of Calibration Parameters	19
2.4.1. Overview	19
2.4.2. Ongoing Calibration	19
2.4.3. M-factors	19
2.4.4. Level 0 to 1b Processing of Calibration Constants	20
2.5. Operational aspects of Level 0 to 1c processing	21
2.6. Algorithms Overview	22
<b>3. Level 0 to 1c Algorithms Description</b>	<b>25</b>
3.1. <i>Pre-processing of Mueller Matrix elements</i>	25
3.1.1. Introduction to Mueller Matrix elements	25
3.1.2. Rationale	27
3.1.3. Conversion of Key Data for polarisation sensitivity	27
3.1.4. Conversion of Key Data for radiance sensitivity	27
3.1.5. Calculation of Instrument Response	27
3.1.5.1. Generic Mueller Matrix and Contamination Layers	30
3.1.5.2. Scanner Mueller Matrices	31
3.1.6. Calculation of errors on Mueller matrix elements	32
3.1.6.1. Errors for radiance response parameters	32
3.1.6.2. Errors for polarisation sensitivity parameters	33
3.2. Calculate Geolocation and Synchronise PMDs	34
3.2.1. Determine integration time grid	34
3.2.2. Integrated PMD values	36
3.2.3. Extract Line of Sight	37
3.2.3.1. Extraction of scan mirror positions	38
3.2.3.2. Calculation of the effective scan angle	40
3.2.3.3. Conversion to the ILOS angles at Satellite	40
3.2.4. Calculate geolocation	40
3.2.5. Conversion to TOA angles	42
3.2.6. Calculate Doppler shift	43
3.2.7. Determine SAA region	44

3.2.8. Calculate orbit phase	44
3.3. Correct Detector Readout Memory and Non-Linearity	44
3.3.1. Calculation if no previous measurement available	46
3.3.2. Scaling with PMDs at co-adding for memory effect	47
3.3.3. Scaling with PMDs at co-adding for non-linearity	48
3.4. Calculate Dark Signal	50
3.4.1. Introduction	50
3.4.2. Calculation of FPN and LC from dedicated 'Dark' measurements	50
3.4.3. Operational aspects	52
3.4.4. Modelling of LC over the orbit	53
3.4.5. Calculation of Solar Stray light from dedicated 'Dark' measurements	54
3.4.6. Quality check on Dark Signal using Limb States	55
3.5. Apply Dark Signal	57
3.6. Calculate PPG and Etalon Parameters	59
3.6.1. Introduction	59
3.6.2. Operational aspects	59
3.6.3. WLS preprocessing	60
3.6.4. Calculate Etalon	61
3.6.5. Calculate PPG	63
3.7. Apply PPG and Etalon Parameters	65
3.8. Calculate Spectral Calibration Parameters	66
3.8.1. Using Fraunhofer lines	68
3.8.2. Additional quality control parameters	69
3.8.3. Doppler shifts	69
3.9. Apply Spectral Calibration Parameters	70
3.10. Determine Spectral Straylight	71
3.10.1. Uniform stray light	71
3.10.2. Ghost stray light	72
3.10.3. Channel 1 stray light	74
3.10.4. Straylight parameters on the Level 1b product	74
3.11. Apply Straylight Correction	75
3.12. Apply BSDF and calculate SMR	76
3.12.1. Introduction	76
3.12.2. Solar Mean Reference spectrum from Sun diffuser measurements	77
3.12.3. Solar Mean Reference spectrum from other measurements	78
3.12.4. Calculation of average PMD signals	78
3.12.5. Calculation of out-of-band PMD signal	79
3.12.6. Calculation of the Doppler-shift at 500 nm	79
3.13. Determine Fractional Polarisation Values	80
3.13.1. Introduction to polarisation measurements	80
3.13.2. The theoretical point near 300 nm	85
3.13.3. Polarisation fractions from PMDs	88
3.13.4. Polarisation fractions from channel overlaps	95
3.14. Wavelength interpolation of polarisation values	99
3.14.1. Introduction	99
3.14.2. Interpolation - default case with all points available	100
3.14.3. Interpolation - only few points available	103
3.15. Apply Radiance Response	104
3.15.1. Sun-normalised radiance	104
3.16. Quality Flagging	106
3.16.1. Dead or bad pixel mask	106
3.16.2. Dark signal quality assessment	106
3.16.3. Wavelength calibration check	106
3.16.4. Sunlint and Rainbow flag	106
3.16.5. Saturation	107
3.16.6. Hot pixels	107

---

3.16.7. Red Grass	107
3.16.8. Decontamination flag	108
3.17. Notes on algorithm description	109
<b>4. Limitations of the Algorithms</b>	<b>110</b>
<b>5. Measurement Uncertainty Analysis</b>	<b>113</b>
5.1. Introduction	113
5.2. Overview of errors on Level 1c data	114
<b>A. Level 1b product structure</b>	<b>117</b>
<b>B. References</b>	<b>119</b>
B.1. Applicable Documents	119
B.2. Literature References	119
B.3. Project References	121
B.4. GOME project documentation and study reports	122

# List of Figures

2.1. <i>SCIAMACHY optical lay-out.</i> . . . . .	14
2.2. <i>Data flow of science measurements and of calibration measurements.</i> . . . . .	24
3.1. <i>Definition of the polarisation plane for Q, U on the level 1b product. top panel: nadir geometry. bottom panel: limb geometry.</i> . . . . .	26
3.2. <i>Definitions for Equations 3.8 and 3.9. The light comes from medium <math>i</math>, goes through medium <math>j</math> and is reflected at surface <math>j + 1</math>.</i> . . . . .	31
3.3. <i>Conversion from sampled PMD points to PMD integrals. The thin line represents the delayed signal after filtering.</i> . . . . .	36
3.4. <i>Definition of angles at the elevation mirror for Nadir measurements.</i> . . . . .	39
3.5. <i>Definition of angles at the elevation and azimuth mirror for Limb/Occultation measurements.</i> . . . . .	39
3.6. <i>Definition of footprint points A-D and ILOS points E-G for Nadir scan pattern.</i> . . . . .	41
3.7. <i>Schematic representation of orbit regions, and of harmonic fit of dark signal over the orbit (harmonic fit only for channels 6-8 and PMDs E,F; solar stray light for all channels/PMDs).</i> . . . . .	54
3.8. <i>Quantities used in the determination of SLS before (left) and after continuum correction (right).</i> . . . . .	66
3.9. <i>POLDER image showing polarisation parameters over a partially clouded scene:</i> <i>a) RGB image of total reflectance (Red= 865 nm, Green= 670 nm, Blue= 443 nm)</i> <i>b) RGB image of Degree of Polarisation</i> <i>c) Polarisation angle <math>\chi</math> at 443 nm</i> <i>d) Polarisation angle <math>\chi</math> at 670 nm</i> <i>The FOV of this scene is <math>\sim 102^\circ \times 86^\circ</math> (compare with SCIAMACHY <math>15^\circ \times 2^\circ</math> for 1 second exposure time at nominal swath width); West on top. Panel b) clearly shows a rainbow phenomenon. Outside the rainbow, polarisation is low over thick clouds, where the residual polarisation is predominantly in the blue.</i> <i>POLDER data courtesy CNES/NASDA</i> . . . . .	81
3.10. <i>Data flow of the polarisation correction algorithm (simplified).</i> . . . . .	83
3.11. <i>Example of clustered readout (see text).</i> . . . . .	85
3.12. <i>Wavelength interpolation of polarisation values.</i> . . . . .	99
A.1. <i>Schematic structure of the Level 1n Product.</i> . . . . .	118

## List of Tables

2.1. <i>Calibrated channel boundaries (cut off at 5% level) and PMD boundaries (20% level)</i> . . . . .	15
3.1. <i>New Key Data.</i> . . . . .	29
3.2. <i>Solar spectrum Identifiers on the ADS.</i> . . . . .	77
5.1. <i>Summary of error sources on Level 1c data.</i> . . . . .	116

## Changelog

Change	Page	Section
<b>for changes Issue <math>\leq 5</math> see issue 5</b>		
<b>Issue 6 ()</b>		
- adjustments for the fact that SciCal/IECF is no longer used	all	all
- Updated processing scheme (usage of calibration DB)	24	2.5
- pre-processing MM deleted and scan mirror model introduced	25	3.1
- Memory Effect Correction improved and corrected	47	3.3.2
- Non-Linearity correction improved	48	3.3.3
- Selection of dark states for dark correction	50	3.4.2
- Hot pixel correction Limb changed	55	3.4.6
- Uniform stray light corrections	71	3.10.1
- Intensity check for SMR averaging removed	77	3.12.2
- In-band correction calculation updated (scan mirror model)	78	3.12.4
- Out-of-band correction calculation updated (scan mirror model)	79	3.12.5
- Description of SPH updated in L1b structure	117	A

# 1. Introduction

## 1.1. Overview of the SCIAMACHY mission

SCIAMACHY (SCanning Imaging Absorption SpectroMeter for Atmospheric CHartographY) is one of the earth observation research instruments that was included as part of the payload of the ESA (European Space Agency) ENVISAT-1 platform that was launched in the year 2002. The main scientific objective of SCIAMACHY was to measure distributions of a number of chemically important atmospheric trace species on a global basis. SCIAMACHY has a spectrometer and telescope system designed to observe light transmitted through and reflected and scattered from the earth's atmosphere over a spectral range of 240 - 2400 nm. It has an alternate limb and nadir viewing capability, and will be able to perform solar and lunar occultation measurements.

Nadir measurements provide Top of the Atmosphere (TOA) radiance and reflectance, together with limited polarisation information, in the Level 1c data product; Level 2 processing generates UV/visible global column distributions of O<sub>3</sub>, NO<sub>2</sub> and a number of other trace species (BrO, H<sub>2</sub>CO, OClO, SO<sub>2</sub>). Level 2 processing of Nadir infrared measurements will generate column distributions of , CH<sub>4</sub> and CO.

Limb observations will provide in the Level 1c data product TOA radiance and reflectance and limited polarisation, at ≈ 3 km spacing in tangent height between 0 and 100 km; Level 2 processing will generate vertical profiles of many of aforementioned trace gas species, with particular emphasis on O<sub>3</sub> and NO<sub>2</sub> (UV/visible)..

Solar occultation measurements will have only crudely calibrated radiance in Level 1c.

Cloud parameters and additional aerosol parameters will also be produced from a number of Level 2 pre-processing algorithms.

## 1.2. Purpose and scope

This Algorithm Theoretical Basis Document (ATBD) describes all algorithms required for the operational processing of SCIAMACHY Level 1b data products, and for the processing from Level 1b to 1c by the end user. This comprises the calibration algorithms for calculating calibrated TOA radiances and polarisation information, and the calculation of various instrument calibration constants.

This ATBD provides physical descriptions of the level 0 to 1c algorithms as (to be) implemented in the operational Level 0-to 1b processor, as well as in the operational Level 1b-2 processor. Therefore, the algorithms have been prepared to cope with certain constraints of product generation and associated issues related to use in an operational environment.

The ATBD describes the algorithms necessary for L1b or L1c product generation, but does not provide a detailed overview of the output data. For this, the reader is referred to the data product specification, the I/ODD [4]. The purpose of this ATBD is to describe in detail the processing steps which are used in creating the Level 1b and Level 1c data. A product specification will also be included in ESA's BEAT/CODA software packages, which may be used to examine SCIAMACHY data products (the former EnviView package has been discontinued for SCIAMACHY). Note that the processing from Level 1b to 1c by the user is done via the SciaL1c Tool which may be downloaded from ESA.

## 1.3. Document Overview

Chapter 2 gives background information on the SCIAMACHY instrument properties, instrument operation and general calibration considerations. A concise overview of the instrument and the calibration requirements

can be found in Sections 2.1 and 2.2; Sections 2.3 and 2.4 provide background information on the calibration procedures; Sections 2.5 and 2.6 give an overview of the data processing logic and the algorithms implemented in the software for SCIAMACHY level 0 to 1b processing, and of the algorithms for level 1b to level 1c processing (part of the latter are implemented as pre-processing for the NRT level 1b to 2 processor).

Chapter 3 is concerned with the detailed algorithm description for SCIAMACHY level 0 to 1c processing. Each algorithm exposition includes a physical description, along with the most important mathematical formulae. All algorithms in this chapter have both NRT and off-line processing applications.

Chapter 4 gives a listing of limitations of the algorithms described in chapter 3.

Chapter 5 deals with the analysis of the measurement uncertainties. It reflects the general considerations for the calculation of accuracy and precision errors on the level 1c data product. A review of the errors from the available information (mission and on-ground measurements) is planned for the post-operational phase.

A short overview of the ENVISAT level 1b product definition is given in the appendix A. This clarifies a few of the product building blocks referred to in Chapter 3.

## 1.4. Document Status and History

Issue 6 provides the description of the Level 0 to 1 processing software for IPF version 8. A major change is a new formulation of the radiometric and polarisation key data, including a revision of the definition of the 45<sup>0</sup> polarisation direction (U). The keydata from on-ground calibration are now combined with a "scan mirror model" to provide the Mueller Matrix elements of the instrument, corrected for instrument degradation. The degradation-dependent inputs for the scan mirror model are taken from the (daily updated) M-factor file.

Issue 5 provides the description of the Level 0 to 1 processing software for IPF version 7. The main change is an improved stray light correction in channel 2; the algorithm change will also enable future improved stray light correction for the other channels.

Issue 4 provides the description of the Level 0 to 1 processing software for IPF version 6. The main changes are in calibration of the NIR channels 6-8 (non-linearity, use of Darks from same orbit, integration time), polarisation correction (option to disable use of PMD-45), and calculation of additional SMR spectra without irradiance calibration.

Issue 3 provides the description of the Level 0 to 1 processing software after finishing the "Alignment and Improvement" of the industrial ground segment processor (IPF version 5, written by DJO) and the DLR prototype processor, in December 2003. The document update consists of a few additional clarifications and of algorithm modifications, in particular regarding the polarisation correction algorithm (in concordance with a re-analysis of on-ground calibration key data, version 3.0). A chapter on algorithm limitations has been added.

The second issue of the document was written by S.Slijkhuis, with useful inputs from ESA's reviewer R. de Beek [46]. The document now contains more introductory text and references, and the algorithm specifications are updated to reflect the status of the second industrial software implementation. This was finalised before all results of the on-ground calibration were fully analysed. Therefore, some instrument effects are not fully accounted for (e.g. Red Grass in channels 1-5, detector non-linearity in channels 6-8, new ASM diffuser). Although these effects will not be taken into account by the operational level 0 to 1b processing in the first post-launch phase, it will be possible to create workarounds in the calibration database or in off-line level 1b to 1c processing.

The draft version of this document has been prepared by S. Slijkhuis (DLR) in December 1998, following an ESA request for an ATBD for the level 0 to 1c algorithms in September 1998, to be released for presentation at the ESAMS conference (18-22 January 1999). The first issue was released February 1999. The document reflected the status of algorithm specifications for the first industrial software implementation, as laid down in the first issue of the DPM for level 0 to 1b processing written by W. Balzer and S. Slijkhuis in March 1998. The first version of the ATBD was written before detailed results from the on-ground calibration of the SCIAMACHY instrument were available.

Post-launch updates of this ATBD will have to incorporate new experience gained from on-ground calibration c.q. operational processing during and after the commissioning phase. The algorithms will be fine-tuned in

response to results and feedback from verification and validation programmes, and further improved on the basis of relevant scientific research.

The author would like to thank W. Balzer, B. Aberle, U. Boettger, and other colleagues at DLR, and J. Frerick at ESTEC.

## 1.5. Abbreviations and Acronyms

ADC	Analogue to Digital Converter
ADD	Architectural Design Document
ADS	Annotation Data Set (on level 1b product)
AO	Announcement of Opportunity
ASM	Azimuth Scan Mirror
ATBD	Algorithm Theoretical Basis Document
BCPS	Broadcast Pulse Signal
BISA	Belgian Institute for Space Aeronomy (aka BIRA, IASB)
BSDF	Bi-directional Scattering Distribution Function
BU	Binary Unit
CFI	Customer Furnished Items
CNES	French Space Agency
CRR	Computer Resource Requirements
CSF	Common Software Facility
DFD	Deutsches Fernerkundungsdatenzentrum, DLR
DLR	Deutsches Zentrum für Luft- und Raumfahrt e.V.
DOAS	Differential Optical Absorption Spectroscopy
DORIS	Doppler Orbitography and Radiopositioning by Satellite
D-PAC	German Processing and Archiving Centre
DPM/PDL	Detailed Processing Model / Parameter Data List
DS	Data Set
DSD	Data Set Description
DSR	Data Set Record
ECMWF	European Centre for Medium-range Weather Forecasting
ENVISAT	Environmental Satellite
ERS	European Remote Sensing Satellite
ESA	European Space Agency
ESM	Elevation Scan Mirror
ESTEC	European Space Centre of Technology
FD	Fast Delivery
FTS	Fourier Transform Spectrometer
FOV	Field of View

---

FPN	Fixed Pattern Noise
FS	Fokker Space B.V.
FWHM	Full Width Half Maximum
GADS	Global Annotation Data Set (on level 1b product)
GDF	General Distribution Function
GDP	GOME Data Processor
GOME	Global Ozone Monitoring Experiment
GPPR	Ground Processing Performance Requirement
ICU	Instrument Control Unit
IECF	Instrument Engineering and Calibration Facility
IFE	Institut für Fernerkundung der Universität Bremen
IFOV	Instantaneous Field of View
ILOS	Instantaneous Line of Sight
IMF	Remote Sensing Technology Institute, DLR
I/ODD	Input/Output Data Definition
IPF	Instrument Processing Facility (SCIA on-ground data processor)
IR	Infra-red
ISP	Instrument Science Packet
IT	Integration Time
KNMI	Koninklijk Nederlands Meteorologisch Instituut
LRAC	Low rate Reference Archive Centre
MDS	Measurement Data Set
MJD	Modified Julian Date
MPH	Main Product Header
NDF	Neutral Density Filter
NIR	Near Infra-red
NRT	Near Real Time
OBM	Optical Bench Module
PAC	Processing and Archiving Centre
PCA	Polarisation Correction Algorithm
PCD	Product Confidence Data
PDS	Payload Data Segment
PET	Pixel Exposure Time
PF_HS	Processing Facility Host Structure
PMD	Polarisation Measurement Device
PPG	Pixel-to-Pixel Gain
P-T	Pressure and Temperature
RTCS	Relative Time Command Sequences

---

SAA	Southern Atlantic Anomaly
SAGE	Stratospheric Aerosol and Gas Experiment
SAO	Smithsonian Astrophysical Observatory
SBT	Satellite Binary Time
SCIA	shorthand for SCIAMACHY
SCIAMACHY	Scanning Imaging Absorption Spectrometer for Atmospheric Chartography
SJT	SCIAMACHY Joint Team (industrial consortium with FS, SRON, TNO-TPD)
SLS	Spectral Light Source
SGP	SCIAMACHY Ground Processor
SGP_01	SCIAMACHY Ground Processor for Level 0 to 1b Processing
SMR	Sun Mean Reference
SOST	SCIAMACHY Operations Support Team
SPH	Specific Product Header
SRD	Software Requirements Document
SRON	Space Research Organisation of The Netherlands
SSAG	SCIAMACHY Scientific Advisory Group
SVD	Singular Value Decomposition
SZA	Sun Zenith Angle
TOA	Top of Atmosphere
TNO-TPD	Technisch Physische Dienst of TNO, The Netherlands
UTC	Universal Time Co-ordinate
UV	ultra-violet
VIS	Visible
VMR	Volume Mixing Ratio
WLS	White Light Source

## 1.6. Applicable Documents

Moved to Appendix [B.1](#)

## 2. SCIAMACHY Background Information and Algorithms Overview

### 2.1. Introduction to mission and data processing

SCIAMACHY is an AO (announcement of opportunity) instrument for ESA's ENVISAT mission [7]. The AO-Providers, which fund the instrument, are the space agencies of Germany (DLR-Bonn, formerly DARA) and of The Netherlands (NIVR), with a contribution from Belgium (BISA). The instrument is build by an industrial consortium with prime contractors Astrium (formerly Dornier Satellite Systems) and SJT (itself a consortium of Fokker Space, TNO-TPD and SRON) - a large part of the project documentation referenced in the Bibliography of this ATBD stems from these sources. Apart from the project documentation, technical details of the instrument can be found in [17, 19].

A detailed discussion of scientific objectives for SCIAMACHY may be found in the original mission proposal [15] and in e.g. [14]

The mission planning, in terms of instrument configuration and timelines (measuring modes), is prepared and supported by the SCIAMACHY Operations Support Team (SOST), a team of scientists from University of Bremen (IFE) and DLR-IMF. For a detailed description of instrument configurations and timelines see [3]. The other main activity of SOST lies in monitoring of the instrument health and the generation of a set of correction factors for the in-flight calibration of the instrument (M-factors, described in detail in Section 3.1), see [6] and [37]. For an overview of the instrument operation, see [24, 23].

Operational Level 1 and Level 2 data products will be generated at DPAC.

#### 2.1.1. Processing Requirements

Specific scientific requirements on algorithms have been laid down in the Report of the SCIAMACHY Algorithm Development and Data Usage Subcommittee [5].

Detailed requirements for the level 0 to 1b processing are laid down in the GPPR document[1], which amongst others takes account of the SCIAMACHY requirements for calibration [2] and the SCIAMACHY Calibration Plan [54] (based on the instrument design), and of the requirements imposed by the generic environment for all ENVISAT ground processors, by the level 0 data availability scenarios, and by the data product definition.

#### 2.1.2. Inheritance: relation to the GOME Data Processor

The Global Ozone Monitoring Experiment (GOME) was originally conceived as a scaled-down version of SCIAMACHY. It was given fast-track development status by ESA [62] and was launched on 21 April 1995 on board the second European Remote Sensing Satellite (ERS-2). It has 4 spectral channels covering the range 240-790 nm, and is a nadir-only instrument. The measurement capability of GOME closely matches the UV/visible nadir capability of SCIAMACHY; the mission objectives are very similar [16].

The GOME Data Processor (GDP) was developed and implemented at DFD with the help of several scientific institutions, notably the KNMI (especially for Level 1), Univ. of Heidelberg, Univ. of Bremen (IFE), SAO Cambridge, IMGA-CNR (now part of ISAO-CNR, Bologna) [60]. The GDP became operational in July 1996, with calibrated earthshine spectra and retrieved total O<sub>3</sub> columns the main products generated on a routine basis. The experience gained with GOME in the implementation of operational Level 0 to 1 processing has

been very valuable. Parts of the current ATBD have their heritage from the descriptions in the GDP Technical Documentation [61].

Nevertheless, the enhanced capabilities of SCIAMACHY, the technical differences in optics and electronics, in instrument operation, and last but not least the completely different concept of the ENVISAT ground segment infrastructure, have lead to algorithms which in detail have few things in common with the original GOME algorithms, except for the general scientific background. However, part of the algorithm development [63] has been parallel with new developments for EUMETSAT's GOME-2 instrument on METOP, since it shares some of the enhanced calibration possibilities, as well as a similar structure of the ground segment.

## 2.2. SCIAMACHY Instrument Characteristics

### 2.2.1. Instrument Hardware

SCIAMACHY is a medium-resolution UV-VIS-NIR spectrometer, fed by two nearly-orthogonal scan mirrors which enable across-track scanning in Nadir and in Limb, as well as sideways viewing

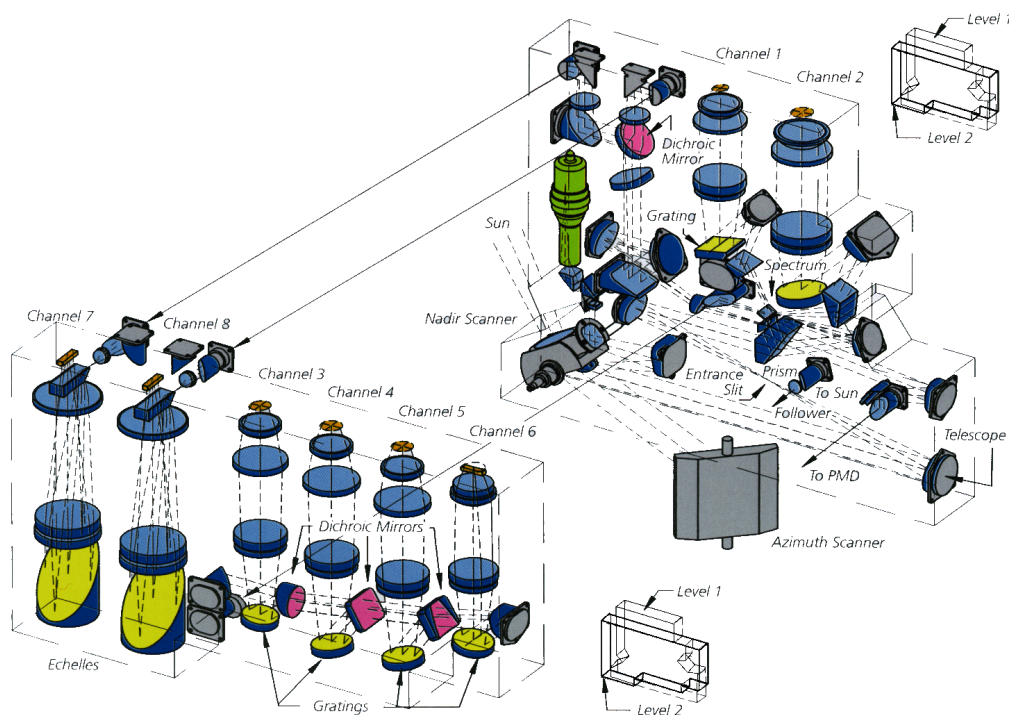


Figure 2.1.: SCIAMACHY optical lay-out.

for occultation and calibration measurements of Sun and Moon.

SCIAMACHY contains 8 channels which focus the spectrum on linear detector arrays of 1024 pixels each, and 7 Polarisation Measurements Devices (PMDs) containing photodiodes which measure linearly polarised intensity over a  $\approx 100$  nm wide spectral band. Six PMDs measure polarisation parallel to the spectrometer slit, and one measures polarisation at a  $45^\circ$  direction.

Channels 1-6 provide continuous spectral coverage of the wavelengths between 240-1750 nm with a resolution between 0.2 nm (at 240 nm) and 1.5 nm (at 1750 nm). Channels 7 and 8 provide 0.4 nm resolution in bands around 2.0 and 2.3  $\mu\text{m}$ . Calibrated channel and PMD ranges, taken from [47], are listed in Table 2.1. The spectra are formed by reflection gratings. Since the reflecting properties of these gratings are polarisation-dependent, the intensity calibration of SCIAMACHY has to take account of the polarisation of the incoming light, using information from the PMDs.

The optical layout of the instrument is schematically shown in Figure 2.1. Light enters the telescope via two ultra-smooth (reduced straylight) scan mirrors. In Nadir observation mode, only the Nadir (or 'Elevation') scan mirror (ESM) is used. In Limb and in Solar/Lunar measurement modes, the light is directed to the Nadir Scanner via the Azimuth scanner (ASM); in these modes the Nadir scanner determines the elevation (in Limb or Occultation: the limb tangent height) of the measurement. In order to monitor a possible degradation of the Azimuth Scanner, which is the optical element most exposed to contaminants and

Channel Nr.	Spectral Range [nm]	PMD	Spectral Range [nm]
1	240 - 314		
2	307 - 405	A	302 - 385
3	391 - 605	B	441 - 527
4	598 - 809	C	602 - 707
5	776 - 1051	D	785 - 913
		45°	≈ 800 - 912
6	1033 - 1765	E	1447 - 1641
7	1938 - 2043		
8	2259 - 2383	F	2262 - ≈ 2400

**Table 2.1.:** Calibrated channel boundaries (cut off at 5% level) and PMD boundaries (20% level)

solar UV radiation, a special Sun port is present which enables viewing the Sun over the Nadir Scanner only (if the geometry is favourable). In normal operations, a solar irradiance calibration is performed once a day with the Sun shining over the Azimuth scanner on a diffuser plate which is mounted on the backside of the Nadir scan mirror. Other calibration sources such as the Spectral Light Source (SLS, for wavelength calibration) and the White Light Source (WLS, for pixel-to-pixel gain and etalon correction) are directed to the Nadir scanner using auxiliary optics.

The telescope (3 cm diameter) projects the light beam onto the slit which determines the instantaneous field-of-view of 1.8° by 0.045°. For direct Sun viewing, an aperture can be inserted which reduces the amount of light entering the telescope. After the slit, the beam is collimated again and enters a predisperse prism, which has two functions. Brewster reflection at the back of the prism splits off part of one polarisation direction to the PMDs. The prism furthermore forms a low-dispersion spectrum, from which parts are picked-off to separate the light into the channels. Picked off are channel 1, channel 2, channels 3-6, and channel 7 - 8. In the channel 3-6 light beam a 20% Neutral Density filter may be inserted to cut down high light levels. Further channel separation is performed using dichroics. A grating in each channel then further disperses the light which is subsequently focused onto the detector array. Details can be found in [39].

The detectors are cooled to temperatures between 235 K (UV channels) and 150 K (NIR channels) to reduce dark signal. SCIAMACHY's optical bench is cooled to a stabilised temperature of -18° C to provide a stable, low thermal background for the NIR channels 7 and 8.

A late addition to the instrument is a second diffuser plate, mounted on the back of the Azimuth scanner (not shown in the figure). This diffuser plate is not absolutely calibrated, but can provide additional information to check in-flight properties of the default diffuser, and it can provide relative solar measurements useful in certain level 1 to 2 applications (DOAS).

## 2.2.2. Instrument Operation and Data Packet structure

A basic concept in the operation of the SCIAMACHY instrument, which is also reflected in the structure of the level 0 and level 1 data products, is that of the instrument 'State'. A State is defined by a set of parameters such as scan mirror position, scan swath width, scan rate, detector exposure time, use of sun aperture, NDF, or calibration sources. During the orbit the instrument executes a sequence of States, with a typical duration of ≈ 1 minute per State.

There are up to 70 different States possible. The States are subdivided into  $\leq 30$  'Measurement Categories'. The Nadir, Limb and Solar Occultation are the three measurement categories most relevant to the end-user. Other measurement categories comprise States for calibration and instrument monitoring. A detailed description is provided in [3].

Another important concept for especially the data packet structure is that of the 'cluster'. A cluster is a subdivision of a channel and contains data of a certain wavelength region. The cluster concept was partly driven by the wish to have certain important spectral windows with a higher spatial resolution (i.e. a faster readout during scanning) than would be possible on grounds of data rate limitations.

The consequence is that on the data product not each readout contains the whole spectrum, but that depending on which readout is finished more or less clusters (spectral regions) are present. Several clusters are in fact read out at high rate, but then co-added on-board to reduce the data rate between SCIAMACHY and on-ground receiving stations (in particular, the detector array in each channel can only be read out as a whole, and therefore the cluster with the shortest integration time in the channel determines the detector readout time; clusters which shall have a longer integration time have these short exposures co-added to obtain their nominal integration time). In Nadir, not all clusters are contiguous i.e. certain pixel ranges are read out but not transmitted to ground; these are referred to as 'unused pixels'.

For each State, the State identifier, Measurement Category and the cluster configuration parameters are written to the Level 0 and Level 1b data products. An overview of the latest status (and history) of these and further instrument configuration parameters can be found on the SOST homepage [38].

The readout of the clusters is synchronised via a clock which every 1/16 second sends a BCPS (Broadcast Pulse Signal), hence all detector exposure times are multiples of 1/16 second. The photodiodes of the PMDs are providing a continuous signal which is sampled at 40 Hz through a filter with a time constant of  $\approx 20$  Hz. Unfortunately, the sampling of the PMDs is in no way synchronised with the BCPS, and one of the tasks of level 0 to 1b processing is to interpolate the PMD signals onto the detector-readout time grid.

For Nadir, the nominal integration time is 1 second, corresponding to a footprint on the ground of 240x30 km. A complete swath of 960 km consist of 4 such integrations, plus one fast reverse scan where the scan mirror returns to the initial position. Channels 2b-6 are read out at a higher rate; the smallest integration time is for the cluster from 425-530 nm (for  $\text{NO}_2$ ,  $\text{O}_3$  retrieval) which under sufficiently high light levels attains a minimum footprint of 30x30 km.

For Limb, the nominal integration time is 1.5 second, corresponding to a 'column pixel' of  $\approx 960 \times 3$  km at the tangent height. The minimum integration time (under sufficiently high light levels) is for channel 3 (400-600 nm) with a column pixel size of  $\approx 120 \times 3$  km. All clusters in one channel have the same integration time in Limb mode. Limb scanning is performed in 34 steps of 3 km height intervals, starting at approximately 2 km below the horizon up to 100 km. Subsequently a 'dark' exposure is made by looking in dark space at 250 km above the horizon (before orbit 6456 this was 150 km). During the across-track swath of 960 km, the nadir scan mirror follows the Earth's curvature, so that at every point in the swath the field-of-view remains centred on the same tangent height.

In nominal operation, Limb and Nadir viewing is alternated in such a way that a packet of air observed during Limb observation is a few minutes later covered by the Nadir observation; projected on the Earth surface this leads to footprints where both Limb and Nadir are measured, alternated with footprints where no measurements are available. In order to retain a global latitude coverage, the location of gaps and measurements is alternated every orbit ('chess-board' pattern).

For Sun Occultation measurements, SCIAMACHY is first pointed to the approximate location at which the sun is expected to be situated some 17 km above the horizon (this avoids problems with atmospheric refraction). Because the position of the sun is not known exactly (spacecraft pointing inaccuracies), the elevation mirror scans continuously up and down. When the sun enters the field-of-view, a sun-follower locks the azimuth mirror on the sun, but the elevation mirror continues to scan the slit up and down over the solar image. We thus get a sequence of spectra for which the position on the solar surface is not accurately known. Since different horizontal slices of the solar image cover different surface areas, there is no accurate radiance calibration of these spectra.

In general, platform pointing inaccuracies pose a problem in the determination of tangent height for both Limb and Occultation measurements.

### 2.2.3. Instrument Calibration requirements for Level 0 to 1c processing

There are four basic calibration steps needed to convert the instrument binary data into calibrated physical quantities.

1. Signal processing: correction of electronic anomalies (memory effect, cross-talk) and PMD synchronisation; correction for dark signal (including thermal background in channel 7 and 8), pixel-to-pixel gain, etaloning and straylight
2. Wavelength calibration: assigning to each detector pixel its associated wavelength
3. Radiance calibration: conversion of the corrected detector signals of the earth-shine spectra to radiance units; this includes a polarisation correction which takes into account the different response of the instrument to input radiance with different polarisation directions
4. Irradiance calibration: conversion of the corrected detector signals of the solar spectra to irradiance units; this includes correction for the BSDF of the diffuser plate.

Furthermore the measurements have to be geolocated, i.e. the geographical position of the footprint on the Earth's surface (Nadir) or of the tangent height point (Limb) has to be determined from the instrument's scan mirror angles and from the spacecraft data.

Performing these calibration steps is the task of level 0 to 1c processing.

## 2.3. The generic calibration equation

The generic expression for the signal detected by each detector pixel, as function of the incident radiation and as function of the instrument characteristics, can be written as:

$$S_i = I(\lambda_i) \cdot T(\lambda_i) \cdot Q_i + SS_i + DS_i$$

with

$S_i$	measured signal at detector pixel i
$\lambda_i$	wavelength of detector pixel i
$I(\lambda_i)$	incident radiation as function of wavelength
$T(\lambda_i)$	optical transmission function of instrument as function of wavelength
$Q_i$	detector efficiency (including conversion to 'binary units') of detector pixel i
$SS_i$	straylight signal at detector pixel i (depending on all signals in the channel)
$DS_i$	dark signal of detector pixel i

which by inversion yields the expression for the retrieved atmospheric intensity (on the Level 1b product given in units of photons/(s.cm2.sr.nm) for Earth-shine measurements c.q. photons/(s.cm2.nm) for the Sun measurements):

$$I(\lambda_i) = \frac{S_i - SS_i - DS_i}{T(\lambda_i) \cdot Q_i}$$

Instrument calibration comprises the determination of all quantities (except  $S_i$ ) in the right-hand side of this equation. The quantities in the denominator deserve special attention, since they are in practice varying with time due to:

- wavelength shifts
- general degradation of the optics

- degradation of detector pixels
- varying interference patterns on detector (e.g. build-up of thin ice layers).

The latter problem is called Etaloning [35]. The changes in etalon manifest themselves as a changing sinusoidal pattern, with typically 3-10 waves per channel in the UV and visible (in the near-infrared, the etalon frequency becomes of the order of the channel width and the pattern cannot be detected anymore). Etalon can be determined from measurements of the internal white light calibration source (WLS). To separate out the changes in etalon from the changes in the WLS itself (or the optics in its light path) a Fourier filtering technique is used to determine all changes in the expected frequency range of 3-10 waves per channel.

When correcting the Response function of the instrument,  $T(\lambda_i) \cdot Q_i$ , for wavelength shifts we encounter the problem that only its wavelength-dependent part must be shifted and not its pixel-dependent part (the wavelength-dependent part is formed by the transmission of the optics and the quantum efficiency of the detector material; the pixel-dependent part is formed by pixel size and possible radiation damages to pixels). This separation into a wavelength- and a pixel-dependent part is difficult to make since in practice only the end-to-end throughput is measured. The usual approach is to postulate that the wavelength-dependent part is a smooth function of wavelength. The instrument response function is smoothed with a certain filter and this is taken as its wavelength-dependent part; the remaining structure on a pixel-to-pixel scale is taken as the pixel-dependent part. However, there is a certain arbitrariness in this approach by the choice of the smoothing filter.

The pixel-dependent part of the Response function, called pixel-to-pixel gain (PPG) is determined by illuminating the detector with a light source with a smooth spectrum. To this end the WLS can be used, although care has to be taken since experience from the SCIAMACHY on-ground calibration shows that the WLS spectrum may contain ripples with a frequency near the pixel-to-pixel separation, probably caused by an Etaloning effect in the glass bulb of the lamp.

Changes in instrument response function other than the above are usually caused by a gradual degradation in optics or electronics. This degradation must be monitored by scientific analysis of the data set. Such changes in instrument response are in the calibration equation accounted for by so-called monitoring factors.

An additional complication is that the instrument response function depends on the polarisation state of the incoming light. This is implemented as a polarisation correction factor, applied to the response function measured for unpolarised light. The polarisation state of the incoming light is determined for each measured channel signal, using the PMD-detector measurements recorded during the integration time of the channel signal.

Taking all of the above effects into account, we can rewrite the generic calibration equation as:

$$I(\lambda_i) = \frac{S_i - SS_i - DS_i}{c_{pol}(\lambda_i, p_t(\lambda_i)) \cdot (R_{0,i}/PPG_{0,i})(\lambda_i) \cdot PPG_{t,i} \cdot m_t(\lambda_i) \cdot E_t(\lambda_i)}$$

where subscript 0 denotes the quantity at a reference time  $t = 0$  and subscript t denotes the quantity at the time of measurement, and

$(R_{0,i}/PPG_{0,i})(\lambda_i)$	smooth part of response function as function of wavelength, for unpolarised input
$c_{pol}(\lambda_i, p_t(\lambda_i))$	polarisation correction factor as function of wavelength and input polarisation
$PPG_{t,i}$	pixel-to-pixel part of response function at detector pixel i
$m_t(\lambda_i)$	degradation monitoring factor as function of wavelength
$E_t(\lambda_i)$	etalon change as function of wavelength

The above equation is valid for the atmospheric measurements. For the observation of the Sun there is additionally a diffuser plate (plus auxiliary optics) in the light path. The scattering properties of the diffuser plate depend both on the elevation angle of the incident beam (which is a function of time in the orbit) and on its azimuth angle (which is a function of time of the year); this 2-dimensional dependency is expressed in the bi-directional scattering function (BSDF) of the diffuser. Noting that the sunlight is unpolarised, the generic calibration equation then takes the form:

$$I(\lambda_i) = \frac{S_i - SS_i - DS_i}{BSDF_0(\lambda_i) \cdot m_{BSDF,t} \cdot (R_{0,i}/PPG_{0,i})(\lambda_i) \cdot PPG_{t,i} \cdot m_t(\lambda_i) \cdot E_t(\lambda_i)}$$

## 2.4. Determination of Calibration Parameters

### 2.4.1. Overview

Calibration of the instrument is performed on 3 different levels:

- **Onground Calibration:**  
determines the instrument response to calibrated radiance and irradiance sources as function of wavelength and scan mirror angles; determines the straylight properties of the instrument; provides preliminary calibration of wavelength and dark signal.
- **M-factors:**  
uses in-orbit dedicated observing modes ('monitoring States') to obtain the so-called M-factors (monitoring factors) which describe the degradation of the instrument in space.  
The M-factors are defined as the factors which have to be applied to the measured signals to correct them to begin-of-life levels, such that the onground-calibration data on the (ir)radiance response can be applied.  
M-factors are to be updated at regular time intervals by the SCIAMACHY Operations Support Team (SOST) consisting of scientists from Univ.Bremen and from DLR-DFD. The m-factor files are subsequently used in the Level 0-1b Processor to calculate the scan angle dependent degradation correction with the scan mirror model.
- **Level 0 to 1b Processing of Calibration Constants:**  
Calibration constants which can be directly derived from measurements using on-board calibration sources are determined during the operational Level 0 to 1b processing. This comprises dark signal measurements on the night side of each orbit, and at regular intervals wavelength calibration using the SLS measurements and PPG/Etalon calibration using the WLS measurements.

### 2.4.2. Onground Calibration

The onground calibration is performed by the SCIAMACHY Joint Team (SJT), a consortium consisting of SRON, TNO-TPD and FSS for the design, building and on-ground calibration of the SCIAMACHY instrument. The output of the on-ground calibration relevant to the operational Level 0 to 1c processing, is a data set containing the so-called 'Calibration Key Data'.

A complication of the onground calibration has been that the instrument had to be calibrated in thermal vacuum (to enable cooling the instrument to operational temperatures without frosting, and to avoid H<sub>2</sub>O and CO<sub>2</sub> absorption features in the infrared calibration data) but that the available measurement setup did not allow calibration over the full range of viewing directions. Therefore, the angular dependence of the calibration constants has been derived from measurements on the isolated scanner mechanism alone, but the integration of these angular dependence in the calibration constants leads to a rather complex mathematical description, especially for the polarisation sensitivity. Details are given in Section 3.1.

### 2.4.3. M-factors

The degradation of the instrument can be monitored by combining measurements from several instrument States. These States have been designed in such a way that they include or exclude various optical elements, thus enabling to determine the reflectance/transmittance of these elements.

The M-factors describe the ratio of begin-of-life to actual end-to-end instrument efficiency, both for the channel detectors and for the PMDs. They are split in two components:

1. The *scanner degradation* which describes the change of mirror/diffuser (combinations) are calculated with the scan mirror model using refractive indices and thickness of the contamination layers. This degradation depends on the scan angle and the wavelength.
2. The *OBM degradation* describes the change of all optical elements behind the scanners.

The m-factors are calculated by fitting various in-flight measurements with the scan mirror model. The fitting parameter is the thickness of the contamination layers. An additional multiplicative term gives the residual degradation not captured by the model. In the ideal case this corresponds to the degradation of the OBM. These m-factors are called *residual m-factors*.

The M-factor concept assumes that the degradation does not influence the polarisation sensitivity and that the scan angle dependence can be modelled. In how far these assumptions really apply remains to be seen. A validation of these assumptions might be possible using observations of the Moon, which shows polarisation depending on phase angle.

In Level 0 to 1c processing, the M-factors are applied to update the radiance- and irradiance response as given by the Calibration Key Data. Residual M-factors, refraction and thickness of the contamination layers are provided externally to the operational processors through the SOST.

This calibration concept has only one gap, which is that M-factors are determined w.r.t. the begin-of-life in orbit (driven by the necessity to use in-orbit measurements). However, the on-ground calibration was finished before launch, and degradation of the instrument while in ground storage, or during its first days in space, is not covered. Details can be found in section 3.1.5 and in [53, 45]

#### 2.4.4. Level 0 to 1b Processing of Calibration Constants

Dark signal from the detectors and PMDs, including the thermal background in the infrared channels, is measured at regular intervals around the orbit by staring at 'Deep Space' (like limb viewing geometry with a tangent height of 150 km). Dark signal has a fixed component, the so-called fixed-pattern noise (FPN), as well as a component due to charge leaking which increases linearly with detector exposure time. The thermal background component also increases linearly with detector exposure time. Therefore, the dark signal can be characterised by 2 calibration constants: the offset (FPN) and the slope of the dark signal versus exposure time. To this end 5 Dark States are implemented, with different exposure times which are executed after each other, from which the 2 parameters plus error estimate can be derived. The dark signal is derived as function of the orbital phase (see below), to allow for thermal gradients over the orbit.

Another background component which increases linearly with exposure time is a possible contamination by solar straylight, which might occur when the Azimuth Scanner is directly illuminated by the Sun for a short period after the instrument emerges from the dark side of the orbit. This component will be modelled as a polynomial function of orbit phase, but only for that part of the orbit where the Azimuth Scanner is directly illuminated.

Spectral calibration is performed at regular intervals (typically weekly) using the sharp emission lines of an internal Pt/Cr-Ne hollow cathode lamp (the SLS). For each channel, a 4th order polynomial will be fitted to the spectral line positions to obtain wavelength as a function of pixel number. Since the number of strong lines in the infrared channels is insufficient, the wavelength polynomial for these channels will be derived from Solar observations, using the Fraunhofer lines in the Sun.

The wavelength calibration depends on the temperature of the optical bench. Although the instrument is temperature stabilised, thermal gradients may occur as function of orbit phase due to single-sided heating by the Sun.

Just as with the Dark Signal, the polynomial coefficients of the wavelength calibration will be modelled by a harmonic (sinusoidal) function, as function of orbit phase. Since within one orbit not all orbit phases may be covered by the measurements, the calculation of the harmonic function is done outside the operational Level 0 to 1b processing chain (in particular, this is a requirement for the NRT processing at the receiving station, which may not have access to orbits received by another station). The result is offered to the processor via an auxiliary input file. As a consequence, the processor never uses calibration data obtained from the orbit which is being processed, but always from (an) earlier orbit(s).

Calibration measurements from the White Light Source (WLS), which approximately delivers a continuous,  $\approx 3000$  K blackbody, spectrum are used for flat-fielding the spectra of each detector array. This comprises the calculation of pixel-to-pixel gain (PPG) and the characterisation of the etalon effect - a low-frequency spatial (i.e. as function of pixel number) oscillation in detector response caused by a changing thickness of ice deposits

on the detector (see e.g. [35]). Incidentally, first results from the on-ground calibration indicate that the etalon is very stable and no in-orbit correction may be required here. The WLS calibration is also done only at regular (typically weekly) intervals.

The WLS measurements are also used to generate a 'bad pixel mask'. This is a mask which determines which detector pixels are dead or yield potentially unreliable signals, and shall be ignored during processing. Bad pixels are only expected in the new-technology detectors [21] employed in the NIR channels 6-8; first results indicate that up to 10% of all pixels in these channels may be bad [40]. Unlike the PPG and Etalon data, the input bad pixel mask is not automatically updated by the processor; this needs a human intervention.

Daily observations of the Sun over a diffuser plate provides a solar reference which is used in the calculation of the Earth-shine reflectivity spectra. The calibrated solar irradiance spectrum is output as measurement data on the product of the orbit containing the solar measurement; for subsequent orbits it is used as calibration data for reflectivity, until a new Sun is observed. This calibration data is referred to as the **Sun Mean Reference** (SMR) spectrum.

## 2.5. Operational aspects of Level 0 to 1c processing

The algorithms described in this ATBD are primarily driven by the scientific needs to convert measured signals into calibrated radiances. However, constraints from the operational environment may force one to take different strategies as one would employ for a ground-based instrument. This mainly affects the way how calibration data are processed and stored on the data products.

The dataflow of the scientific measurements from Level 0 to level 1c, and the dataflow of the calibration measurements, is schematically shown in Figure 2.2.

The main input to the SCIAMACHY Data Processor is the level 0 product, comprising data streams of ADC signals for the scientific nadir, limb and occultation States, for calibration and monitoring States, and separate data streams for ADC signals of PMDs and instrument housekeeping data. The level 0 product contains data from 1 satellite orbit. Also required as input is a list of parameters controlling the execution of the algorithms in level 0 to 1b processing; this comprises the 'Initialisation File'.

Additional real-time auxiliary data are also required; instrument calibration data, ENVISAT orbit parameters (state vector), SCIAMACHY pointing model, for example.

The level 0 product and the auxiliary data products are input to the level 0 to 1c processor system.

In order to keep the data product as small as possible, the SCIAMACHY processing is done in two steps. All necessary calibration constants are processed from the calibration measurements in the operational processing from level 0 to 1b. The level 1b data product contains the raw detector signals (binary ADC units) of the science measurements plus calibration constants.

The end-user has to run an application tool which applies the calibration constants to the data; this inflates the level 1b product to a much larger level 1c product containing fully calibrated data. An additional advantage of this procedure is that the user can optionally omit certain calibrations to investigate their influence (or perform the calibration himself), and that by optionally filtering out only a subset of the data (i.e. geographical coverage or measurement category) the final level 1c product may be kept as small as possible.

A significant complication arises from the fact that:

- the instrument needs calibration data, but it also generates new calibration data
- the newly generated calibration data can only be processed per orbit, but the needed amount of calibration data may span several orbits (it may even occur that the data of one orbit are "sliced" i.e. the orbit file is split to different processors and concatenated afterwards - this makes it impossible to perform in the operational processor modelling over one orbit)
- According to PDS architecture rules, there can be only one (!) output product, the level 1b product, as specified in [4].

As a consequence of especially the last point, the level 1b product must not only hold processed science data, but also calibration data (measurements) and instrument monitoring data, as well as newly calculated calibration parameters (the latter are collected in a special part of the product, the ADS's, see Appendix A - usually an ADS is generated after each processed instrument state). In order to keep the size of the product as small as possible, dark signal calibration data are discarded after calculation of the dark signal calibration parameters. All other calibration data and monitoring data are retained, albeit in unprocessed form.

## 2.6. Algorithms Overview

In this and the following section, summaries of algorithms are given without references (these will be given in the main text). The summaries given include both the Level 0 to 1b and the Level 1b to 1c algorithms; the latter are often also referred to as 'Applicator' algorithms because they are part of an application tool which has to be run by the end user on the Level 1b data product, in order to generate the level 1c data product. Noted in italics is if the algorithm belongs to the operational Level 0 to 1b processing (*OP*) or to the Level 1b to 1c applicator (*A*). The sequence below also reflects the sequence of signal processing.

Note that certain processing steps depend on the type of measurement: the 'Calculate...' processing steps (except 'calculate geolocation') are only invoked if the corresponding calibration sources are being observed. The type of measurement is in the Level 0 to 1b processing determined from the field 'MEASUREMENT CAT[EGORY]' in the data field header on the Level 0 file. The link between measurement category and processing mode is established via the GADS 'Processing Categories' on the initialisation file [4].

***Pre-processing of Mueller Matrix elements (OP)*** These algorithms calculate the Mueller Matrix elements of the instrument from the Calibration Key Data (for an introduction to Mueller Matrix elements see the corresponding algorithm description). These basic calibration data are interpolated to a fine grid of scan angles, and to the wavelength of the SMR spectrum. Those interpolated Mueller Matrix elements which are also needed by the application program are output to the Level 1b product.

***Calculate Geolocation and synchronise PMDs (OP)*** In the geolocation processing, the instrument scan angles and time information is converted to geographical coordinates, and the solar illumination condition is determined. This relies heavily on the use of ESA's ENVISAT Orbit Propagator, whose routines will be referenced but not explained in detail. The stream of PMD signals is synchronised with the BCPS of the channel readout, and the PMD signals are averaged over time chunks of 1/32 second which is an integer fraction of the channel exposure time (2 times the shortest possible readout).

***Correct Detector Readout Memory (OP, A)*** The algorithm calculates the magnitude of the memory effect in the Reticon detectors (channels 1-5) and codes this as a byte on the Level 1b data product (*OP*). The memory effect is subtracted from the measurement (*OP, A*).

***Correct Detector Non-Linearity (OP, A)*** The algorithm calculates the magnitude of the non-linearity in the SWIR detectors (channels 6-8) and codes this as a byte on the Level 1b data product (*OP*). The memory effect is subtracted from the measurement (*OP, A*).

***Calculate Dark Signal (OP)*** The algorithms describe how to use the Dark Measurement States to derive calibration constants for FPN and leakage current (including thermal background). Output to the Level 1b product is a set of calibration constants as function of orbit phase. Similarly, calibration constants for the possible solar straylight from the Azimuth Scanner are derived. The pointing to the dark sky during Limb measurements is not used for dark signal calibration, but a quality flag is set for the limb measurements.

**Apply Dark Signal (OP, A)** Applies the calibration constants for Dark Signal to the measurement spectrum and calculates the relevant errors.

**Calculate PPG and Etalon Parameters (OP)** Calculates from the WLS calibration data the PPG (detector pixel-to-pixel gain) and the Etalon (interference pattern), using a Fourier filtering technique. For the latter a solar spectrum may be used as backup for the WLS.

**Apply PPG and Etalon Parameters (OP, A)** Applies the calibration constants for PPG and Etalon to the measurement spectrum and calculates the relevant errors.

**Calculate Spectral Calibration Parameters (OP)** All algorithms listed above are applied to detector signals without need of knowledge of the precise wavelength of each pixel. This changes for the algorithms which follow, which need wavelength information in order to use the correct calibration constants. The algorithms described here provide this wavelength calibration, using information from the SLS or from the SMR spectrum.

**Apply Spectral Calibration Parameters (OP, A)** Calculates for each detector pixel its wavelength [nm] from the spectral calibration parameters.

**Determine Spectral Straylight (OP)** Uses pre-flight straylight characteristics and measured polarisation fractions to calculate for each detector pixel the straylight from other wavelengths. The straylight intensity is coded on the level 1b product.

**Apply Straylight Correction (OP, A)** Decodes the straylight from the level 1b product (**A**) and subtracts it from the measurements.

**Apply BSDF and calculate SMR (OP, A)** Uses measurements of the Sun over the diffuser to calculate a (daily) Sun Mean Reference spectrum, where the irradiance is calibrated via the BSDF function of the diffuser (**OP**). The application of BSDF is also performed in the radiometric calibration of science measurements using the Sun (**A**). The out-of-band signal of the PMDs is calculated (**OP**).

**Determine Fractional Polarisation Values (OP)** Calculates the Fractional Polarisation Values at 12 wavelengths over the SCIAMACHY range from the ratio of PMD to channel signals, from the ratio of 2 overlapping channel signals, or from single-scatter theory (at 300 nm). This is not only done for all readouts with the points then available, but also for averaged readouts to cover all possible ground pixel sizes in a State.

**Interpolate Fractional Polarisation Values and Apply Polarisation Correction (OP, A)** Calculate the parameters of the polarisation curve in the UV (**OP**). The Fractional Polarisation Values are interpolated to wavelength (**A**). This is partly done using modified spline interpolation (Akima), partly using the UV parameterisation from the Level 1b product. The interpolated polarisation values are used in the calculation of the polarisation correction of Earth-shine measurements (**A**). Note that the calculation of the spectral straylight (**OP**) may also require polarisation information - here a simplified approximation of the polarisation is used.

**Apply Radiance Response (A)** Perform the absolute radiometric calibration of the detector signals, including polarisation correction using the wavelength-interpolated Fractional Polarisation Values. Optionally a Sun-normalised spectrum (the reflectivity) is calculated.

**Quality Flagging (OP)** Several data quality flags are written to the Level 1b product. These may apply to the whole orbit, or only to a State, or only to a (cluster) readout in a State.

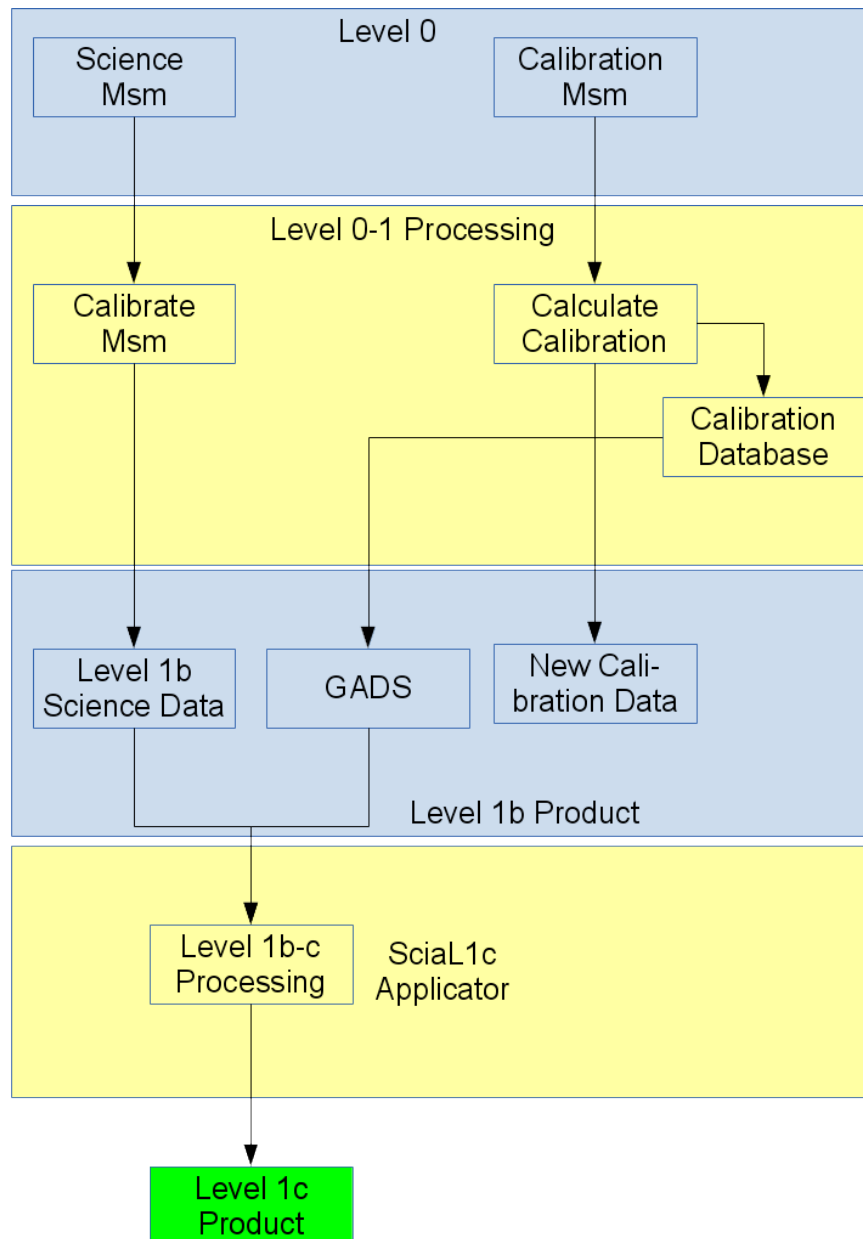


**Figure 2.2.:** Data flow of science measurements and of calibration measurements.

## 3. Level 0 to 1c Algorithms Description

### 3.1. Pre-processing of Mueller Matrix elements

The sensitivity of the instrument to polarised radiance is described by a set of calibration constants which are named Mueller Matrix elements (see below).

The algorithms in this section calculate the Mueller Matrix elements of the instrument from the Calibration Key Data. The Mueller Matrix elements are interpolated to a fine grid of scan angles, and to the wavelength of the SMR spectrum; they are corrected with the M-factors. Those interpolated *Mueller Matrix elements*, which are not only needed for the Level 0 to 1b processing but also for the Level 1b to 1c processing, are output to the Level 1b product, together with their errors.

The reason for doing this in a pre-processing step on a predefined grid of scan angles has to do with the special way how the PDS may cut the orbit into slices, and collate these slices into one level 1b product - there is no further algorithmic reason for doing things this way.

#### 3.1.1. Introduction to Mueller Matrix elements

Every optical system can be described in terms of a Mueller matrix which transforms an input Stokes vector  $(I_0, Q_0, U_0, V_0)$  to a Stokes vector in front of the detector  $(I_d, Q_d, U_d, V_d)$  [13, 10]. The first element of the Stokes vector,  $I$ , describes the total intensity of the light. The second component,  $Q$ , describes the amount of linear polarisation along the X-axis of the (chosen) coordinate system. It is equivalent to the quantity  $I_X - I_Y$  where  $I_X$  is the intensity of light with polarisation parallel to the X-axis and  $I_Y$  is the intensity of light with polarisation parallel to the Y-axis; note that  $I = I_X + I_Y$ . The third component,  $U$ , describes the amount of linear polarisation along the  $45^\circ$  direction (going from +X to +Y) of the (chosen) coordinate system. One can write  $I_{45^\circ} - I_{135^\circ}$  (note that  $I$  can also be written as  $I = I_{45^\circ} + I_{135^\circ}$ ).

Although not further needed in this Section, it is mentioned that the total amount of linearly polarised light,  $P$ , and the polarisation angle,  $\chi$ , are given by:

$$P = \sqrt{\left(\frac{Q}{I}\right)^2 + \left(\frac{U}{I}\right)^2}$$

and

$$\chi = \arctan\left(\frac{Q}{U}\right)$$

See Section 3.13 for further details.

Unlike  $Q$  and  $U$ , the quantity  $P$  is independent of the choice of coordinate frame.

The last component of the Stokes vector,  $V$ , describes the amount of circular polarised light. For the radiation from the Earth's atmosphere, Stokes element  $V_0$  is expected to be very small, and the Mueller matrix elements of the SCIAMACHY instrument which could mix  $V_0$  into  $I_d$  are small enough that we can neglect  $V$  altogether.

The radiative transfer through the instrument can then be written in the form

$$\begin{pmatrix} I_d \\ Q_d \\ U_d \end{pmatrix} = \begin{pmatrix} M_1 & M_2 & M_3 \\ \dots & \dots & \dots \\ \dots & \dots & \dots \end{pmatrix} \cdot \begin{pmatrix} I_0 \\ Q_0 \\ U_0 \end{pmatrix} \quad (3.1)$$

Since the detector only measures intensity (its quantum efficiency is independent of polarisation) the first row of the Mueller matrix is the only significant one. Therefore, the signal  $S$  of any detector in SCIAMACHY (channel array or PMD) can be expressed as

$$S = M_1 \cdot I_0 + M_2 \cdot Q_0 + M_3 \cdot U_0 = M_1 \cdot I_0 \cdot \left\{ 1 + \frac{M_2}{M_1} \cdot Q_0^* + \frac{M_3}{M_1} \cdot U_0^* \right\} \quad (3.2)$$

where the matrix elements now implicitly include the detector efficiency and electronics amplification. The task of level 1 processing is to invert this equation and derive the intensity  $I_0$  from the signal.

The matrix elements are dependent on wavelength and on scan mirror angles. At calibration they have been measured at certain wavelengths and scan angles; at level 1 processing they have to be interpolated to the exact wavelengths and scan angles of the measurement in process.

A note on co-ordinate frames: for the users of SCIAMACHY data it is convenient to use a co-ordinate frame which is only related to the geometry of the scattering of light in the atmosphere. The choice is to define  $Q_0$  as parallel to the local meridian plane - the plane through satellite, zenith, and centre-of-FOV (where the z-axis of the polarisation frame points in the travel direction of light i.e. towards the instrument). However, the calibration Key Data as delivered by SRON are measured w.r.t. an instrument co-ordinate frame which is different.

In the processor, we will evaluate the calibration of radiance using this instrument calibration co-ordinate frame with Stokes fractions  $Q_0^*$ ,  $U_0^*$  simply denoted as  $Q$ ,  $U$ .

On the Level 1b data product, the derived polarisation values will be presented on the co-ordinate frame based on the local meridian plane as defined above.

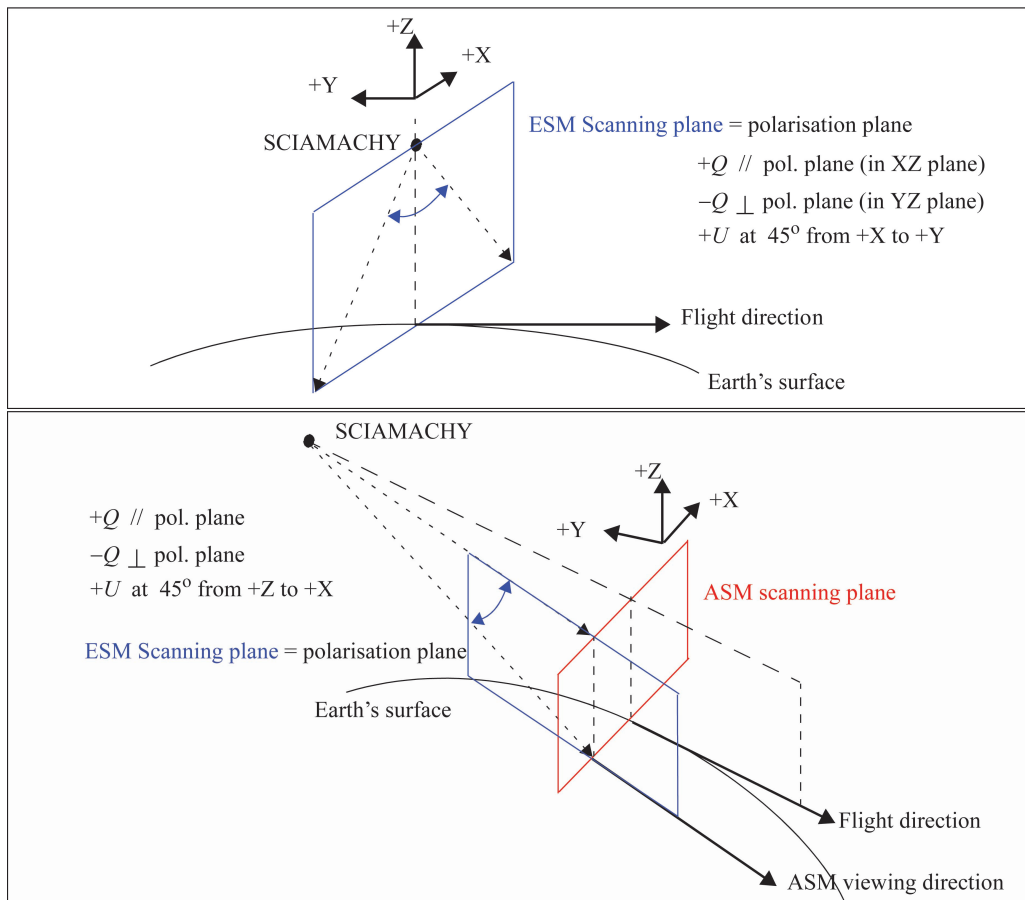


**Figure 3.1.:** Definition of the polarisation plane for  $Q$ ,  $U$  on the level 1b product. top panel: nadir geometry. bottom panel: limb geometry.

This plane is depicted in Figure 3.1 for Nadir-viewing geometry (upper panel) and for Limb-viewing geometry (lower panel). Note that XYZ refers here to SCIAMACHY instrument coordinates, not the coordinates of the polarisation frame. The polarisation vector corresponding to  $Q=1$  lies in the ESM scanning plane, perpendicular to the viewing direction. The polarisation vector corresponding to  $U=1$  lies in a plane perpendicular to the viewing direction. In Nadir mode, the  $U=1$  vector lies  $45^\circ$  clockwise out of plane, looking into the instrument (in the exact Nadir direction this is  $45^\circ$  from  $+X$  to  $+Y$ ). In Limb, similar definitions apply, i.e. when the viewing direction is in flight direction, the  $U=1$  vector lies  $45^\circ$  from  $+Z$  to  $+X$ , clockwise when looking into the instrument. Note that in Limb the polarisation plane may make an angle with the flight direction, depending on the azimuth viewing direction.

### 3.1.2. Rationale

The original SCIAMACHY calibration plan [54] describes the calibration of the instrument directly in terms of the calibration Key Data. Polarisation is described using the fractions of light polarised on 2 instrument axes. These polarisation parameters are denoted  $p$  and  $q$  and are, depending on the chosen co-ordinate frame, simple transformations of the Stokes fractions  $Q$  and  $U$  respectively. This formalism is very well suited to perform the on-ground instrument calibration using ratios of measurements (i.e. avoiding as much as possible the needs for absolute intensity calibration), but it leads to a rather complex formulation of the retrieval of the atmospheric radiances and polarisation from the signals measured in-orbit.

The expressions for calculating e.g. polarisation fractions or stray light from the in-orbit measurements become much more transparent when using the Mueller matrix formalism. This is especially important for the validation of the algorithms. For this reason, the level 0 to 1b processor was based on the Mueller matrix formalism.

Another advantage is that the retrieval using the Mueller matrix formalism is independent of the observing mode (Nadir or Limb). This has become advantageous now that it appears that the polarisation properties of SCIAMACHY are more complex than anticipated in [54] (although the GOME on-ground calibration already showed anomalies which indicated that the assumptions might be too simple) [30, 28]. The Mueller matrix formalism can cope with this without major modifications, which is advantageous because at the time of calibration the bulk of the processing software was already being coded.

### 3.1.3. Conversion of Key Data for polarisation sensitivity

A separate conversion of polarisation key data is no longer needed. With the introduction of the scan mirror model, see Section 3.1.5, the polarisation-sensitive Mueller Matrix Elements are directly obtained from the key data using the model.

### 3.1.4. Conversion of Key Data for radiance sensitivity

A separate conversion of the radiometric key data is no longer necessary, because the values for the Mueller Matrix elements are directly obtained from the scan mirror model to calculate the radiometric sensitivity.

### 3.1.5. Calculation of Instrument Response

The scan unit model is used to calculate polarisation and radiance sensitivities of the SCIAMACHY instrument depending on

- Elevation scan mirror position
- In case of limb and occultation measurements the azimuth scan mirror position
- In case of sun-diffuser measurements the solar elevation angle
- Usage of the Neutral Density Filter (NDF), true or false

- The used sensor (science detector, PMD or PMD\_45)
- The date of the measurement used for selecting the corresponding M-Factor file, which contains time dependent values: the thickness and refractive index of contamination layers on the optical surfaces, and the residual (OBM) m-factors.

The polarisation and radiance sensitivities of the Optical Bench Module (OBM), the Neutral Density Filter (NDF) and the diffuser (characterised by the BSDF) have to be applied depending on the light path for which polarisation and radiance response shall be calculated. These key-data can be read from key-data files. For the variable part of the instruments polarisation and radiance sensitivities a Mueller Matrix shall be calculated which is defined by the current viewing angles and the modelled contamination status of the instrument.

For the calculation of polarisation and radiance response we start with the following formula, which describes the light by a Stokes vector and the instrument by a series of matrices. The light, which goes through the instrument and which is changed by the instruments characteristics can then be calculated by multiplying the incoming light vector by the instrument matrices. The light vector consists of 8192 elements according the eight SCIAMACHY channel arrays with 1024 detectors each:

$$\begin{aligned}
 I(\lambda_i) &= \underline{I}_0(\lambda_i) \times \underline{M}_1^{OBM}(\lambda_i) \times mf_{OBM}(\lambda_i) \times \mu_{OBM}(\lambda_i) \times \underline{M}_{scanner}(\lambda_i, \alpha_{esm}, \alpha_{asm}, \alpha_{elev}, n_j, d_j) \\
 &=: \underline{I}_0(\lambda_i) \times \underline{M}_{instr}
 \end{aligned}
 \tag{3.3}$$

with

$\lambda_i$	Wavelength for pixel $i$
$I$	The Stokes vector of the light in front of the detector with 8192 elements
$\underline{I}_0$	The Stokes vector for the incoming light
$\underline{M}_1^{OBM}$	the constant radiance sensitivity of the OBM given as key-data vector
$mf_{OBM}$	the M-factor of the measurement day
$\mu_{OBM}$	the (constant) polarisation sensitivity of the OBM given as key-data
$\underline{M}_{scanner}$	the contamination- and scan-mirror dependent part of the instrument depending on scanner angles $\alpha_{esm,asm}$ or sun elevation angle $\alpha_{elev}$ , refractive index $n$ and layer thicknesses $d$ and on the light path. For details, see [53].
$n_j$	refractive index of layer $j$
$d_j$	layer thickness of layer $j$

The new key data for that serve as an input for the scan mirror model, are:

Key Data	Description
$\lambda_{keydata}$	Wavelength grid of the key data
$\mu_{2,OBM}^D$	Polarisation Sensitivity $Q$ of the OBM (Detector Light Path)
$\mu_{3,OBM}^D$	Polarisation Sensitivity $U$ of the OBM (Detector Light Path)
$\mu_{4,OBM}^D$	Polarisation Sensitivity $V$ of the OBM (Detector Light Path)
$\mu_{2,OBM}^P$	Polarisation Sensitivity $Q$ of the OBM (PMD Light Path)
$\mu_{3,OBM}^P$	Polarisation Sensitivity $U$ of the OBM (PMD Light Path)
$\mu_{4,OBM}^P$	Polarisation Sensitivity $V$ of the OBM (PMD Light Path)
$\mu_{2,OBM}^{P45}$	Polarisation Sensitivity $Q$ of the OBM (PMD45 Light Path)
$\mu_{3,OBM}^{P45}$	Polarisation Sensitivity $U$ of the OBM (PMD45 Light Path)
$\mu_{4,OBM}^{P45}$	Polarisation Sensitivity $V$ of the OBM (PMD45 Light Path)
$M_{1,OBM}^D$	Radiance Sensitivity of the OBM (Detector Light Path)
$M_{1,OBM}^P$	Radiance Sensitivity of the OBM (PMD Light Path)
$M_{1,OBM}^{P45}$	Radiance Sensitivity of the OBM (PMD45 Light Path)
$BSDF_{scaling}$	BSDF Ambient Scaling Factor
$BSDF_{slope}$	BSDF Slope Coefficients
$NDF$	Neutral Density Filter Transmission
$NDF_{sp}$	Neutral Density Filter Polarisation Sensitivity
$RM_{1,OBM}^{P,D}$	Ratio of polarisation sensitivities of PMD 1-6 and Detectors
$RM_{1,OBM}^{P45}$	Ratio of polarisation sensitivities of PMD45 and Detectors
$mf_{OBM}$	Residual m-factors for the OBM .
$n_j$	Refractive indices of the contamination layers.
$d_j$	Thickness of the contamination layers.

**Table 3.1.:** New Key Data.

The radiometric sensitivity is the  $M_1$  element and the polarisation sensitivity are the  $M_2/M_1$  and the  $M_3/M_1$  elements of the matrix  $M_{instr}$  calculated for the different instrument paths (see also Equation 3.2). The key data serve as direct input for equation 3.3 or are used to calculate the Mueller matrices for the different light paths. The Mueller Matrix for the complete light path is obtained by calculating the Mueller Matrix for all elements from the scanner to detector ( $M_{scanner}$ , see section 3.1.5.2) and insert the result into equation 3.3.

### 3.1.5.1. Generic Mueller Matrix and Contamination Layers

The Mueller Matrix of a given surface can be calculated as a function of the incidence angle  $\beta$ :

$$\underline{M}_{scanner}(\beta) = \begin{pmatrix} \frac{1}{2}(r_p^2 + r_s^2) & \frac{1}{2}(r_p^2 - r_s^2) & 0 & 0 \\ \frac{1}{2}(r_p^2 + r_s^2) & \frac{1}{2}(r_p^2 - r_s^2) & 0 & 0 \\ 0 & 0 & |r_p| \cdot |r_s| \cdot \cos \Delta & |r_p| \cdot |r_s| \cdot \sin \Delta \\ 0 & 0 & -|r_p| \cdot |r_s| \cdot \sin \Delta & |r_p| \cdot |r_s| \cdot \cos \Delta \end{pmatrix} \quad (3.4)$$

where  $\Delta = \arg(r_s) - \arg(r_p)$  is the phase jump. The complex refraction coefficients  $r_p$  and  $r_s$  for p- and s-polarised light are given by the Fresnel equations:

$$r_p = \frac{n_2 \cos \beta - n_1 \sqrt{1 - \left(\frac{n_1}{n_2} \sin \beta\right)^2}}{n_2 \cos \beta + n_1 \sqrt{1 - \left(\frac{n_1}{n_2} \sin \beta\right)^2}} \quad (3.5)$$

$$r_s = \frac{n_1 \cos \beta - n_2 \sqrt{1 - \left(\frac{n_1}{n_2} \sin \beta\right)^2}}{n_1 \cos \beta + n_2 \sqrt{1 - \left(\frac{n_1}{n_2} \sin \beta\right)^2}} \quad (3.6)$$

with  $n_1, n_2$  being the refractive indices of medium 1 and 2 (e.g. mirror surface and decontamination layer).  $r_p$  and  $r_s$  have to be calculated for each layer.

The rotation matrix for the polarisation coordinate frame over an arbitrary angle  $\gamma$  is given as

$$\underline{\mathfrak{R}}(\gamma) = \begin{pmatrix} 1 & 0 & 0 & 0 \\ 0 & \cos 2\gamma & \sin 2\gamma & 0 \\ 0 & -\sin 2\gamma & \cos 2\gamma & 0 \\ 0 & 0 & 0 & 1 \end{pmatrix} \quad (3.7)$$

For a surface of material  $j + 1$  with a layer medium  $j$ , the total reflectance  $R_{ij}$  to medium  $i$  becomes (see also Figure 3.2)

$$R_{ij} = \frac{r_{ij} + r_{j,j+1} \cdot e^{-2i\delta_j}}{1 + r_{ij} \cdot r_{j,j+1} \cdot e^{-2i\delta_j}} \quad (3.8)$$

using

$$\begin{aligned} \delta_j &= \frac{2\pi}{\lambda} \cdot d_j \cdot n_j \cos \phi_j \\ \cos \phi_j &= \sqrt{1 - \left(\frac{n_i}{n_j} \sin \beta\right)^2} \end{aligned} \quad (3.9)$$

Currently the scan mirror model uses two layers and the total reflectance of the system becomes (Index 1,2 and 3 represent ambient, contamination layer 1, and contamination layer 2, respectively)

$$R_t = \frac{r_{12} + R_{23} \cdot e^{-2i\delta_2}}{1 + r_{12} \cdot R_{23} \cdot e^{-2i\delta_2}}$$

where  $R_{23}$  is to be calculated using Equation 3.8.  $R_t$  replaces the reflectance coefficients in equation 3.4 and is valid for p- and s-polarised light when using equations 3.5 and 3.6 for  $r_{ij}$ . More details can be found in [31] and [10].

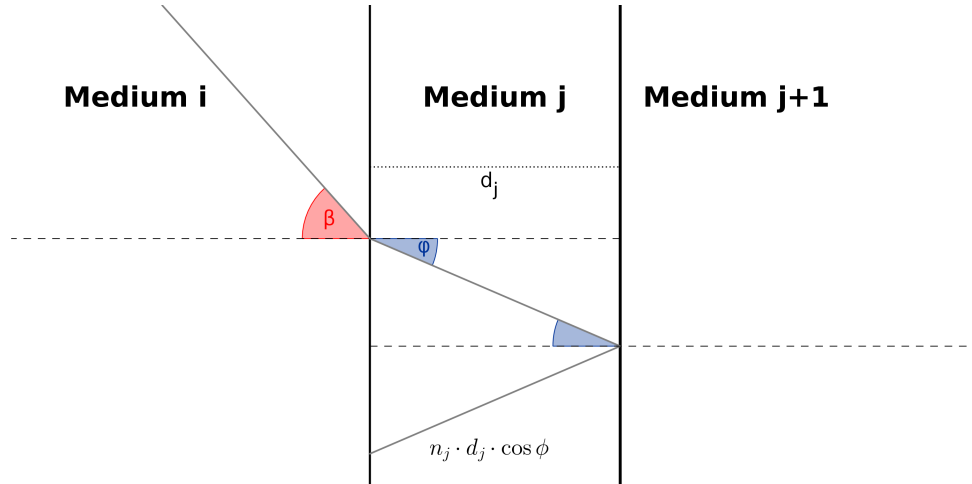


**Figure 3.2.:** Definitions for Equations 3.8 and 3.9. The light comes from medium  $i$ , goes through medium  $j$  and is reflected at surface  $j + 1$ .

### 3.1.5.2. Scanner Mueller Matrices

The total throughput is described by Eq. 3.3. In order to calculate the Mueller Matrix of the scanner  $\underline{M}_{scanner}$ , we have to go from the scan mirror coordinate frame to the polarisation coordinate frame. The formulae for the scanner matrices are given in the following according to the light path:

**Limb Path:** The matrix for light paths using the Limb configuration (no diffuser) is:

$$\underline{M}_{scanner}^{Limb}(\lambda_i, \alpha_{esm}, \alpha_{asm}) = \underline{\mathfrak{R}}(\gamma_{esm}) \times \underline{M}(\lambda_i, \beta_{esm}, n_i, d_i) \times \underline{\mathfrak{R}}(\gamma_{asm}) \times \underline{\mathfrak{R}}(\gamma_{asm}) \times \underline{M}(\lambda_i, \beta_{asm}, n_i, d_i) \times \underline{\mathfrak{R}}(\gamma_{asm}) \quad (3.10)$$

The incidence and rotation angles on the mirror can be calculated from the commanded angle  $\alpha$  and the incidence angle  $\beta$  as

$$\begin{aligned} \beta_{esm} &= -\alpha_{esm} \\ \gamma_{esm} &= 90^\circ \end{aligned}$$

for the elevation scan mirror and as

$$\begin{aligned} \beta_{asm} &= \arccos(\cos \alpha_{asn} \cdot \cos(2\alpha_{esm})) \\ \gamma_{asm} &= \arcsin(\cot \beta_{asm} \cdot \tan(2\beta_{esm})) \end{aligned}$$

for the azimuth scanner.

**Nadir Path:** The Mueller Matrix for the Nadir light path becomes

$$\underline{M}_{scanner}^{Nadir} = \underline{\mathfrak{R}}(\gamma_{esm}) \times \underline{M}(\beta_{esm}, n_i, d_i, \lambda_i) \times \underline{\mathfrak{R}}(\gamma_{esm}) \quad (3.11)$$

with the same conversion from incidence angle to commanded angle as for the Limb path.

**ESM Sun Diffuser Path:** The sun diffuser path contains the ESM diffuser on the back of the nadir mirror and the ASM mirror. For absolute irradiances we first calculate the a radiometric correction factor for the ESM diffuser for each wavelength using the key data  $BSDF_{scaling}$  and  $BSDF_{slope}$ , which were derived from in-flight and on-ground measurements [22]. The latter describes the slope of the ESM diffuser BPDF as a function of the changing solar zenith angle. It is parametrised as a 3<sup>rd</sup> degree polynomial in the key data for all wavelengths:

$$P_{BSDF_{slope}}(\lambda_i) = BSDF_{1,i}^{slope} + BSDF_{2,i}^{slope} \cdot \alpha_{delta} + BSDF_{3,i}^{slope} \cdot \alpha_{delta}^2$$

with  $\alpha_{delta} = \frac{SZA}{2} - 45^\circ$ . Together with the  $BSDF_{scaling}$  key data and some additional scaling, the radiometric correction factor for the diffuser becomes

$$M_1^{BSDF}(\lambda_i) = (1 + 0.07 \cdot \alpha_{delta}) / BSDF_{scaling}(\lambda_i) \cdot P_{BSDF_{slope}}(\lambda_i)$$

For the whole light path, the Mueller Matrix becomes

$$\underline{M}_{scanner}^{BSDF} = (\underline{M}(n_{i,diff}, d_{diff}, \alpha_{delta}, \lambda_i) \times \underline{M}(n_{i,ASM}, d_{ASM}, \beta_{ASM}, \lambda_i)) \cdot M_1^{BSDF} \quad (3.12)$$

**NDF Mueller Matrix** The Mueller Matrix for the NDF can be calculated as follows

$$M_{NDF} = \frac{1}{2} \cdot \begin{pmatrix} p_x + p_y & p_x - p_y & 0 & 0 \\ p_x - p_y & p_x + p_y & 0 & 0 \\ 0 & 0 & p \cdot p_y & 0 \\ 0 & 0 & 0 & p_x \cdot p_y \end{pmatrix} \quad (3.13)$$

using  $p_x$  and  $p_y$  calculated from the NDF key data

$$p_x = \frac{2 \cdot NDF}{(1 + NDF_{sp}) + \left(\frac{M_2}{M_1}\right)_{OBM} \cdot (1 - NDF_{sp})}$$

$$p_y = NDF_{sp} \cdot p_x$$

### 3.1.6. Calculation of errors on Mueller matrix elements

The errors on the level 1b product will be given as relative errors. The formulae presented below denote absolute errors on parameters; these have to be divided by the parameter value in order to obtain relative errors.

Whereas the new scan mirror model solves several issues that existed with the old formulation of the keydata, the model does not [yet] provide an error estimate. For the time being, the level 0-1b processor still uses the old keydata to provide error estimates on accuracy (not precision!) of (ir)radiance and polarisation.

#### 3.1.6.1. Errors for radiance response parameters

The basic assumption is made that the errors are equal for all scan angles. A further assumption is that the error made in the calibration at one scan angle is independent of the calibration error at another scan angle.

The Mueller matrix elements for absolute (ir)radiance response had the form:

$$M_1^{i,\alpha} = ABS\_RAD_i \cdot \frac{OBM_{s\_p_i} \cdot X_{s_i,\alpha} + X_{p_i,\alpha}}{OBM_{s\_p_i} \cdot ELEV_{s_i,\alpha_0} + ELEV_{p_i,\alpha_0}}$$

where  $X$  stands for  $ELEV$  in Nadir, for  $EL\_AZ$  in Limb, and for  $BPDF$  in Sun+diffuser measurement mode. As usual, the assumption is made that the errors are equal for all scan angles.

Denote

$$X_{0,i} = OBM_{s\_p} \cdot X_{s_{i,\alpha_0}} \cdot X_{p_{i,\alpha_0}}$$

for each pixel  $i$ , then the error propagation law gives for the error on the (ir)radiance response:

$$(\epsilon_{M_{1,X}^2})_i = \frac{1}{ELEV_{i,\alpha_0}^2} \cdot \left( [X_{0,i} \cdot \epsilon_{ABS\_RAD_i}]^2 + [ABS\_RAD_i \cdot \epsilon_{X_i}]^2 + \left[ \frac{X_{0,i} \cdot ABS\_RAD_i}{ELEV_{i,\alpha_0}} \cdot \epsilon_{ELEV_i} \right]^2 \right) \quad (3.14)$$

where

$$\epsilon_{X_i^2} = (X_{0,i} \cdot \epsilon_{OBM_{s\_p_i}})^2 + (OBM_{s\_p_i} \cdot \epsilon_{X_{s_i}})^2 + \epsilon_{X_{p_i}}^2$$

where the  $\epsilon_{<xx>}$  are the errors from the Key Data file, interpolated to the SMR wavelength of detector pixel  $i$ ;  $\epsilon_{ABS\_RAD_i}$  is additionally scaled with the conversion factor from W/sr.cm<sup>3</sup> to photons/s.cm<sup>2</sup>.sr.nm.

The error on the BSDF relevant to sun-normalised radiances (reflectance) is the error on the ratio  $M_1^{irrad}/M_1$ . Using the same notation as above with  $\epsilon_{X_i}$  calculated as above for  $BSDF$ , the relevant error is given by:

$$\epsilon_{BSDF_i^2} = \left( \frac{1}{EL\_AZ_{i,\alpha_0}} \right)^2 \cdot \left( \left[ \frac{BSDF_{i,\alpha_0}}{EL\_AZ_{i,\alpha_0}} \cdot \epsilon_{EL\_AZ_i} \right]^2 + \epsilon_{X_i^2} \right) \quad (3.15)$$

where  $EL\_AZ_{i,\alpha_0}$  and  $BSDF_{i,\alpha_0}$  are calculated similar to  $ELEV_{i,\alpha_0}$  above.

### 3.1.6.2. Errors for polarisation sensitivity parameters

The errors on ratios of Mueller matrix elements which refer to the detector arrays (variables with superscript  $D$ ) are to be calculated for each pixel  $i$ . The errors on the 'Greek Key data' on the Calibration Key Data file are given independent of scan angle. These errors will only be used by the calculation of the polarisation correction factor in Level 1b to Level 1c processing; they are written to the Level 1b product:

$$\begin{aligned} \epsilon_{\mu_{2,i}^D} &= \frac{2 \cdot \eta}{(1 + \eta)^2} \cdot \epsilon_{\eta} \\ \epsilon_{\mu_{3,i}^D} &= \frac{2 \cdot \zeta}{(1 + \zeta)^2} \cdot \epsilon_{\zeta} \end{aligned} \quad (3.16)$$

The ratios of Mueller matrix elements for the PMDs are used only in the retrieval of the Stokes fractions  $Q$  and  $U$ ; the errors of these matrix elements will be used in the error calculation of the Stokes parameters. It is very difficult to make a really clean error estimate for these matrix elements, for several reasons.

One of the reasons is that these ratios use a combination of 'Greek' key data, but these key data are often based on one and the same calibration measurement. Hence the errors on the key data are strongly correlated. If one works out the expressions for the Muller matrix ratios in terms of basic calibration measurements, one will discover that several measurements included in separate 'Greek' key data in fact fall out of the equation, and the error component of these measurements which is included in the 'Greek' key data error should not be taken into account. A further complication is that even for the basic calibration measurements the errors are correlated, since the major error component is not due to measurement 'noise' but to systematic errors sources (e.g. residual polarisation) in the calibration set-up.

Note further that for the retrieval of the Stokes fractions (see the Equation for the 'PMD virtual sum' in Section 3.13) some ratios of Mueller matrix elements always appear multiplied with another one, e.g.  $\mu_2^P$  is always multiplied with  $M_1^P/M_1^D$ . In the following we will for the error on the latter assume that the errors on its

constituting ‘Greek’ key data can be regarded as being independent; for  $\mu_2^P$  and  $\mu_3^P$  we take into account the error on their physically most significant ‘Greek’ component and regard the others as error-free multiplication factors (whose error is already counted in the error on  $M_1^P/M_1^D$ ). A more lengthy justification for the approach, taking into account the basic calibration measurements from which the ‘Greek’ key data are derived, can be found in [56].

In principle the error calculation is to be done for all pixels contained in the PMD bandwidth. However, since the error estimate is rather coarse anyway, and since also the error on the Stokes fractions will be estimated using some simplifying assumptions, it is sufficient to come up with one representative value for each PMD. This is done by calculating the errors for each of a dozen central pixels in the PMD response curve (current default is 11 pixels for PMDs A-D, 45 and 17 pixels for PMDs E,F) .

For each of these central pixels,  $ip$ , the errors are estimated as:

$$\begin{aligned} \epsilon_{-\left(\frac{M_1^P}{M_1^D}\right)_{ip}} &= \left(\frac{1}{1+\eta}\right) \cdot \left(\left[\frac{\xi}{1+\eta} \cdot \epsilon_{-\eta}\right]^2 + \epsilon_{-\xi}^2 + [\eta \cdot \epsilon_{-\kappa}]^2\right)^{\frac{1}{2}} \\ \epsilon_{-\mu_{2,ip}^P} &= 2 \cdot \frac{\eta}{\xi} \cdot \epsilon_{-\kappa} \\ \epsilon_{-\mu_{3,ip}^P} &= 2 \cdot \frac{1+\eta}{\xi} \cdot \epsilon_{-\omega} \end{aligned} \quad (3.17)$$

where for typographical clarity the indices  $ip$  have been omitted from the ‘Greek’ key data.

For the matrix elements involved on the calculation of PMD-450 the same formulae hold, but replace  $(\xi, \kappa, \omega)$  by  $(\tau, \psi, \sigma)$ .

For each PMD, the errors for each ratio of Mueller matrix elements are averaged over the pixels  $ip$ , with the exclusion of bad pixels (as indicated by the bad pixel mask), to obtain one typical error estimate per PMD.

## 3.2. Calculate Geolocation and Synchronise PMDs

The algorithms described in this section calculate a number of quantities which have in common that they all rely on basic instrument data such as raw timing data or raw scan mirror decoder position.

The first task is therefore to convert raw timer data to UTC (Universal Time Co-ordinate) time. Once this is achieved, the PMD data can be synchronised with the channel readout, and the Orbit Propagator software (supplied by ESA) can be used to retrieve the geolocation. Auxiliary quantities such as orbit phase and SAA location are calculated.

For those readers less interested in this low-level instrument stuff: this section also provides a definition of the viewing geometry and a description of the geolocation format on the Level 1b product (see part on calculation of the geolocation).

### 3.2.1. Determine integration time grid

The retrieval of the integration time grid starts with the extraction of the Broadcast Pulse Signals (BCPS) from the data packet, and the extraction of the Delta Time values of the PMD data packets (this is the time between the BCPS and the PMD SYNC). There are in fact several BCPSs:

1. (a) for the last detector module electronics (DME) readout or the end of the integration time of the channel,
2. (b) for the time at which the encoder counter and scanner control error data was read (on the Auxiliary Data Packet),
3. (c) for the time after which the PMD data was assembled in the Measurement Data Interface (MDI) (on the PMD Data Packet).

The next step is the transformation of the instrument control unit (ICU) time, as given in the data packets time, or the satellite binary time (SBT) into the Universal Time Co-ordinate (UTC) time given in the Modified Julian Date (MJD) format and into days. The conversion to MJD is done by use of an ESA-supplied routine (CFI routine) 'pl\_sbtutc' described in [41]. The conversion to days is straightforward. Note that ICU and SBT time are physically different, but synchronised clocks.

To link the BCPS time to the ICU time one has to take account of delay times in the State start-up for the channel data, and of PMD readout time and filter time delay for the PMD data. The UTC time of an arbitrary BCPS may be calculated as follows [44]:

$$t_{BCPS}(n) = t_{ICU} + \Delta t_{start} + n_{BCPS} \cdot 62.5 \text{ ms} \quad (3.18)$$

where:

$t_{ICU}$  is the UTC time [days] in the corresponding data packet

$n_{BCPS}$  is the counter of an arbitrary BCPS

$t_{start}$  is a combination of two delay times after the start of the state:

$$\Delta t_{start} = \Delta t_{ICU} + \Delta t_{start\_BCPS}$$

where:

$\Delta t_{ICU}$  is a delay between the start of the BCPS relative to the command to start it which is a characteristic of the ICU H/W. This delay time was measured to be 90.625 ms.

$\Delta t_{start\_BCPS}$  is a delay based on the commanding defined in the state's RTCS. Due to the fact that different states required a different RTCS each state may have its own delay time. The delay times are taken from [44] as the "ICU-OBT" plus the response time of the Reticon detectors to the leading edge of the BCPS.

The UTC time of an arbitrary PMD measurement may be calculated as follows [44]:

$$t_{PMD} = t_{BCPS} + \Delta t_{PMD} \cdot 2\mu s - 12.5 \text{ ms} + T_{PMDdelay} - T_{filter} \quad (3.19)$$

where:

$t_{BCPS}$  is the UTC time [days] of the BCPS counter given in the PMD Data frame

$\Delta t_{PMD}$  is the Delta Time counter in the PMD Data frame

$T_{PMDdelay}$  is an increasing delay time for each PMD readout; this value is calculated from

$$T_{PMDdelay} = 1.999 + m \cdot 0.5 \text{ ms}$$

where

$m$  is a counter for the sequential PMD readout; this counter runs from 0 for PMD-A amplifier A, via 1 for PMD-A amplifier B, to 12 for PMD-45o amplifier A, and 13 for PMD-45° amplifier B.

$T_{filter}$  is an 'analogue delay' introduced by a low pass filter; due to the relaxation (averaging) in the filter, the moment which corresponds to maximum information of the current measurement appears with a time lag after the current measurement. The filter is a 3rd order Butterworth filter having a cut-off frequency of  $\approx 20$  Hz (data by Fokker Space at SSAG meeting Feb.2, 1998). The corresponding 'analogue delay' value is taken from [44] it's value lies around 14 ms. However, the corresponding parameter on the initialisation file has been set to a larger value. This has been done to synchronise the PMDs with the approximate wavelength centre of the PMD bandwidth on the Reticon (UV-VIS) detectors, where detector pixel  $i$  is read out  $i \cdot 0.028$  ms ms after the BCPS.

### 3.2.2. Integrated PMD values

The PMD time-tagging performed above brings the PMD data stream and the channel detector data stream to a synchronised time grid. What is really needed for the polarisation correction algorithm, is the ratio of channel detector signal to a PMD signal which is integrated over the same detector exposure time. In the Level 0 to 1b processor we perform this integration time in two steps. First the PMD values are integrated over time intervals of 1/32 seconds (half the minimum channel integration time) synchronised with the channel detector (DME) BCPS. Then these '**PMD integrals**' need only be added later to obtain the PMD signal integrated over the actual exposure time of the cluster which is used for the calculation of polarisation parameters.

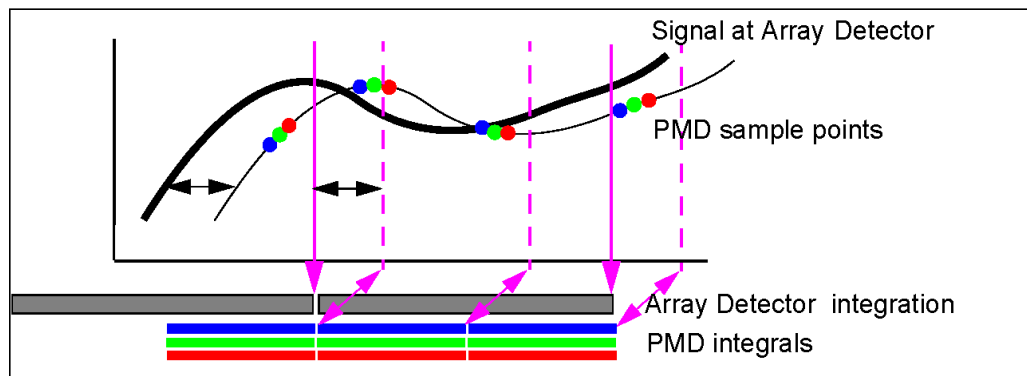


**Figure 3.3.:** Conversion from sampled PMD points to PMD integrals. The thin line represents the delayed signal after filtering.

The synchronised PMD integrals are also written to the Level 1b product, where they are useful for e.g. cloud recognition purposes in the Level 1b to 2 processing. Although the PMD integrals probably contain all the information one would usually need, the original PMD data stream is copied to the Level 1b product as well (as annotation data).

For each PMD two read-out values (value A and B) are given for one measurement. Value A is the output of the first amplifier stage (low gain), value B the output of the second amplifier stage (high gain) in the PMD electronics. Therefore, the two read-outs correspond to different gain factors and unfortunately have different offsets.

Primarily the PMD signals shall be taken from amplifier stage B. Whenever the signal read-out of amplifier stage B is saturated ( $S_{PMD} > pmd\_saturataion\_limit$ , currently set to 50000 BU), the signal value shall be taken from amplifier stage A, and then converted to the signal value that would have been measured by B without saturation. This is done as follows:

$$S_{PMD}(B) = \frac{C_A}{C_B} \cdot (S_{PMD}(A) - PO_A) + PO_B \quad (3.20)$$

where  $C_A = 1$  and  $C_B \approx 24.7$  are the gain factors (given on the initialisation file) and  $PO_A$  and  $PO_B$  are the different PMD-offsets (taken from the calibration data).

In case the amplifier stage B is used directly (i.e. not derived from stage A) a correction for cross-talk is necessary [59]. The PMD stage B signals are influenced by the stage A signals of the previous PMD, except for the first PMD (PMD-A) which is influenced by stage B of the PMD-45 in the previous readout, and except for PMD-45 which is not affected by crosstalk. The behaviour of the cross-talk depends on the signal level of the PMD which causes the cross-talk. The following corrections are applied on PMD signals after subtraction of the offset ( $A, B$  denotes amplifier stage,  $k$  denotes a measurement counter,  $X$  denotes the PMD number in sequence A-F,45, all other constants are from key data PMD\_CROSS\_COEF):

$$\begin{cases} S_{PMD,X}(k, B) = S_{PMD,X}(k, B) - a_1 \cdot S_{PMD,X-1}(k, A) & \text{for } S_{PMD,X-1}(k, A) \leq f_1 \\ S_{PMD,X}(k, B) = S_{PMD,X}(k, B) - b_0 & \text{for } f_1 < S_{PMD,X-1}(k, A) \leq f_2 \\ S_{PMD,X}(k, B) = S_{PMD,X}(k, B) - c_0 - c_1 \cdot S_{PMD,X-1}(k, A) & \text{for } S_{PMD,X-1}(k, A) > f_2 \end{cases} \quad (3.21)$$

where  $S_{PMD,X}(k, B)$  is calculated for  $X = B - F$ ; for  $X = A$  use above formulas but replace  $S_{PMD,X-1}(k, A)$  by  $S_{PMD,45}(k - 1, B)$ .

After above correction, the offsets are added again to the PMD signals (because calibration for offset appears elsewhere in the processor).

For each 31.25 ms (half the time of a BCPS duration) in the State being processed a set of integrated PMD values will be calculated as follows, using the corrected PMD signals of stage B:

$$I_{PMD} = \int_{t_{start}}^{t_{end}} 40 \cdot S_{PMD}(t_{PMD}) dt \quad (3.22)$$

For this integral, the PMD signal in BU is interpreted like a number of photons which would have been measured in an integration time of 1/40 second ('integration' instead of 'sampling') - hence the function to be integrated has at each time  $t_{PMD}$  a value of  $40 \cdot S_{PMD}$  (this value integrated over 1/40 second would yield  $S_{PMD}$ )

The start and the end time of these integrals shall be synchronised to the BCPSs given in the detector data packets, as follows:

$$t_{end} = t_{BCPS(n)} \text{ (at BCPS readout) or } t_{end} = (t_{BCPS(n)} + t_{BCPS(n+1)})/2 \text{ (in-between BCPS readout) and } t_{start} = t_{end} - 31.25 \text{ ms.}$$

This integral is numerically calculated using quadratic interpolation and Simpson integration, taking into account the precise time stamps ( $t_{PMD}$ ) of the used PMD measurements (e.g. time is different for stage A and stage B of the same PMD!).

Note that for a constant PMD signal we thus get:  $I_{PMD} = 40/32 \cdot S_{PMD}$  where the unit of the integral is again in [BU] (because it is [BU/s]\*s).

### 3.2.3. Extract Line of Sight

The instantaneous line of sight (ILOS) is obtained by converting the instrument's Scanner decoder positions to scan angles in the coordinate frame used by ESA's Orbit Propagator. These scan angles can then later be used to calculate the Geolocation.

The co-ordinate system which is required for ESA's CFI routines on input is the Satellite Relative Actual Reference CS. It is the co-ordinate system that constitutes the reference for the definition of a look direction relative to the satellite to express the pointing of an instrument. The co-ordinate system is defined as follows:

- the ( $-z$ )-axis points vertically downwards to approximately Nadir,
- the ( $-y$ )-axis points approximately into the flight direction and
- the  $x$ -axis is added according to a right-handed co-ordinate system (Eastward direction on the descending part of the orbit).

The parameters that define a direction in the Satellite Relative Actual Reference co-ordinate system are the satellite related **azimuth**  $\theta_{Az}$  and the satellite related **elevation**  $\theta_{Ele}$  which are defined as follows:

- the azimuth is given in the (x-y)-plane starting from the negative y-axis in clockwise direction
- the elevation is the angle out of the (x-y)-plane to the negative z-axis.

For SCIAMACHY observations this implies that the elevation is always counted positive; on the descending part of the orbit (the 'illuminated side' of Earth) Westward is indicated by positive Azimuth angles from 0° onwards, and Eastward is indicated by Azimuth angles up to 360°. On basis of this reference co-ordinate system the ILOS may be retrieved with the following three steps:

### 3.2.3.1. Extraction of scan mirror positions

There are several pieces of information in the Scanner Position Data frame which may provide input to the scanner position retrieval, but only the AZIMUTH ENCODER COUNTER ( $n_{azi}$ ) and the ELEVATION ENCODER COUNTER ( $n_{elev}$ ) entries on the level 0 product are used for this purpose. All other entries just provide diagnostics information about scanner operation which shall not be used for scanner position retrieval. The formulas to calculate the angular position of an individual scan mirror in degree is given as follows:

- for the ASM:  $\alpha_{ASM} = n_{azi} \cdot \frac{360}{64000} + ASM\_offset$
- for the ESM:  $\alpha_{ESM} = n_{elev} \cdot \frac{360}{64000} + ESM\_offset$

The offsets in the formula above are provided on the initialisation file. There are two sets, depending on which instrument side is used. If the CONFIGURATION\_ID on the level 0 product is an odd number, then instrument side A is used, else instrument side B.

The scan mirror positions are defined as follows (see Figure 3.4 and Figure 3.5 for illustration):

- the position when the elevation mirror is looking directly back into the instrument is defined to be zero
- the position when the azimuth mirror is looking back into the direction of the elevation mirror is defined to be zero
- the angles are running counter clockwise from 0° to 360°.

Note that in various instrument documentation sources the angles of scan mirrors appear negative which would be undefined according to the definition above. This describes angles running clockwise from the zero position.

#### Patch for missing scan mirror position update

Due to a rare synchronisation error, it happens occasionally that a scanner position readout is not updated, i.e.  $n_x(i+1) = n_x(i)$  ( $x = azi$  or  $elev$ ), although the scanner itself has moved. A correction is made for the scanning measurements in Nadir with Measurement Category = 1, and scanning measurements in Limb with Measurement Category = 2. The correction algorithm uses the fact that the scan pattern repeats itself after  $n\_repeat$  BCPS with  $n\_repeat = 80$  for ESM Nadir and  $n\_repeat = 54$  for ASM Limb.

The correction is done as follows:

find  $i$  where  $n_x(i+1) = n_x(i)$  ( $x = azi$  or  $elev$ )

if  $i > n\_repeat$  then  $n_x(i+1) = n_x(i+1 - n\_repeat)$  else  $n_x(i+1) = n_x(i+1 + n\_repeat)$

Only measurements modes with fully repetitive scan mirror movement can be corrected this way. No correction is made for measurements other than nadir and limb scanning. In Limb, only the ASM is corrected (ESM movements during the scan are negligible, ESM movement to the next tangent height is in the middle of the 3 BCPS readout which is not transmitted). For the Limb dark measurements (the last 27 BCPS) this correction is not done, because the ASM mirror is in a fixed position.

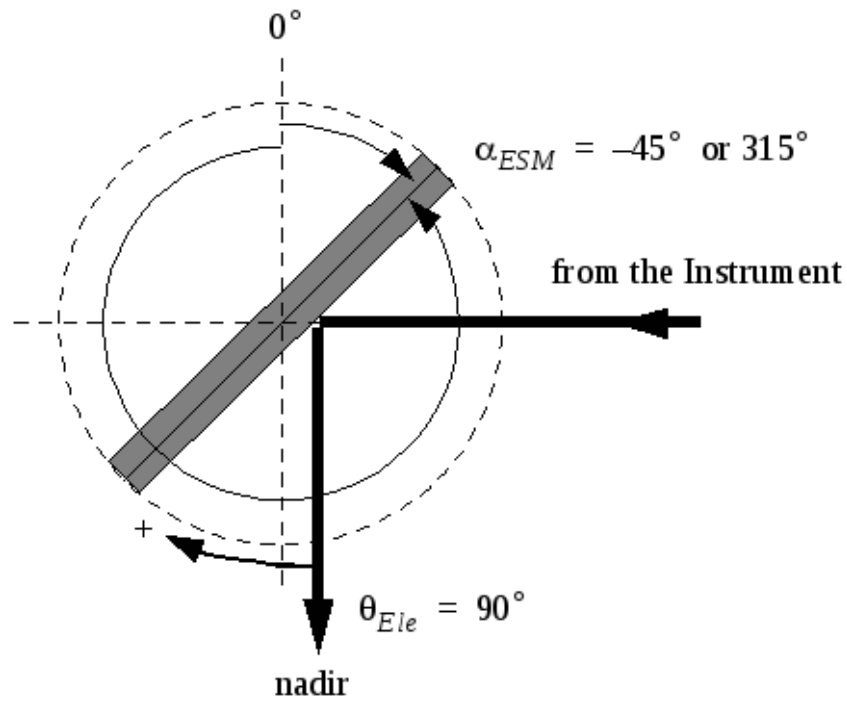


Figure 3.4.: Definition of angles at the elevation mirror for Nadir measurements.

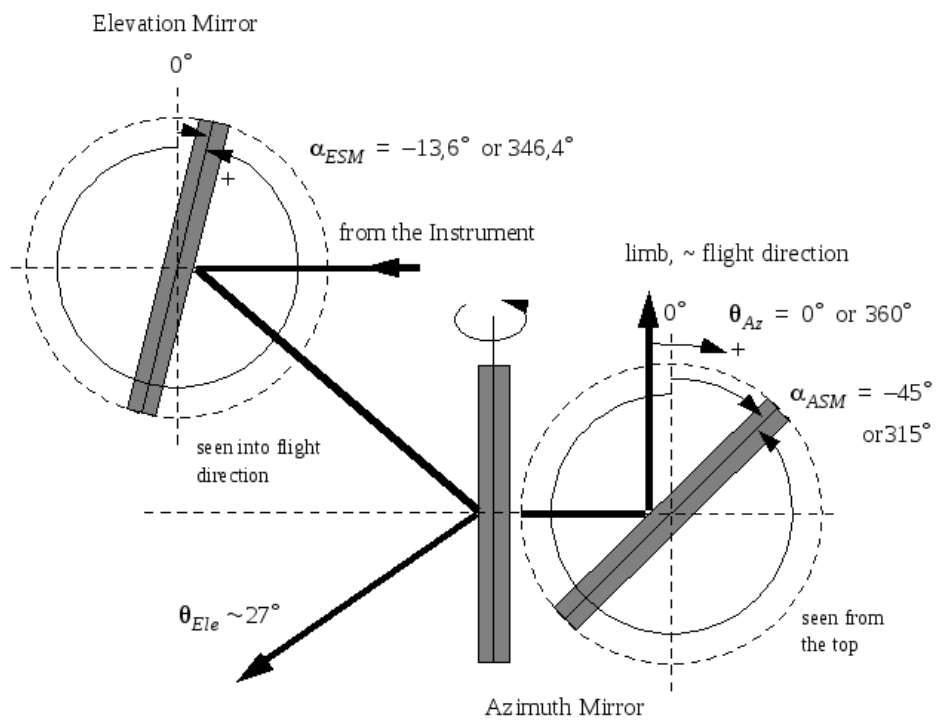


Figure 3.5.: Definition of angles at the elevation and azimuth mirror for Limb/Occultation measurements.

### 3.2.3.2. Calculation of the effective scan angle

The effective scan angle describes the viewing direction, running clockwise, with respect to the default Nadir (for the ESM) or default Limb (for the ASM) viewing directions. The effective scan angles given in the optical zero reference frame may be calculated as follows:

- for the ASM:

$$\psi_{eff} = -2 \cdot (\alpha_{ASM} - \alpha_{asm,0}) \quad (3.23)$$

- for the ESM:

$$\phi_{eff} = +2 \cdot (\alpha_{ESM} - \alpha_{ESM,0}) \quad (3.24)$$

where  $\alpha_{ASM,0}$  and  $\alpha_{ESM,0}$  (both  $\approx 315^\circ$  [or  $-45^\circ$ ]) are zero offsets determined during alignment.

### 3.2.3.3. Conversion to the ILOS angles at Satellite

The effective scan angles may be transformed to the ILOS angles in the Satellite Relative Actual Reference CS as follows:

$$\theta_{Ele} = \begin{cases} 90^\circ - \phi_{eff} & \text{if } \phi_{eff} \geq 0^\circ \\ 90^\circ + \phi_{eff} & \text{if } \phi_{eff} < 0^\circ \end{cases} \quad (3.25)$$

$$\theta_{Az} = \begin{cases} \psi_{eff} & \text{if } \psi_{eff} \geq 0^\circ \\ 360^\circ + \psi_{eff} & \text{if } \psi_{eff} < 0^\circ \end{cases} \quad (3.26)$$

For Nadir, the definition of viewing Azimuth is independent of the Azimuth Scanner:

$$\theta_{Az} = \begin{cases} 90^\circ & \text{if } \phi_{eff} > 0^\circ \\ 270^\circ & \text{if } \phi_{eff} < 0^\circ \end{cases} \quad (3.27)$$

For  $\phi_{eff} = 0^\circ$  the azimuth is not defined. In this case it shall be set to  $\theta_{Az} = 0^\circ$ .

Note that on the Level 1b product, the geolocation record contains viewing zenith angles (not elevation angles). These are defined by  $\phi_{eff}$  in Equation 3.24. The quantity  $\theta_{Ele}$  is used only for the Orbit Propagator (see below).

Note: the quality check for the allowed angle ranges in the observational modes, which was done in an earlier version of the software, has been removed to allow unlimited use of dark calibration measurements in an observational state.

### 3.2.4. Calculate geolocation

The geolocation parameters which are determined are the following:

- precise date & time at the beginning of the ground pixel
- solar zenith and azimuth angles (possibly more than one set per ground pixel)
- line-of-sight zenith and azimuth angles (possibly more than one set per ground pixel)
- satellite height and earth radius (geoid)
- the sub-satellite point

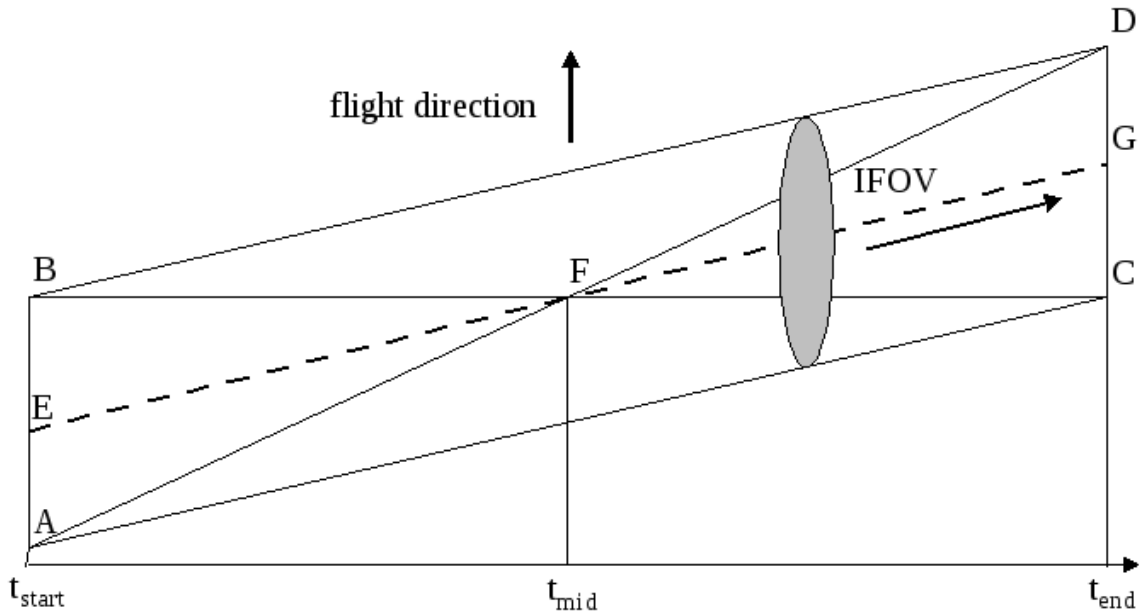


**Figure 3.6.:** Definition of footprint points A-D and ILOS points E-G for Nadir scan pattern.

The geolocation information is calculated in granules of the shortest integration time in the present State. Geolocation information for clusters with larger integration times have to be constructed out of the corresponding sets of geolocation information for the shortest integration time.

For Nadir, the geolocation parameters are given for the footprint on the ground as defined by Figure 3.6. Geographical coordinates (lon,lat) will be given for the 4 corner points A-D and the centre point F. Zenith and azimuth angles are given for points E, F, G. Here the solar angles are calculated at the TOA height.

For Limb and Occultation measurements, tangent height (geoid) and geographical coordinates of the tangent will be given for the start, middle and end of the exposure time (equivalent to points E, F, G in Nadir). Corresponding viewing and solar zenith/azimuth angles will be given at TOA.

For all other measurement modes (calibration and monitoring) only the geographical coordinates for the centre sub-satellite position, and the solar angles for the start, middle and end of the exposure time will be given.

Please note that for the Limb and Occultation modes, the accuracy of the tangent height due to the pointing error of the spacecraft may be limited to  $\approx 2$  km. In off-line processing mode (not NRT) this can be improved by an order of magnitude by using star tracker information, via the AUX\_FRA auxiliary input file. See also Sect. 4.

Note further that the shortest integration times in the Nadir and Limb States are always such that it never occurs that the scan mirror changes direction during the integration; therefore the extremes of the footprint can be calculated from the start and end of the integration time (no wrap-around).

The geolocation parameters are derived from ESA's Orbit propagator, using as input the orbit state vector, the UTC time of the measurement points, and the viewing angles. The integration time IT and the UTC time at the end of the measurement tend (corresponding to point G) are given on the data packet. The UTC times at the middle of the integration time ( $t_{mid}$ , corresponding to point F) and at the start of the integration time ( $t_{start}$ , corresponding to point E) are given by:

$$\begin{aligned} t_{start} &= t_{end} - IT \\ t_{mid} &= t_{end} - IT/2 \end{aligned}$$

For each of these times the corresponding azimuth and elevation angle shall be selected. For the middle time these will not be available if the integration time is 62.5 ms (the BCPS period). A linear interpolation (of

the azimuth and elevation angle) between the start and end is done in this case. This is legal, because the scanners are moving with constant speed.

The angles for the 4 corner co-ordinates A-D of a Nadir measurement cannot be taken directly, but have to be calculated from the IFOV dimensions as follows. First the angles are calculated at satellite, for the conversion to TOA see the paragraph on the next page. The angles at satellite are:

$$\theta_{Ele} = \arcsin(\cos \phi_{eff} \cdot \cos \delta) \quad (3.28)$$

$$\theta_{Az} = \begin{cases} 90^\circ & \text{if } \phi_{eff} > 0^\circ \text{ and } \delta = 0 \\ 270^\circ & \text{if } \phi_{eff} < 0^\circ \text{ and } \delta = 0 \\ \arctan\left(\frac{\sin \phi_{eff} \cdot \cos \delta}{\sin \delta}\right) & \text{otherwise} \end{cases} \quad (3.29)$$

where  $\delta$  designates the offset angle from the centre of the IFOV:

$\delta = +IFOV/2$  for points A, C ;  $\delta = -IFOV/2$  for points B, D ;  $\delta = 0$  for E, F, G.

and  $\phi_{eff}$  is the effective scan angle. The value of IFOV is the average value of the IFOV of all channels (small deviations between channels are possible due to detector misalignment errors, but these are not taken into account for the geolocation):  $IFOV \approx 1.8^\circ$ .

For Limb, the scan is in the direction of the length of the slit. The extreme ends of the field of view are also here obtained by adding  $IFOV/2$  to the azimuth angles at start and end of the integration time. But because these extremes are only exposed to light for a short time (the edge turns directly away when starting the scanning), in contrast to e.g. the centre of the scan (where light enters during the full scanning over the slit length), this extreme is not very meaningful. The points with 50% of the effective exposure time for each 'air column' lie in fact at the centre of the IFOV at the start and end of the scan. Hence we directly take these points as the effective boundaries of the scan, without further correction.

The timing of the Limb scan is such, that the actual measurement scan starts after 3 BCPSs. In-between each tangent height, a gap of 2 BCPSs exists in which the ASM scan mirror reverses direction and the ESM is positioned at the next tangent height. The last 1.5 sec of the state are used for taking a dark spectrum. The first 3 BCPSs, the 2 BCPS gaps, and the last 1.5 sec are not included in the geolocation on the Level 1b product.

### 3.2.5. Conversion to TOA angles

The solar angles and viewing angles in Nadir, Limb, and Occultation are converted from angles at satellite to angles at the top of the atmosphere (TOA). The TOA height is a parameter from the initialisation file; currently set to 100 km above the geoid (in seldom cases, the measurement tangent height in Limb/Occultation may be above 100 km; in this case we replace the value by tangent height + 1m). The conversion is done using ESA's Orbit Propagator. Input to the Propagator are the  $\theta_{Ele}$  and  $\theta_{Az}$  calculated above. Output for the Level 1b product are the Zenith angles (not elevation angles !) and the Azimuth angles at TOA. Solar azimuth is taken from output field [66], solar zenith angles are calculated as  $90^\circ - [67]$ . Line-of-sight azimuth is calculated as  $180^\circ + [8]$ , LOS zenith angles are calculated as  $90^\circ - [9]$ . The propagator is called with mode=1 (target determined by viewing angle and height), except for solar angles in Limb/Occultation with mode=7 (target at tangent point determined by viewing angle). The propagator output fields are following: [8]=target to satellite azimuth (topocentric CS, 0 to 360); [9]=target to satellite elevation (topocentric CS, -90 to +90); [66]=target to Sun (centre) azimuth (topocentric CS, 0 to 360), [67]=target to Sun (centre) elevation (topocentric CS, -90 to +90).

Note:

- The azimuth angle is defined w.r.t. North
- The orientation of azimuth is from +Y to +X (X,Y as in Figure 3.1)

- The angles are calculated at the intersection point of the line-of-sight from the spacecraft with a layer height of  $h=h(\text{TOA})$  above the WGS84 ellipsoid

For Limb and Occultation, this orientation is the same as for  $\theta_{Az}$  in Figure 3.5 on page 39, but the zero point is different (For forward Limb direction, the difference on the descending part of the orbit is  $\approx 170^\circ$ ).

SCIAMACHY has a small misalignment w.r.t the ENVISAT spacecraft. In the call to the Orbit Propagator, we pretend that the misalignment of SCIAMACHY is equivalent to an attitude offset of the spacecraft (this is not always true and must then be corrected again, see below). We subtract a value of 0.227460 from attitude input parameter `att[2]`, which is based on an on-ground misalignment determination. In addition, we add to `att` the small extra pitch, yaw, and roll misalignments from in-flight measurements as given by [20].

### 3.2.6. Calculate Doppler shift

For Limb, Occultation, and Solar measurements, the instrument is looking more or less in the direction of the flight direction. This implies that the spectra which are recorded will be Doppler-shifted. For Nadir measurements the FOV is perpendicular to the flight direction and no Doppler-shift is present. It is the policy that on the Level 1b product all data are calibrated as measured by the instrument without geophysical interpretation, i.e. spectral calibration is given in the instrument rest frame. Hence the Doppler-shift is no issue for level 0 to 1b processing, but it will be needed for matching measured spectra to reference spectra in level 1b to 2 processing.

Since the Doppler-shift varies linearly with wavelength, it is sufficient to specify on the Level 1b product the Doppler-shift at one wavelength, for which 500 nm is chosen. The Doppler-shift depends on spacecraft velocity and viewing angles in elevation and azimuth; expressed in units of nm the shift is given by (velocities given in units of m/s):

$$D_{500nm} = 1.66782 \cdot 10^{-6} \cdot \sqrt{\dot{x}^2 + \dot{y}^2 + \dot{z}^2} \cdot \cos \theta_{Az} \cdot \cos \theta_{elev} \quad (3.30)$$

For Limb/Occultation the angles are given for the centre position in the geolocation (based on the shortest integration time in the State). For the Solar Reference spectra the angles are taken as the average angles of the State; the variation of the Doppler-shift over these States is below 2%. For solar States when a diffuser is used, replace in above Equation the viewing elevation angle by Solar Elevation angle, and the viewing azimuth angle by Solar Azimuth angle. As the solar angle should be measured here w.r.t. the spacecraft direction, and not w.r.t. the SCIAMACHY viewing direction, we must undo here the SCIAMACHY misalignment correction discussed above (which was falsely, though conveniently, interpreted as spacecraft misalignment in the call to the orbit propagator). A value of 0.227460 is therefore added to the calculated Solar Azimuth angle before using Eq. 3.30.

Note that the spectrum recorded on the detector will be blue-shifted, i.e. a positive amount of shift has to be added to convert from Level 1b wavelengths to atmospheric/solar wavelengths.

### 3.2.7. Determine SAA region

The SAA region will be specified as a rectangular region in longitude and latitude. The SAA will be a 'zone of avoidance' for calibration measurements. If one of the data packets of the calibration measurements are within this region, the whole state will be skipped for calibration processing. In the Level 0 to 1b processing context, the SAA is defined by four corner points in (lon,lat) as follows: the data package is in the SAA if the following conditions are fulfilled:

$$\begin{aligned} \frac{lon_{SAA,lt} + lon_{SAA,rt}}{2} &\geq lon_{data} \geq \frac{lon_{SAA,lb} + lon_{SAA,rb}}{2} \\ \frac{lat_{SAA,lt} + lat_{SAA,rt}}{2} &\geq lat_{data} \geq \frac{lat_{SAA,lb} + lat_{SAA,rb}}{2} \end{aligned} \quad (3.31)$$

where the  $(lon_{SAA,*}, lat_{SAA,*})$  are the four pre-defined corner points of the SAA box: lt = left/top, lb = left/bottom, rt = right/top and rb = right/bottom. Preliminary values of this box are taken as  $(-120^\circ, 10^\circ)$ ,  $(-120^\circ, -60^\circ)$ ,  $(50^\circ, 10^\circ)$ ,  $(50^\circ, -60^\circ)$ .

### 3.2.8. Calculate orbit phase

The position in orbit for selecting position-dependent dark signal or spectral parameters will be related to the orbit phase after eclipse (see also Figure 3.7 on page 54); this phase after eclipse can be seen as a measure for the 'warm-up time' or 'cooling-down time' of the instrument after entering or leaving the sunlight. For numerical reasons we define sunrise (SZA=90°) as phase 0.5 (the phase 0 then corresponds more or less to start of eclipse over the Antarctic), so that we do not have the jump in phase from 1 to 0 in the region where we wish to make the polynomial fit on the solar stray light. The eclipse time is calculated from the orbit state vector, using ESA's Orbit Propagator software to calculate the point in time where the solar zenith angle reaches +90°. Then the orbit phase may be calculated as:

$$\phi_{orb} = \frac{t_{measurement} - t_{eclipse}}{\Delta t_{orbit}} + 0.5 + n \quad (3.32)$$

where:

$t_{measurement}$  is the time of the measurement in the middle of the State,

$\Delta t_{orbit}$  is the duration of one orbit and

$n$  is an integer number to get  $\phi_{orb}$  into the range between 0 and 1.

This equation has to be solved by iterative calls to the Orbit Propagator. Convergence is assumed when the difference in orbit phase between iteration steps is smaller than 0.001 .

## 3.3. Correct Detector Readout Memory and Non-Linearity

It appears that after each detector readout, a certain amount of the signal is retained in the electronics as charge memory. This charge is transferred (added) to the next measurement. This problem was specifically noted with the Reticon detectors (channels 1-5) at qualification at SRON. Therefore, each measurement must be corrected with a certain percentage of the previously measured signal.

In channels 6-8 a non-linearity in the electronics has been found. Each measurement must be corrected with a certain amount, depending on signal level. The procedure is very similar to that of the memory effect, except that not the previous signal is used as basis for the calculation, but the signal itself.

As of IPF version  $\geq 6$  , the calculation of the memory effect has changed: look-up tables (generated by SRON [55]) are now used instead of the less accurate polynomial approximation. This now also includes a correction for signals below 10,000 BU where previously no correction was made.

The correction for non-linearity is also based on look-up tables (LUTs) [51]. Both for memory effect correction and for non-linearity correction, the index of the LUT-entry to be used is the raw signal value of each detector readout (there are thus 65536 elements per table; the LUTs on the key data file are specified for a selection of signals and are expanded by linear interpolation to 65536 elements).

Memory effect calculation for channels 1-5 uses one LUT for each channel. Non-linearity correction for channels 6-8 uses in total 14 LUTs for the (sub)channels 6, 6+, 7, 8. Each of these four (sub)channels has one LUT for even- and one for odd-numbered pixels. Then there is a separate LUT for the first half and for the second half of the (sub)channel. The combination (channel 6+, first half of channel) does not exist, hence we have 16-2=14 different LUTs. In the key data, each LUT is identified by a start pixel number. If this is an odd number, the LUT is valid for odd pixels larger or equal than the start number; similar for even pixel numbers.

The amount of memory effect correction [BU] for pixel  $i$  in optical channel  $j$  ( $j = 1 - 5$ ) is calculated from the LUT, where the first index to the LUT is the raw signal value of the previous measurement:

$$C_{ij} = Lut_{mem}(\text{ROUND}(S_{ij}^{prev}), j) \quad (3.33)$$

where ROUND rounds to the nearest integer. In case of co-adding, the value of  $C_{ij}$  is derived for each detector readout and then summed, see below.

The amount of non-linearity correction [BU] for pixel  $i$  in near-infrared channel  $j$  ( $j = 6, 7, 8$ ) is calculated from the LUT, where the first index to the LUT is the raw signal value of the measurement itself, and the second index refers to the LUT (0-13) to be used:

$$C_{ij} = Lut_{NL}(\text{ROUND}(S_{ij}^{raw}), LUTindex_{ij})$$

The memory effect or non-linearity is coded on the Level 1b product on a single byte (256 available values). To reduce the dynamic range, the correction is divided by a factor  $f_{byte,j}$  (one value per channel, specified on the initialisation file, in practice smaller than 1.5) and an offset is added to bring data in the range [-128, 127] :

$$CC_{ij} = \text{ROUND}(C_{ij}/f_{byte,j}/f_{Coadd} + offset_{byte,j}) \quad (3.34)$$

Values of  $CC_{ij}$  below -128 or above 127 are clipped to -128, 127, respectively. Clipping is expected for signals in channels 6-8 close to the saturation limit.

In the level 1b>1c application of memory effect/non-linearity, the signal of pixel  $i$  in channel  $j$ , corrected for memory effect ( $j = 1 - 5$ ) or non-linearity ( $j = 6 - 8$ ), is given by:

$$S_{ij}^{corr} = S_{ij}^{raw} - f_{byte,j} \cdot f_{Coadd,j} \cdot (CC_{ij} - offset_{byte,j}) \quad (3.35)$$

In the level 0>1b processor internally, the same formula is used for the memory effect correction of the calibration measurements. For non-linearity, we use the float values of the correction (i.e.  $S_{ij}^{corr} = S_{ij}^{raw} - C_{ij}$ ). This is because there are several calibration states in Level 0 to 1b processing which have very high co-adding factors in the NIR channels, where we do not want to multiply the errors, due to rounding or due to high-signal cut-off, by the co-adding factor (in level 1b to 1c processing we have of course to use the same formula as for memory effect, but there the limb/nadir states have small co-adding factors). For memory effect we have in praxis a maximum rounding error of  $0.25 \cdot f_{Coadd,j}$  which is considered negligible since the uncertainty in the correction itself is around 5 BU. For details on memory effect, see [58].

Three specific problems arise from the fact that the previously measured spectrum has to be used in the correction:

- At the begin of a State, no previous measurement is available to calculate the memory effect (the readout has of cause been made, but is discarded immediately on-board). The detectors have been integrating during a part of the set-up time, which is known, but different for each State. For the memory effect correction, we assume that the spectral intensity on the detectors during this last part of the set-up was identical to the one of the first spectrum in a State; the signal of the previous spectrum is then taken as the signal of the current spectrum scaled with the ratio of the respective integration times.

- In limb mode, a reset measurement is made while the scan mirror moves to the next tangent height. This reset measurement is discarded and hence no previous measurement is available. The previous measurement must be estimated from the signals at the lower and at the higher tangent height, taking into account the mirror movement.
- In case of co-adding, only the sum of the signals of all co-added readouts is known, not the individual readout signals. But for the memory effect correction we need to know all readout signals, because the correction on the co-added signals is the sum of the corrections on each individual readout; the strong non-linearity of the effect makes that the sum of the corrections is not equal to the correction on the sum (there might even be a sign difference in the most extreme case!). For an estimate of the individual signals we use the variation of the PMD signal during the measurement (including the last readout of the previous measurement: for example for a co-adding factor of 4 we need to estimate the signal of the 4th readout of the previous co-added measurement plus the signals of the 1st, 2nd, 3rd readout of the current co-added measurement). This is only strictly valid if the polarisation would not change during the measurement; in fact it usually does but GOME measurements have shown that changes in PMD signals are usually to a much larger extend due to intensity variations, than to polarisation variations (at least within the same orbit region).

### 3.3.1. Calculation if no previous measurement available

If no previous measurement is available (which, except for limb measurements, only occurs at the beginning of each State, else the State is incomplete and is not processed anyway) then assume that the previous spectrum is equal to the current one, and calculate the signal from the ratio of integration times

$$S_{previous} = S_{current} \left( \frac{IT_{previous}}{IT_{current}} \right) \quad (3.36)$$

At the beginning of a State, take as  $IT_{previous}$  the set-up time of the State (specified on the Initialisation file). The States are identified by the State ID on the level 0 product.

The second case where no previous measurement is available is at the beginning of each new tangent height in limb, as a measurement in the transition time between tangent heights is discarded [52]. The transition time is 3 BCPS. The scan mirror waits around 0.5 BCPS (1/6th of the measurement time) before it starts to move to the next tangent height. This waiting time assures that also the last pixel of each detector array has been read out before the mirror moves. The movement itself lasts 2 BCPS. The previous measurement signal is then taken as a weighted average of the previously transmitted signal (at the last tangent height) and the current signal (at the new tangent height). The weighting depends on exposure time in relation to the 3 BCPS, and due to the sequential readout of the detectors, this may also lead to a weighting dependend on pixel number.

One can define  $reset\_ratio = (3/16)/IT * f_{Coad,,j}$ , which leads to the following cases:

1.  $reset\_ratio > 2$ : The mirror is already at the higher TH; and the previous signal equals the measured one.
2.  $reset\_ratio > 1$ : Similar to the previous case, but the exposure time is truncated. The previous (not co-added) "illuminated" signal is half the current (not co-added) "illuminated" signal, where "illuminated" signal is the one corrected for Dark. As we do for coadding (see below), we correct the signals for dark using only the FPN:

$$S_{ij}^{prev} = FPN_{ij} + 0.5 \cdot (S_{ij} - FPN_{ij})$$

3.  $reset\_ratio \leq 1$ : Take the applicable weighting of upper and lower height's "illuminated" signal. Due to the sequential readout of the detector, pixel 0 stays longer at the lower height than pixel 1023. Also the weighting factor varies linearly with the pixel number. For pixel 0 the weights are equal, and for the last one it is 2/6:4/6

$$\begin{aligned} S_1 &= reset\_ratio \times (S_{lower,ij} - FPN_{ij}) \\ S_2 &= reset\_ratio \times (S_{ij} - FPN_{ij}) \\ S_{ij}^{prev} &= FPN_{ij} + [(3 - k/1023) \cdot S_1 + (3 + k/1023) \cdot S_2]/6 \end{aligned}$$

where  $S_{lower}$  is the signal of the last readout at the lower TH,  $k$  is the pixel index, which is written like  $k = 1023 - i$  for channel 2 (due to its reversed readout) and  $k = i$  for the other channels.

### 3.3.2. Scaling with PMDs at co-adding for memory effect

In case of co-adding, calculate the 'previous' signals from the ratio of PMD signal during each individual measurement, with the PMD signal integrated over the co-adding time. Use for each channel the corresponding (or nearest-in-wavelength) PMD, i.e. use for channels 1, 2, 3, 4, 5 the PMDs A, A, B, C, D respectively. For this PMD scaling we use the "illuminated signal", i.e. the signals corrected for dark signal. For channels, 1-5, where the leakage current is very low, it is sufficient to correct the signals with FPN only.

Let there be  $N_{ij}$  co-addings for each detector pixel  $i$  in channel  $j$  (this number is cluster-dependent); let the current measurement be indicated with index  $m$ . Then the total memory correction for the co-added signal is given by

$$C_{ij} = C_{ij}(m-1, N_{ij}) + \sum_{n=1}^{N_{ij}-1} C_{ij}(m, n) \quad (3.37)$$

where  $C_{ij}(m, n)$  is the correction for each (unknown) individual readout in the co-adding (note: base for  $m, n$  is 1 not 0 here); this amount of correction is calculated (using the formulae above) from the corresponding, estimated, signal  $S_{ij}^{previous}(m, n)$  (see below).

A complication arises when  $t_{PET} = 1/32$ . As a data packet can be generated only every 1/16 second, the first channel readout of each data packet is discarded (but it is this readout which causes the memory effect of the readouts which are kept). Let  $n$  be the index over 1/16 s readouts for  $N_{ij}$  co-addings then the total memory correction for the co-added signal is given by

$$C_{ij} = \sum_{n=1}^{N_{ij}-1} C_{ij}(m, n32) \quad \text{if } t_{PET} = 1/32 \quad (3.38)$$

where  $n32$ , the index over 1/32 s readouts, is given by  $n32 = 2 \cdot n - 1$ .

$S_{ij}^{prev}(m, n)$  is obtained from scaling the co-added measurement with the PMD integrals (i.e. it is assumed that the ratio of PMD signal to channel signal is constant during co-adding). Therefore, the signal is temporarily corrected for dark signal (since scaling only applies to the signal from the ground scene, not to dark). As the leakage current is very small for channel 1-5, it is sufficient to correct for FPN only. The PMD integrals are not corrected for dark here - that is not quite correct, but guards against negative scaling factors that otherwise might occur for low, noisy, PMD signals.

For  $t_{PET} \geq 1/16$ :

$$S_{ij}^{prev}(m, n) = \frac{\sum_{it=it1}^{it2} I_{PMD}(it)}{\sum_{n=1}^{N_{ij}} \sum_{it=it1}^{it2} I_{PMD}(it)} \cdot (S_{ij}(m) - FPN_{ij} \cdot f_{Coadd,j}) + FPN_{ij} \quad (3.39)$$

using the integration during cluster readout of the PMD integrals from  $it1$  to  $it2$  (relative to start of measurement  $m$ ):  $it1 = 1 + (n - 1) \cdot t_{PET} \cdot 32$  and  $it2 = n \cdot t_{PET} \cdot 32$

where one has to take for each cluster the pixel exposure time  $t_{PET}$  [seconds] of the channel it is located in.

For the case  $t_{PET} = 1/32$ , the previous signals for Eq. 3.38 are estimated according to:

$$S_{ij}^{prev}(m, n32) = \frac{I_{PMD}(it1)}{\sum_{n=1}^{N_{ij}} I_{PMD}(it2)} \cdot (S_{ij}(m) - FPN_{ij} \cdot f_{Coadd,j}) + FPN_{ij} \quad (3.40)$$

for  $n32 = 2 \cdot n - 1$ , with  $it1 = 1 + 2 \cdot (n - 1)$  and  $it2 = 2 \cdot n$

### 3.3.3. Scaling with PMDs at co-adding for non-linearity

The procedure here is very similar to that of the memory effect, except that the measurement  $S_{ij}^{raw}$  itself is used instead of the previous measurement  $S_{ij}^{prev}$ . This results in essentially the same formulae but a shift in indices.

The total non-linearity correction for the co-added signal, corresponding to Eq. 3.37, is given by

$$C_{ij} = \sum_{n=1}^{N_{ij}} C_{ij}(m, n) \quad (3.41)$$

and

$$C_{ij} = \sum_{n=1}^{N_{ij}} C_{ij}(m, n32) \text{ for } t_{PET} = 1/32s$$

where  $n32$ , the index over 1 / 32 s readouts, is given by  $n32 = 2 \cdot n$ .

$S_{ij}^{raw}(m, n)$  is obtained from scaling the co-added measurement with the PMDs (i.e. it is assumed that the ratio of PMD signal to channel signal is constant during co-adding). Both, PMD integrals and channel Signals, are corrected for dark signal as in Apply\_leakage (see Equation 3.59, 3.60) but setting the stray light component to zero. To obtain the total signal, the dark signal is added to the scaled dark-corrected signal. For the non-linearity we have a similar scaling as for the memory effect (superscript  $DC$  indicates dark-corrected measurements). For  $t_{PET} \geq 1/16s$  we have the same scaling as in Eq. 3.39 for the memory effect:

$$S_{ij}^{raw}(m, n) = \frac{\sum_{it=it1}^{it2} I_{PMD}^{DC}(it)}{\sum_{n=1}^{N_{ij}} \sum_{it=it1}^{it2} I_{PMD}^{DC}(it)} \cdot S_{ij}^{DC}(m) + (S_{ij}^{raw}(m) - S_{ij}^{DC}(m)) / f_{Coadd,j} \quad (3.42)$$

using the integration during cluster readout of the PMD integrals from index  $it1$  to  $it2$  (relative to start of measurement  $m$ ):

$$it1 = 1 + (n - 1) \cdot t_{PET} \cdot 32, \quad it2 = n \cdot t_{PET} \cdot 32$$

where one has to take for each cluster the PET of the channel it is located in, and the corresponding PMD, i.e. for channels 6,7,8 the PMDs E, F, F respectively.

For the case  $t_{PET} = 1/32s$  the raw signals for Eq. 3.38 are estimated according to:

$$S_{ij}^{raw}(m, n32) = \frac{I_{PMD}^{DC}(n32)}{\sum_{n=1}^{N_{ij}} I_{PMD}^{DC}(n32)} \cdot S_{ij}^{DC}(m) + (S_{ij}^{raw}(m) - S_{ij}^{DC}(m)) / f_{Coadd,j}$$

with  $n_{32} = 2 \cdot n$ .

To avoid introducing spurious noise, scaling with the PMD signal is only performed if the PMD signal is high enough. For all dark states, defined by measurement category 12, PMD scaling is not applied (this is implemented by temporarily setting all PMD signals to 1 before applying above formulas). For other states, PMD scaling is only applied if the PMD signal is 3 times larger than the PMD noise, with a minimum threshold of 20 BU. For each integration time it is checked if the corresponding PMD signals are above this noise threshold. If one PMD in the integration time is below the threshold, all PMD values in that it are temporarily set to the threshold values (so that effectively no PMD scaling takes place).

The threshold noise level  $I_{min}$  is calculated from the PMD signal-to-noise  $SN_{PMD}$  as determined in the Apply Leakage routine:

$$I_{min} = (3 \cdot I_{PMD}^{DC}(it) / SN_{PMD,j}(it)) > 20$$

## 3.4. Calculate Dark Signal

### 3.4.1. Introduction

The dark signal has four possible components:

- a bias component which is for each pixel a fixed amount; this component is often called fixed-pattern noise (FPN);
- a time-dependent component which is caused by charge leaking in the detector pixel, called leakage current (LC) - the resulting signal is  $leakage\ current \times integration\ time$  (IT);
- a time-dependent component which is caused by photons from the thermal background in the instrument - only significant for the infrared channels 6-8 and for PMDs E and F. This signal increases linearly with IT, therefore we will implicitly include it in the LC parameter which is calculated in this section.
- in Limb mode, the possibility exists that the azimuth scan mirror is illuminated by the Sun. This may generate diffuse stray light in the instrument at a detectable level. This signal also increases linearly with IT and is therefore implicitly included in determination of LC from dark sky measurements.

For a number of reasons the FPN and LC parameters may vary during one orbit:

- The thermal background (in channels 6-8 and PMD-E,F) depends strongly on the temperature of the optical bench module (OBM). Although the OBM is temperature controlled, the changing illumination of SCIAMACHY during an orbit may cause a changing gradient of the temperature within the OBM. The resulting changes in thermal background are expected to depend only on the position in orbit relative to the sun.
- Possible stray light from the azimuth mirror in Limb dark sky depends on the solar illumination geometry. It is therefore expected that this also can be derived as function of position in orbit.
- A presently unsolved problem is how to proceed in regions with a high background of cosmic rays, notably in the South Atlantic Anomaly (SAA, roughly in the region between and including Latin America and Southern Africa). Dark signal calibration measurements from these regions will be in any case excluded from calibration processing.

The leakage current and FPN will therefore be determined separately for a number of intervals within the orbit. We make a distinction between the solar stray light component, which is expected to be present only in Limb mode around sunrise, and the other LC components which are modelled over the whole orbit.

### 3.4.2. Calculation of FPN and LC from dedicated 'Dark' measurements

SCIAMACHY measures 5 dark states with different PETs and co-adding factors. The processor allows to select individual darks. For channel 1-7 all five dark states are used, for channel 8 we leave out the dark state with the shortest PET, since it degraded the results for longer exposure times. The apparent reason is a dependence of the non-linearity on the exposure time. Since the shortest PET is not representative for the observations, including it introduces an error into the correction. All pixels in one channel have the same PET and co-adding factor; all channels have the same integration time but may have different PET and co-adding factor.

Note that for the LC part of the dark signal only the integration time (product of PET and co-adding factor) is significant. However, each co-adding adds a FPN component to the measured signal. Example:

- a dark measurement with  $x$  co-addings of  $y$  seconds each has a signal of  $x \cdot FPN + x \cdot y \cdot LC$ ;
- a dark measurement with  $y$  co-addings of  $x$  seconds each has a signal of  $y \cdot FPN + x \cdot y \cdot LC$ .

The following describes the procedure for a single detector channel. This has to be done for each channel.

First a measurement health check is performed. It regularly occurs that a pixel is hit by a cosmic particle, resulting in a high signal spike, and these measurements (called 'hot pixels') must be discarded. Because the detector memory effect cannot be well corrected in case of co-adding, the next measurement of this pixel

must be discarded too. Health checking is done on the basis of pixel intensity; a hot pixel threshold is given as one value per channel in the initialisation file. A pixel is discarded from the calibration processing if its value exceeds its median value in the State by more than the threshold amount. The number of discarded measurements for each State is kept as quality control parameter. Bad pixels are excluded from this quality control parameter as they may have such a high intrinsic variability that they may also be detected as 'hot'; as a result no dark signal will be calculated there. This is no problem since these pixels are effectively not usable. The PMDs are similarly checked; here the quality control parameter is the average of the number of hot pixels for amplifier A and amplifier B.

For each pixel  $i$  in channel  $j$  the FPN and LC are calculated by a linear least square fit from the equations (one for each State):

$$S_{ij}/f_{Coadd,j} = FPN_{ij} + t_{PET,j} \cdot LC_{ij}$$

where  $f_{Coadd,j}$  is the co-adding factor for each (cluster in the) channel  $j$  and  $t_{PET,j}$  is its pixel exposure time (IT of each detector before co-adding).

The formal solution of this equation is given by (see, e.g. [32]):

$$LC_{ij} = \frac{1}{T} \cdot \sum_k w_k \cdot (t_{PET,j}(k) - \langle t_j \rangle \cdot S_{ij}(k)/f_{Coadd,j}(k)) \quad (3.43)$$

and

$$FPN_{ij} = \frac{\sum_k w_k \cdot S_{ij}(k)/f_{Coadd,j}(k)}{\sum_k w_k} \quad (3.44)$$

where index  $k$  runs over the Dark States and  $\langle t_j \rangle$  is the weighed average of the PET over all dark States

$$\langle t_j \rangle = \frac{\sum_k w_k \cdot t_{PET,j}(k)}{\sum_k w_k}$$

and

$$T = \sum_k w_k \cdot (t_{PET,j}(k) - \langle t_j \rangle)^2$$

and  $w_k$  is a weighting factor for each State. This factor is based on the ratio  $\omega_j$  between electronic noise  $\sigma_{E,ij}$  (see below) and the expected noise on the LC and thermal background:

$$w_k = \left[ \frac{\sigma_{E,ij}^2}{f_{Coadd,j}(k)} + \omega_j \cdot t_{PET}(k) \cdot f_{Coadd,j}(k) \right]^{-\frac{1}{2}} \quad (3.45)$$

Thus, for pixels with a high electronic noise the abscissa point will receive a lower weight to get a better determination of the LC; pixels with a longer integration time receive a lower weight because otherwise they would dominate the fit too much and the abscissa (FPN) could then be inaccurate due to noise. The factor  $\omega_j$  can be set to tune the algorithm.

The formal fit errors (external errors) of the equation are (see, e.g. [32]):

$$\sigma_{LC_{ij}^{ext}} = \sqrt{\frac{1}{T} \cdot \frac{\sum_k w_k \cdot \delta_k^2}{n_{states} - 2}} \quad (3.46)$$

and

$$\sigma_{FPN_{ij}^{ext}} = \sqrt{\left( \frac{1}{\sum_k w_k} + \frac{\langle t_j \rangle^2}{T} \right) \cdot \frac{\sum_k w_k \cdot \delta_k^2}{n_{states} - 2}} \quad (3.47)$$

where  $\delta_k$  is the difference between measurement and fit:

$$\delta_k = S_{ij}(k) / f_{Coadd,j}(k) - FPN_{ij} - t_{PET,j}(k) \cdot LC_{ij}$$

and  $n_{states}$  is the number of states  $k$  used in the fit.

The internal errors on the data points are approximated for the FPN from the electronic noise value  $\sigma_{E,ij}$ , and for the LC by the slope which one gets by dividing the sum of shot noise in State with the shortest IT and the shot noise in State with the longest IT by the difference in IT of these States:

$$\sigma_{FPN_{ij}^{int}} = \sigma_{E,ij} / \sqrt{N_{ij}^{t-min} \cdot f_{Coadd,j}^{t-min}} \quad (3.48)$$

$$\sigma_{LC_{ij}^{int}} = \frac{\sqrt{\frac{\sigma_{E,ij}^2}{N_{ij}^{t-max} \cdot f_{Coadd,j}^{t-max}} + \frac{LC_{ij} \cdot IT_j^{t-max}}{N_{ij}^{t-max} \cdot e_j}} + \sqrt{\frac{\sigma_{E,ij}^2}{N_{ij}^{t-min} \cdot f_{Coadd,j}^{t-min}} + \frac{LC_{ij} \cdot IT_j^{t-min}}{N_{ij}^{t-min} \cdot e_j}}}{IT_j^{t-max} - IT_j^{t-min}} \quad (3.49)$$

where integration time  $IT_j = t_{PET,j} \cdot f_{Coadd,j}$  is the integration time in channel  $j$ ,  $e_j$  is the number of photo-electrons per BU, and  $N_{ij}$  is the number of measurements used for the determination of LC/FPN, superscripts  $t-max / t-min$  refer to the used State with minimum / maximum integration time.

If  $n_{states}$  is smaller than 3, then the internal errors must be used; else the error which is used is the larger one of internal and external error.

Note that usually  $n_{states}$  will be equal to 3. Only if a pixel in one of these 3 states is deleted by the hot pixel check,  $n_{states}$  may be equal to 2 for this pixel.

The electronic noise value  $\sigma_{E,ij}$  of a detector pixel is calculated from the measurements in one preselected Dark State (currently: State 46). Requirements are that the IT of each measurement is short enough that noise is determined by FPN and not by LC, and that the State duration is long enough to get statistics within a State (the latter requirement is less strict since more than one such State can be used per orbit). Let there be  $N$  measurements used, with average signal  $\langle S_{ij} \rangle$ , then

$$\sigma_{E,ij} = \sqrt{\frac{1}{(N-1) \cdot f_{Coadd,j}} \cdot \sum_{n=1}^N (S_{ij}(n) - \langle S_{ij} \rangle)^2}$$

which can be re-written as (avoids a second loop over all measurements):

$$\sigma_{E,ij} = \sqrt{\frac{1}{(N-1) \cdot f_{Coadd,j}} \cdot \left( \sum_{n=1}^N \{S_{ij}^2(n)\} - N \cdot \langle S_{ij} \rangle^2 \right)} \quad (3.50)$$

The PMDs are non-integrating devices and therefore have no IT-dependent component in their dark signal. We calculate a 'zero offset' for the PMDs which is simply the average of the PMD values over the Dark States. The error on the PMD zero offset is the usual square root of the variance. The offsets and their errors are calculated for both amplifier stages A and B.

### 3.4.3. Operational aspects

In level 0 to 1b processing all FPN, LC and PMD-offset values are calculated from the States located in one 'orbit region' (see next subsection 3.4.4); these values are written to a 'Leakage ADS' on the level 1b product.

If two or more identical States lie within one orbit region, the measurements of these States are averaged (excluding hot pixels) before FPN, LC and PMD-offset are calculated. The reason for doing things as function

of orbit region instead of directly as function of orbit phase, is that the calculation combines measurements from 3 different States and therefore no unique orbit phase can be assigned to these dark signal parameters.

If an orbit region contains only 2 or less different Dark States, no dark signal parameters are calculated for that region (although a value for the region may be derived from orbit modelling, see below). Only for individual detector pixels it may occur that just 2 different States are used. This can happen if in one of the States a pixel is detected as hot; rather will we accept a bit lower quality on the dark parameters for this pixel, than leaving a gap in the calibration.

For each Dark State an ADS is written with the averaged dark spectrum in the State (excluding hot pixels from the average) and with a quantity named 'solar stray light' (see below, Equation 3.51) which is nothing but the difference between measured and calculated (from the calibration constants) dark spectrum. The individual dark measurements are discarded to save space on the product.

The processor (see Section 2.5) will use the Leakage ADSs from the Level 1b product to calculate FPN and PMD-offset values averaged over the orbit, and to model LC and solar stray light as function of orbit region, see below.

#### 3.4.4. Modelling of LC over the orbit

The orbit will be subdivided in a number of 'orbit regions' which are defined as intervals in orbit phase (see Section 3.2) - the starting point of each boundary will be given on the initialisation file. The setting of the boundaries must be based on analysis of the dark signal during the commissioning phase; at the point of writing the thermal behaviour of the instrument in space is insufficiently known to make decisions regarding this point. The dark signal parameters are calculated for each region.

Similarly, the solar stray light from the azimuth mirror will be calculated but only for a subset of orbit regions around the time of sunrise (to be more precise: an estimate of the solar stray light is for each State calculated as a diagnostic on the Level 1b product, but for the calibration constants it is given for selected orbit regions). If solar stray light would appear a quickly changing function of time, then the orbit regions around this point will have to be taken much smaller than elsewhere. Solar stray light will be fitted as a polynomial function of orbit phase.

Variation of LC with orbit phase is only expected for the NIR channels 6,7,8 and PMDs E,F. For channels 1-5 the calculation of LC for various orbit phases is only used as diagnostic; the final calibration quantity will be one 'constant' value of LC which applies to the whole orbit (being the average value of LC over the orbit).

Since the thermal behaviour of the instrument is expected to be a smooth function of orbit phase, a harmonic fit is made through the NIR data in order to reduce measurement errors. The regions where solar stray light from the azimuth mirror are expected are excluded from the fit. For the NIR channels/PMDs the LC calibration quantities will be calculated as a 'constant LC' - the average value over the orbit - and a 'variable LC' which gives the variation of LC with orbit region. For the PMDs, the 'variable' PMD offset is only given for amplifier stage B (it is an offset due to thermal radiation and not due to the PMD electronics)

This approach is conform to the calibration requirements laid down in [2], except that a harmonic fit over the orbit is not used there. The requirements [2] specify to use the reading of the OBM temperature sensor as index for dark signal parameters. However, that approach cannot take into account the effects of temperature gradients; for this reason we take the somewhat different approach of modelling as function of orbit phase. Figure 3.7 gives a schematic representation of the method.

Note that the calculation of 'variable LC' needs 3 Dark States with different IT. Hence the orbit phase of a LC measurement is not well defined. All Dark States with the same IT within one region will be averaged before the LC calculation, irrespective of the exact time of measurement. As orbit phase for the LC measurements will be taken the central orbit phase of the region. Since the variation of LC over orbit is expected to be slow, this binning shouldn't introduce significant errors. Furthermore, the phase shifts which could be introduced this way are expected to be random, and the harmonic fit is expected to cancel out such shifts.

Apart from the dedicated 'dark' measurements which are taken over the whole orbit, typically once per month, a few 'dark' measurement states are planned every orbit on the dark side of the Earth. In the present baseline the latter measurements will be used as quality indicators only (this applies to the aforementioned piece of

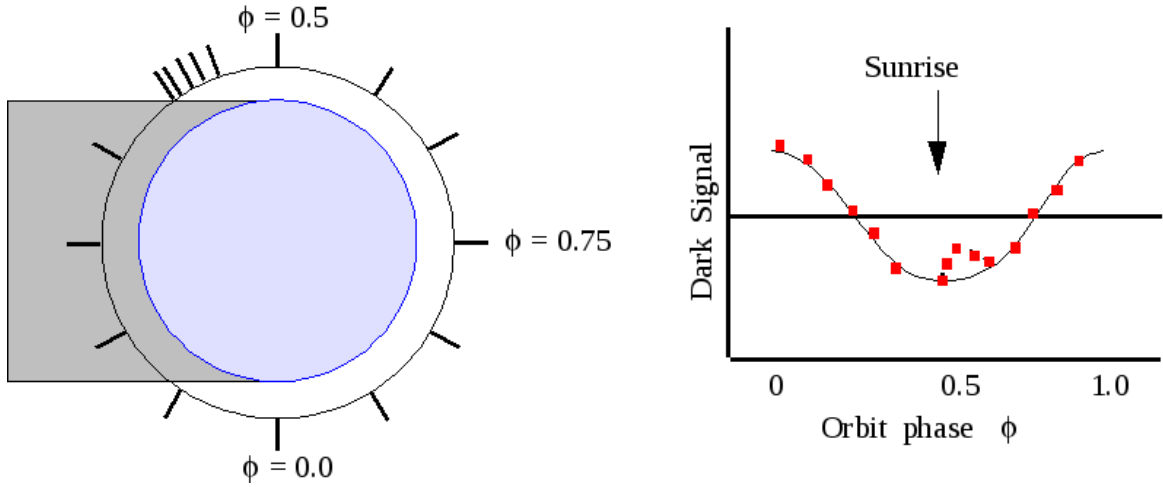


**Figure 3.7.:** Schematic representation of orbit regions, and of harmonic fit of dark signal over the orbit (harmonic fit only for channels 6-8 and PMDs E,F; solar stray light for all channels/PMDs).

software running outside the PDS). The calculation of dark signal parameters shall only be performed if a minimum number of Dark States is available on the orbit to be processed (preliminary value: more than 6 States).

### 3.4.5. Calculation of Solar Stray light from dedicated 'Dark' measurements

For each of the orbit regions after sunrise where solar stray light is expected (the index of these orbit regions are given on the initialisation file), the stray light component of the Dark signal is calculated as the dark measurement corrected for FPN and 'constant' and 'variable' LC, divided by IT to yield units of BU/s:

$$DS_{ij}^{stray} = \frac{\langle S_{ij} \rangle - (f_{Coadd,j} \cdot FPN_{ij}^*)}{IT_j} - (LC_{0,ij}^* + LC_{Var,ij}^*(\phi_{orb})) \quad (3.51)$$

where the superscript \* denotes that values from the calibration GADS have to be taken, not the values determined from the measurement;  $LC_{0,ij}^*$  is the 'constant LC' and  $LC_{Var,ij}^*$  the 'variable LC' (for channels 6-8 only) which is interpolated from the values per orbit region to the orbit phase of the middle of the State using linear interpolation.

The error on  $DS_{ij}^{stray}$  is calculated as the root mean square of the errors of all calibration components in the previous equation:

$$\sigma_{DS_{ij}^{stray}} = \sqrt{[\sigma_{FPN_{ij}^*} \cdot f_{Coadd,j} / IT_j]^2 + [\sigma_{LC_{0,ij}^*}]^2 + [\sigma_{LC_{Var,ij}^*}(\phi_{orb})]^2} \quad (3.52)$$

For the PMD offsets similar quantities are calculated (for the default amplifier stage B only; it is an effect of incident radiation and not of PMD electronics) using the average value of the PMD readings in the State:

$$PO_{stray}(j) = \langle S_{PMD,j}(B) \rangle - (PO_0^*(j, B) + PO_{Var}^*(j, \phi_{orb})) \quad (3.53)$$

$$\sigma_{PO_{stray}(j)} = \sqrt{[\sigma_{PO_0^*}(j, B)]^2 + [\sigma_{PO_{Var}^*}(j, \phi_{orb})]^2} \quad (3.54)$$

In the processor, a polynomial fit of solar stray light over orbit phase will be made - output will be a fitted solar stray light value for the middle of each orbit region where solar stray light may be present. Although the solar stray light might vary much faster than the LC, the correction for solar stray light in level 1b to 1c processing will

be based on the orbit phase of the middle of the State being processed. A prerequisite is that the orbit regions where solar stray light may be present will be spaced close enough. Note that the processor, for calculating new solar stray light calibration constants, cannot take directly the  $DS_{ij}^{stray}$  values calculated above (on the ADSs), since these use 'old' LC parameters and therefore also contain the difference (new–old). Instead, it must calculate new stray light values using:

$$DS_{ij}^{stray} = DS_{ij}^{stray}(ADS) + LC_{0,ij}^* + LC_{Var,ij}^*(\phi_{orb}) + \frac{f_{Coadd,j} \cdot (FPN_{ij}^* - FPN_{ij})}{IT_j} - (LC_{0,ij} + LC_{Var,ij}(\phi_{orb})) \quad (3.55)$$

where the LC and FPN parameters are new dark signal values determined from the harmonic fit.

For the PMDs we get similarly:

$$PO_{stray}(j) = PO_{stray}(j, ADS) + PO_0^*(j, B) + PO_{Var}^*(j, \phi_{orb}) - (PO_0(j, B) + PO_{Var}(j, \phi_{orb})) \quad (3.56)$$

Obviously, the solar stray light calibration parameters may only be updated when dark signal parameters are updated; else there are no 'new' dark signal parameters.

### 3.4.6. Quality check on Dark Signal using Limb States

At the end of each Limb State (at a tangent height of 150 km for early orbits and of 250 km for orbits larger than 6456 for normal Limb states and orbit 7265 for Limb Mesosphere states), SCIAMACHY performs an exposure to 'deep space'. For Limb measurements, there will be an option to use this exposure for dark signal correction of these limb measurements, although the noise on this dark signal will be higher as when using the FPN and LC calibration parameters which have been determined using a whole orbit of data (this option should only be used if the modelled LC over the orbit would prove to be too inaccurate). In any case, this dark exposure is used as quality check on the calibrated dark signal.

For each Limb dark sky measurement a quality check is made by comparing the measured dark signal, averaged per channel, to the one derived from calibration parameters. The percent difference of the two is to be passed as quality flag for this Limb state to the level 1 product (to be written on the SQADS).

Outside the scope of the current level 0 to 1 processing, but still worth mentioning, it is noted that this average "dark signal calibration error" could be used to correct measurements in special circumstances, e.g. in the SAA. In the GOME instrument it is observed that in the SAA the signals in a whole channel are receiving an offset - thus even the average per channel as calculated in this quality flag would be sufficient for correction of this offset. Due to better shielding, it is expected that SCIAMACHY will be much less sensitive for this SAA effect than GOME; therefore currently no special processing for this region is foreseen.

The quality check makes only sense when hot pixels are removed from the average. In processor versions  $IPF \leq 7.xx$ , we took for limb dark sky an average over every 128 pixels and performed a limit check w.r.t. this average. Since this gave too many false flaggings, hot pixels are now only flagged when more than 3 readouts are present in the last 1.5 seconds of the limb state. As "median" value we use the second lowest of 4 readouts as reference signal and discard signals more than hot pixel limit above this reference.

For each channel  $j$  in the Limb State with  $N_j$  usable (i.e. not hot, not bad) pixels, the percent error with the calibrated dark signal is given by:

$$DS_j = 100 - 100 \cdot \sum_{i=1}^{N_j} \frac{f_{Coadd,j} \cdot FPN_{ij}^* + IT_j \cdot (LC_{0,ij}^* + LC_{Var,ij}^*(\phi_{orb}) + DS_{stray,ij}^*(\phi_{orb}))}{S_{ij}} \quad (3.57)$$

where the 'variable LC' (for channels 6-8 only) and the 'solar stray light' (for certain regions after sunrise only) are interpolated from the values per orbit region to the orbit phase of the measurement (middle of State) using linear interpolation.

For the quality check on Limb dark signal for the PMDs (percent error with expected value) we get in analogy with the channels

$$\Delta DS_j = 100 - 100 \cdot \frac{40}{32} \cdot \sum_{i=1}^{N_I} \frac{PO_{0,j}^* + PO_{Var,j}^*(\phi_{orb}) + PO_{Stray,ij}^*(\phi_{orb})}{I_{PMD,j}} \quad (3.58)$$

where  $N_I$  denotes the number of PMD integrals during the measurement, and the  $PO^*$  are the various components of the PMD zero offset, analogue to the LC components in the channels.

#### Added note on operational software implementation and data product

Although the software is in principle fully compatible for dealing with orbit variations of LC and solar stray light, as described above, these features are currently disabled and the corresponding entries in the data product are zero.

Orbit variation in LC is only clearly detectable for channel 8 (for channel 7 it may be present but is currently overshadowed by a light-leak effect). As of IPF version 6 variable LC may be switched on for channel 8.

On the illuminated side of the orbit, not only solar stray light is detected, but also stray light from the Earth's atmosphere is visible in Dark measurements. This is dependent on clouds and surface albedo, and cannot be modelled at present. Therefore the stray light modelling described above is currently switched off. The concept of orbit phase is retained to describe the stray light free regions suitable for dark measurements.

Due to ice build-up on the NIR detectors, dark signal in channels 6-8 may change rapidly, even from orbit to orbit. Therefore, since 15 April 2003 (orbit 5879), Dark measurement states have been scheduled in each eclipse phase of the orbit. The number of different Dark states is increased here from 3 to 5 (this does not affect the formulae above; simply replace  $k=1-3$  by  $k=1-5$  in Eq. - and  $n\_states=3$  by  $n\_states=5$ ) with PETs which match those used in the science measurements as closely as possible, to minimise interpolation errors for non-linearity and to generally improve the fit of FPN and LC. The data processing derives the dark correction from the same orbit when dark measurements are available. The 'constant' part of LC is obtained by subtracting the 'variable' part from the total LC of Eq. 3.43

### 3.5. Apply Dark Signal

The measured spectra are corrected for the dark signal by subtraction of a 'Dark Spectrum' which for each detector pixel is a combination of readout fixed-pattern noise (FPN) and leakage current (LC) including thermal background and solar stray light (for Limb an alternative method may be applied, see below).

All measurements within one State are corrected using the same Dark Spectrum, calculated for the centre orbit phase of the State. Even the State with the longest duration currently foreseen [3] does not cover more than  $\pm 0.02$  in orbit phase, and the LC is not expected to vary significantly over this period.

The Dark Spectrum for each pixel  $i$  in channel  $j$  is calculated from the FPN and LC of this pixel, and from the co-adding factor and PET of the detector cluster to where this pixel belongs to:

$$S_{ij}^{dark} = f_{Coadd,ij} \cdot (FPN_{ij} + [LC_{0,ij} + LC_{Var,ij}(\phi_{orb}) + DS_{ij}^{stray}(\phi_{orb})] \cdot t_{PET,ij}) \quad (3.59)$$

where the variable part of the LC and the solar stray light are linearly interpolated from the set of values per orbit region to the centre orbit phase of the State. The application of the variable part of the LC and the solar stray light may be switched off; this is governed by flags on the initialisation file.

For the PMD zero offset of PMD  $j$  we have similarly:

$$PO_j = PO_{0,j} + PO_{Var,j}(\phi_{orb}) + PO_{Stray,ij}(\phi_{orb}) \quad (3.60)$$

and this zero offset, multiplied by 40 / 32 (see end of subsection 3.2.2) is subtracted from the PMD integral in order to correct it for dark signal.

Note that the variable part of the LC (or PO) is not applied to the UV/VIS channels 1-5 (or PMDs A-D & PMD45), and that the solar stray light is not applied to Nadir States.

To account for the eventuality that the determined parameters for the variable part of the LC or the parameters for solar stray light are noisy and do more harm than good as a correction, the application of these parameters can be switched off (separately for nadir and limb, separately for main channels and PMDs). This is governed by variables on the initialisation file: DO\_VAR\_LC\_\* and DO\_Stray\_LC\_\*.

The error on the measured signal due to the subtraction of the Dark Spectrum is given by:

$$\epsilon_{SD,ij} = \sqrt{f_{Coadd,ij} \cdot \sigma_{FPN_{ij}} + f_{Coadd,ij} \cdot t_{PET,ij} \cdot [\sigma_{LC_{0,ij}} + \sigma_{LC_{Var,ij}} + \sigma_{DS_{ij}^{stray}}]} \quad (3.61)$$

For the PMD integrals (corrected for dark signal) we will later use their signal-to-noise ratio, given by:

$$SN_{PMD,j} = \frac{I_{PMD,j} \cdot 32/40}{\sigma_{PO_{0,j}} + \sigma_{PO_{Var,j}}(\phi_{orb}) + \sigma_{PO_{stray,ij}}(\phi_{orb})} \quad (3.62)$$

For Limb measurements an option exists to use not the formulation above, but to use the (dark) spectrum measured at the end of the limb scan at a height of 150 km (this is currently the default processing). This is governed by the variable 'do\_use\_limbdark' on the initialisation file. Pixels which were flagged as 'hot' in the dark limb spectrum are replaced by values calculated from LC and PPN. Using this dark limb spectrum for correction has the disadvantage that it is noisier than a dark spectrum calculated from LC and FPN parameters which have been smoothed by the harmonic fit over the orbit; the potential advantage is clear if the modelled LC and FPN parameters do not describe the behaviour of the instrument accurately enough.

If 'do\_use\_limbdark' is true, then the error on the measured signal due to the subtraction of the Dark Spectrum is given by:

$$\epsilon_{SD,ij} = 2 \cdot \epsilon_{shot_{ij}} + \sigma_{DS_{ij}^{stray}} \quad (3.63)$$

where  $\epsilon_{shot_{ij}}$  is the shot noise (see below) and where the stray light term reflects the fact that error on stray light is not interpreted as an error on calibration data, but most significantly arises from the uncertainty in stray

light conditions during the measurement (note that the stray light error will only be non-zero in the stray light regions defined on the initialisation file; moreover it can be switched off as mentioned above).

Similarly, if 'do\_use\_limbdark' is true, the signal-to-noise ratio of the PMD integrals (after subtraction of dark signal) is given by:

$$SN_{PMD,j} = \frac{I_{PMD,j} \cdot 32/40}{2 \cdot \sigma_{PO_{0,j}} + \sigma_{PO_{stray,ij}}(\phi_{orb})} \quad (3.64)$$

### Shot noise

The precision (not accuracy) of the SCIAMACHY measurements is to a large extent shot-noise limited. The shot noise is calculated from the raw (or memory-effect corrected) ADC binary units after subtraction of the electronic readout offset FPN:

$$\epsilon_{shot_{ij}} = \sqrt{f_{Coadd,ij} \cdot \sigma_{E,ij}^2(\phi_{orb}) + \left| \frac{S_{ij} - f_{Coadd,ij} \cdot FPN_{ij}}{e_j} \right|} \quad (3.65)$$

where  $e_j$  is the number of photo-electrons per binary unit for channel  $j$ , and  $\sigma_{E,ij}(\phi_{orb})$  is calculated from the electronic noise for each orbit region using linear interpolation, similar to LC.

## 3.6. Calculate PPG and Etalon Parameters

### 3.6.1. Introduction

This section describes the calculation of correction factors for two completely different detector phenomena, PPG (detector pixel-to-pixel gain) and Etalon effect. The common ground of the algorithms for these effects, is that they both use WLS (white light source) data, and that they need a similar comparison to a reference WLS spectrum.

A brief introduction to the physics of the phenomena:

PPG simply means that adjacent pixels on an array detector chip may have (slightly) different Quantum Efficiencies. This implies that calibration data which deal with (polarised) radiometric response, which are usually a smooth function of wavelength in the optical part of the instrument, have this PPG pattern imposed. A problem now arises when the wavelength calibration of the instrument is shifting: if one takes these calibration data as function of pixel, then the wavelength response becomes inaccurate, but if one takes these calibration data as function of wavelength, then the PPG pattern shifts to the 'wrong' pixels.

The solution to this problem is to derive the PPG pattern, and correct both the radiometric calibration data and the measured science data for the PPG, before making any wavelength match.

Note that for best results, the PPG correction shall be performed in the same way as was done by the on-ground calibration team in their determination of PPG correction on the Radiance Response. Trying to implement a 'better' method may lead to inconsistencies with the Radiance Response function which are worse than the improvements in PPG determination itself.

Etalon is an interference phenomenon, which arises in the thin protective layer coated on the detector chip. This causes a wave-like pattern on the radiance response, where the position of the minima and maxima of the wave depend on the ratio between layer thickness and wavelength. The polarisation sensitivity of the instrument is not affected.

At the shortest wavelengths in channel 1 we expect (based on GOME experience) approximately 10 minima and maxima over the channel (i.e. the interference wave has a wavelength of around 100 pixels). At the longest wavelengths of the optical channel 5 this number of waves reduces proportionally with wavelength to around 3 (i.e. 300 pixels interference wavelength). For the IR channels 6-8 Etalon was not apparent, but here the interference wavelength may have been so long that it mingled in appearance with the radiance response function.

The problem with Etalon arises when condensates (ice) settle on the detector, thereby effectively increasing the thickness of the interference layer. This causes a shift of the interference pattern which spoils the radiance response as calibrated on ground. In the GOME instrument which uses the same detectors in channels 1-4, Etalon is still shifting 2 years after launch, especially after each period of instrument switch-off. In GOME, the detectors are the only cold items and therefore any water vapour condenses there. In SCIAMACHY, the whole instrument is cooled below zero and therefore the ice deposit on the detectors is expected to be much less. In fact, on-ground calibration results suggest that the etalon is quite stable.

Since the Radiance Response function measured in the on-ground calibration already contains most of the etalon, we only need to correct for differential etalon caused by condensates in orbit.

The Etalon function is calculated separately for each channel.

### 3.6.2. Operational aspects

The default method of determining Etalon and PPG is using the WLS, since this is the only calibration source which provides a smooth spectrum from which PPG can be derived.

It is essential to obtain a very high signal-to-noise ratio. Especially for PPG correction, but also for Etalon correction at low-intensity levels (channel 1). The first tests on the instrument have shown that the WLS has low signal in the lower half of channel 1. For pixels where the signal-to-noise would be too low, no PPG can

be measured in-flight and the values from the on-ground calibration must be used. However, Etalon can still be derived from solar calibration observations, by comparing the measured solar spectrum with a reference spectrum from the literature (PPG cannot be derived because the ratio measured / reference will be very noisy due to effects of different spectral sampling and small wavelength calibration differences; moreover there may be changes in several Fraunhofer line cores due to solar activity). Both methods are grosso modo similar, but use different inputs. This feature can also be used as backup in case the WLS might fail.

To obtain the highest possible signal-to-noise, the calculation of PPG and Etalon should ideally be done after all WLS measurements from one orbit are collected and averaged into a single spectrum. However, because of the possible 'slicing' of the orbit (see Section 2.5) this is not possible.

Instead, Etalon and PPG will be calculated for each (WLS or solar) State and for each processed State the results will be written to an ADS on the level 1b product.

A switch '*do\_fraunhofer*' is implemented on the initialisation file (and carried to the Level 1b product) for each channel to prepare as calibration data either Etalon calculated from the WLS or Etalon calculated using the solar reference spectrum. Note: the on-ground calibration indicated that use of the small aperture (for Subsolar, Sun Occultation measurements) may cause additional (or better said: different) etalon structures. Therefore, etalon is not only calculated for Sun over Diffuser measurements (which is the default solar calibration) but for all solar measurements.

For PPG (and also for the determination of new bad pixels which is part of the PPG algorithm) a simple average or median (per pixel) over the States is considered to be too inaccurate for calibration purposes. Since PPG and bad pixels are not expected to change rapidly, the values from the Level 1b product *should only be regarded as diagnostics*; off-line scientific analysis over a longer period should show if modification of PPG / bad pixel calibration data is necessary. Operationally this should then not be an automatic update, but a manual exchange of the calibration data derived from the scientific analysis.

### 3.6.3. WLS preprocessing

The measured WLS spectrum is an average of all measurements in one State, excluding hot pixels and excluding the first 8 seconds of the State. The latter is to avoid changes in WLS spectrum observed during warm-up of the lamp. This average spectrum is written to the Level 1b product, together with its noise which is calculated as the RMS sum of shot noise (reduced by the averaging of the spectra) and the dark signal calibration error  $\epsilon_{SD,ij}$  which both have been calculated in Section 3.5:

$$\epsilon_{WLS_{ij}} = \sqrt{\frac{\epsilon_{shot_{ij}}}{N_{ave,ij}} + \epsilon_{SD,ij}}$$

where  $N_{ave,ij}$  is for each detector pixel the number of 'validated' spectra used to calculate the average WLS spectrum. Validated means here that the pixel is neither hot nor saturated; the noise values in the righthand side of the equation are themselves averages of the values at each single validated readout.

The hot pixel detection uses a similar algorithm as described in Section 3.4, with two modifications. The hot pixel thresholds used are different for dark and for WLS measurements: for WLS measurements they have been increased to prevent triggering on WLS signal noise. A second modification is to scale for each readout each pixel value to the average pixel value in a cluster, to compensate for thermally-induced signal drift. The scale factor is calculated as:

$$scale_{fac_{cl}}(n) = WLS_{cl}^{ave}(n) / \langle WLS_{cl}^{ave} \rangle$$

where  $WLS_{cl}^{ave}(n)$  is for each readout  $n$  the average signal in the cluster  $cl$ , and  $\langle WLS_{cl}^{ave} \rangle$  is the average over all readouts of those values.

After scaling, a pixel  $ij$  in cluster  $cl$  is flagged as hot when it exceeds the median value over the measurements:

$$\frac{WLS_{ij}(n)}{scalefac_{cl}(n)} - \text{median} \left( \frac{WLS_{ij}(n)}{scalefac_{cl}(n)} \right) > H_j$$

where  $H_j$  is the hot pixel limit for channel  $j$  in which cluster  $cl$  is located. To obtain enough statistics for the median, the hot pixel check discards only the first 4 seconds of the WLS state, instead of the first 8 seconds as for the average WLS spectrum.

No hot pixel check is performed for the PMDs, as they are not used in WLS processing.

### 3.6.4. Calculate Etalon

Note that since version 8 of the processor the etalon is calculated, but no longer applied automatically. The etalon correction is calculated once for the reference day of the new m-factors, all possible changes of the etalon are covered by the m-factors.

A fundamental question is: does one want to compensate for all changes in radiance response which manifest themselves in the WLS spectrum, or only for the Etalon component. For getting the 'best' calibration, one might be tempted to correct for everything, but this goes against the configuration control philosophy that the processor itself shall not modify the calibration data - in this sense correction for Etalon is already on the brink - without human supervision. The latter being performed using the m-factors delivered by the SOST.

Modelling of the theoretical Etalon indicates that a reasonable approximation can be found by characterising the Fourier spectrum by a main frequency and a beat frequency (modulation); the first harmonic of the two frequencies ( $f_{main} - f_{beat}$  and  $f_{main} + f_{beat}$ ) must also be taken into account.

Similar simple parametrisation of the Etalon effect was reported by users of a ground-based spectrometer for DOAS having the same detector arrays, see [35].

However, practical tests have shown that a good modelling is very difficult to achieve over the whole detector range. We therefore will use as baseline a Fourier-filtering approach, where we will try to filter out only those frequencies which can be assigned to Etalon. We have to accept that our model may not be perfect, and that Etalon residuals may remain, while at the same time an unwanted automatic correction may be made for e.g. shifts in Radiance Response which result in features on the scale of the etalon frequency.

Since we only derive the differences w.r.t. the on-ground calibration, the first step is to divide the WLS spectrum by a Reference WLS spectrum from the Calibration Key data. The Reference WLS spectrum has been corrected for memory effect and for dark signal, but contains the on-ground Etalon and PPG features.

In the Fourier-filtering technique which we will use below, it is best to start working with spectra which are as much as possible normalised to a "flat" spectrum oscillating around 0. Therefore, a linear component is subtracted from the ratio (measured WLS) / (Reference WLS). This linear component may be interpreted as a first order correction in case of changing blackbody temperature of the lamp. Before the ratioing is done, the Reference WLS is interpolated to the wavelengths of the SMR (this is the standard wavelength grid and might only be different from the actual measurements grid by an amount which is very much smaller than the typical Etalon structure), unless the flag 'do\_pixelwise' on the initialisation file is set. Before wavelength interpolation may take place, the Reference WLS must be divided by the on-ground PPG. The measured spectrum is then divided by the actual in-flight PPG from the calibration data. In addition it is divided by an M-factor for the WLS which has to correct for possible changes of a high-frequency WLS feature colloquially known as 'fast etalon'.

Accordingly, the spectrum containing the differential Etalon and PPG structures is given by:

$$\begin{aligned} S_{ij}^* &= \left( \frac{WLS_{ij}}{D_{ij}^{WLS} \cdot PPG_{ij}} \right) / \left( \frac{REF\_WLS}{PPG_0} \right) (\lambda_{ij}) \\ S_{ij} &= \frac{S_{ij}^*}{LIN_{ij}} \end{aligned} \quad (3.66)$$

where  $PPG_{ij}$  is the PPG of the in-flight calibration,  $PPG_0$  is the PPG of the on-ground calibration,  $D_{ij}^{WLS}$  is the M-factor for the WLS, and  $LIN_{ij}$  is the linear interpolation of the spectrum  $S_{ij}^*$  between two pixel boundaries, specified for each channel on the initialisation file, 'etal\_pix\_min' and 'etal\_pix\_max'; these boundaries are set to protect the fourier-filtering from trying to model rogue structures in the overlap regions (caused by overlap shifts or by incorrect stray light subtraction). The above spectrum is calculated separately for each channel. The values at the location of bad pixels are replaced by linearly interpolated values of the neighbouring pixels.

It is an on-going discussion if the spectrum above should be corrected for changes in the instrument's transmission function (using the M-factor for the channel) or not. It certainly would be better to apply such a correction first; otherwise the Etalon function derived will be a mix between 'true' Etalon and degradation, and also the derivation of Etalon might be jeopardised if strong shifts in dichroic structure in the overlaps would occur (although the latter may be corrected again by a new M-factor for the channel, but these updates are expected to be less frequent). However, using an M-factor correction before Etalon is derived requires a recalibration of the Etalon function for each M-factor update; the synchronisation of these two updates is operationally difficult. In particular, one would have to recalculate a new Etalon function using the updated M-factor, and it must be ensured that Etalon calibration file and M-factor calibration file reach the processor at the same time.

M-factor correction may be enabled by a flag 'do\_etal\_mfac' on the initialisation file. In this case, the righthand side of Equation 3.66 is divided by the M-factor for Nadir,  $M_{ij}^{DN}$ . If this flag were to be changed, a synchronised recalculation of both M-factors and Etalon function would be required.

For the backup calculation using the solar SMR spectrum, a template solar spectrum is included on the initialisation file (containing the Etalon structure of the on-ground calibration).

The following spectrum containing the differential Etalon and PPG structures is then used:

$$S_{ij} = \left( \frac{SMR_{ij}}{REF\_SOL(\lambda_{ij})} \right) / AVE_{ij} \quad (3.67)$$

where  $AVE_{ij}$  is the average value of  $SMR_{ij}/REF\_SOL(\lambda_{ij})$  between the boundaries 'etal\_pix\_min' and 'etal\_pix\_max'

The theoretical modelling of etalon shows that Etalon frequency is linear with inverse wavelength, implying that only a clean Fourier spectrum can be obtained if the spectrum is first rebinned to an inverse wavelength scale.

The first operation performed on the spectrum calculated above is therefore rebinning to an inverse wavelength scale. To each pixel  $i$  in channel  $j$  an inverse wavelength is assigned according to  $\lambda_{ij}^{inv} = 3000/(\lambda_{ij}[\text{nm}])$  and subsequently the spectrum is rebinned to an equidistant grid in inverse wavelength, whereby the total number of spectral points is retained. This rebinned spectrum is denoted as 'basis spectrum',  $SB_{ij}$ .

The filtering is done as follows: an FFT of the basis spectrum is made; all but the etalon frequencies are set to 0 by multiplication with a filter  $P_{nj}$  (see below), and this fourier spectrum is transformed back to obtain the filtered etalon spectrum:

$$S\_ETN_{ij} = FFT^{-1}(P_{nj} \cdot FFT(SB_{ij})) \quad (3.68)$$

The fourier filter  $P_{nj}$  ( $n$ =fourier frequency pixel,  $j$ =channel) is a medium-passband filter which cuts off the lowest and the highest frequencies. This filter is set to 1 for the etalon frequencies, and tapers off to 0, using a cosine function, for higher frequencies outside the etalon frequency range. The lowest frequencies should

ideally also taper off to 0 using a cosine, but here we have so few frequency points available that we make a rapid cut-off using a linear function.

If there are  $N$  points in the basis spectrum, the (complex) fourier-transformed spectrum has frequency points from  $-N/2$  to  $+N/2$ . The filter is for each channel specified on the initialisation file by 4 frequencies  $f_0$ ,  $f_1$ ,  $f_2$ ,  $f_3$ , and is defined by:

$$P_{nj} = \begin{cases} 0 & \text{for } |n| > f_3 \text{ or } (-f_0 < n < +f_0) \\ 1 & \text{for } f_1 < |n| < f_2 \\ 0.5 \cdot \left(1 + \cos\left(\pi \cdot \frac{|n| - f_2}{f_3 - f_2}\right)\right) & \text{for } f_2 < |n| < f_3 \end{cases} \quad (3.69)$$

and linear interpolation is used for the ranges  $[-f_1, -f_0]$  and  $[f_0, f_1]$

After regridding  $S\_ETN_{ij}$  back to the measurement wavelength grid we obtain the calibrated Etalon function which provides the ratio of in-flight etalon to on-ground etalon:

$$ETN_{ij} = \frac{S_{ij}}{S_{ij} - S\_ETN_{ij}} \quad (3.70)$$

A Residual Spectrum of the etalon calculation is written to the Level 1b product when the WLS is used as calibration source. This residual spectrum contains all features left uncorrected by the Etalon filtering:

$$RES_{ij} = \frac{S_{ij}}{ETN_{ij}} \quad (3.71)$$

As mentioned above, the whole procedure is only executed on a part of the spectrum specified in the initialisation file. This is to exclude the channel overlap regions, where small shifts in radiance response would cause large amplitudes in the basis spectrum with frequencies which may interfere with the range of etalon frequencies selected in our bandpass filter. Outside the region where the etalon is calculated, it is set to a value of 1.

A channel is considered saturated if 5 or more consecutive pixels are saturated. In this case no etalon is calculated, but it is set to a value of 1.0 for the whole channel. If less than 5 pixels are saturated, this is considered a 'hot pixel' event; the etalon calculation is performed with these missing pixels in the WLS spectrum linearly interpolated to the value of their nearest neighbour.

The Etalon function cannot be derived reliably anymore if the Etalon scale-length becomes a significant fraction of the wavelength coverage of a channel. This is expected to happen for channels 4 and higher. A flag '*do\_etalon*' on the initialisation file determines for which channels Etalon is calculated.

### 3.6.5. Calculate PPG

As basis for the PPG correction an averaged WLS spectrum should be used where all known low-frequency components are taken out. To this end, the Residual Spectrum from the Etalon calculation is used. Note that this may cause spurious effects near the etalon boundaries '*etal\_pix\_min*' and '*etal\_pix\_max*'.

PPG is determined by smoothing this Residual Spectrum over a number of pixels '*PPG\_smooth*' (specified on initialisation file), using a triangular kernel (preliminary width of 5 pixels):

$$PPG'_{ij} = PPG_{ij} \cdot \frac{RES_{ij}}{(RES_{ij})_{smoothed}} \quad (3.72)$$

For channels for which no Etalon was calculated, the residual spectrum is calculated from Equation 3.71 by setting there  $ETN_{ij} = 1.0$ .

Additional output from the PPG calibration is an update of the bad pixel mask. To avoid that coincidental 'hot' pixels are affecting the 'bad pixel mask' used in the processing, the mask derived in the PPG processing should

not be used to update the existing mask, but only used as diagnostic. It should need human intervention to modify the 'bad pixel mask' used in the processing.

Pixels are flagged as 'bad' if

$$PPG_{ij} \geq PPG_{bad} \text{ or } PPG_{ij} \leq 1/PPG_{bad} \quad (3.73)$$

where  $PPG_{bad}$  is a parameter on the initialisation file (preliminary value is 1.2) .

Note that only additional bad pixels can be detected here, since the bad pixels from the calibration data have been replaced by interpolated values is the calculation of  $S_{ij}$ . If such additional 'bad' pixels are found in a channel, then their values are to be replaced by interpolation as above and a final recalculation of PPG is made for that channel.

The PPG values should only be used if they are significantly higher than the noise on the WLS measurement. PPG values which are below  $3\sigma$  noise level must not be used to update the in-flight calibration database.

For this purpose the noise (standard deviation) of the WLS spectrum is written as output on the Level 1b product

$$\epsilon_{ij}^{WLS} = \sqrt{\frac{\epsilon_{shot_{ij}}^2}{N_{Ave}} + \epsilon_{S_{D,ij}}^2} \quad (3.74)$$

where  $N_{Ave}$  is the number of WLS spectra used in building the average WLS spectrum and the errors on the righthand side are calculated as in Section 3.5 (taking the average of the errors calculated for each individual measurement).

### 3.7. Apply PPG and Etalon Parameters

The PPG and the Etalon calibration data are stored in the form of (calibration) spectra. The application of these calibration parameters consist of dividing each measured pixel (the one to be calibrated) by the corresponding pixel in the PPG/Etalon calibration spectrum.

**Remark:** in principle Etalon is a wavelength-dependent phenomenon, and therefore an interpolation to the measured wavelength grid would be required. However, the Etalon frequency is  $>100$  pixels while the expected wavelength shift is  $\ll 1$  pixel. Moreover, the Etalon was derived from spectra averaged over all measurements made in the orbit, without taking into account the exact wavelength calibration (because the same spectra were used for PPG which is not wavelength- but pixel-dependent). Therefore, the wavelength dependence of the Etalon is neglected; the Etalon (i.c. the differential Etalon) is considered to be a pixel-dependent quantity.

The signal  $S_{DP,ij}$  of each pixel  $i$  in channel  $j$  of the spectrum corrected for PPG/Etalon, is calculated from the measured signal (after dark signal correction) by division of the corresponding factors:

$$S_{DP,ij} = \frac{S_{D,ij}}{PPG_{ij} \cdot ETN_{ij}} \quad (3.75)$$

The division by the etalon is not performed for SLS calibration measurements, since spectral fitting by TNO-TPD on GOME spectra showed better results if etalon correction was not performed (possibly due to the monochromatic nature of the SLS lines).

The error on PPG adds to the precision error  $\epsilon_{-}S_{ij}^D$  which has been calculated in the dark signal correction step:

$$\epsilon_{-}S_{DP,ij} = \sqrt{\epsilon_{-}S_{D,ij}^2 + (\delta_{PPG} \cdot S_{DP,ij})^2} \quad (3.76)$$

where  $\delta_{PPG}$  is a general error estimate from the initialisation file based on simulations.

For the accuracy error on etalon correction currently no value is specified; it is expected that this will remain well below the absolute calibration error on the Radiance Response function.

### 3.8. Calculate Spectral Calibration Parameters

The main objective of the spectral calibration is to assign a wavelength value to each individual SCIAMACHY detector pixel during the flight of the sensor. The algorithm uses spectra of the internal SLS, which provides narrow emission lines (quasi-infinite narrow compared to the detector pixel width) over the entire SCIAMACHY wavelength range. Somewhat problematic as far as the number of lines is concerned may be the NIR channels 6-8. If not enough good SLS lines are available there, we will use as fall-back solution Fraunhofer lines from the solar spectrum (discussed later in this Section).

The spectral calibration is described by two functions: a pre-defined 'basis wavelength' calibration and, for each channel, a polynomial which gives wavelength [nm] as function of pixel number. The basis wavelength calibration does not necessarily need to be a polynomial function. It is given as  $8 \times 1024$  values, one for each detector pixel, and the exact values were established during commissioning phase by detailed analysis of measured spectra.

The calibration parameters for spectral calibration, as calculated here, are the coefficients of the polynomial. The order of the polynomial can be specified on the initialisation file, but is not larger than 4. A problem with high order polynomials is that, towards the end of the channel, they tend to 'run away' if no spectral calibration lines are present there. This problem exists for ERS-2/GOME. To reduce this problem, the concept of the 'basis wavelength' has been introduced. The expectation is that the polynomial then needs to account only for relatively small shifts in wavelength over the orbit or during the lifetime of the instrument, and that a low-order polynomial will be sufficient for this purpose. In addition, we propose to use more spectral lines, where the low quality lines can be given a lower weight in the fit, and there is the possibility to curb the polynomial at the detector edges by introducing 'artificial spectral lines'.

Since thermal gradients in the instrument may affect the wavelength calibration, the spectral parameters are defined as function of orbit phase. To this end the orbit is divided into a number of orbit regions (at least 10, according to [2], TBD). The procedure is very similar to the one followed in Section 3.4 for the Dark Signal calibration, but the orbit regions may be differently defined (to be finalised based on commissioning phase results). Calibration results of each SLS State are written to an ADS on the Level 1b product, and one has to make a harmonic fit over orbit region.

The first step in the processing is the determination of the exact spectral line positions on the detector, and diagnostics of the lines. To this end, we use the Falk algorithm [18] which calculates line positions as a centre of gravity, and additional diagnostics such as FWHM and skewness of the lines from the second and third moment - assuming the line shape resembles a statistical distribution.

The spectrum  $S_{ij}$  is taken from the average measurement spectrum in the State, after correction for Dark Signal and PPG/Etalon. In addition, a continuum is subtracted. This continuum is a linear interpolation of the spectrum at the endpoints of the window (a straight line through the spectrum points at  $i = p(k) - w$  and at  $i = p(k) + w$ ), see Figure 3.8

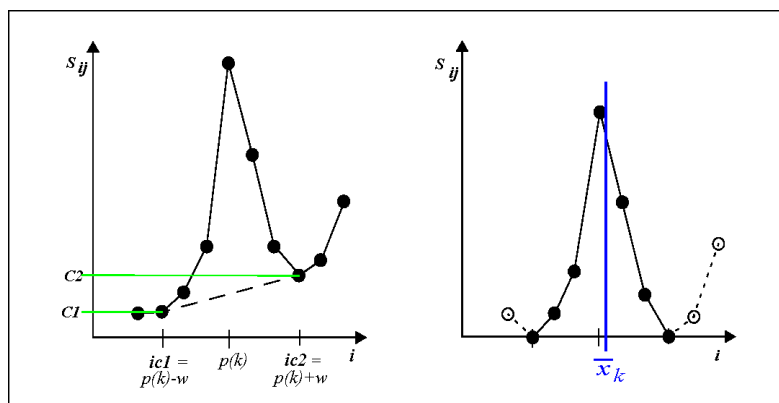


**Figure 3.8.:** Quantities used in the determination of SLS before (left) and after continuum correction (right).

The centre of gravity of a line  $k$ , around a central pixel position  $p(k)$  with a window of pixel width  $2w + 1$ , is given by:

$$\bar{x}_k = \frac{1}{N_c} \cdot \sum_{i=p(k)-w}^{p(k)+w} i \cdot S_{ij} \quad \text{where } N_c = \sum_{i=p(k)-w}^{p(k)+w} S_{ij} \quad (3.77)$$

The full width half maximum of the line is given by:

$$FWHM_k = \sigma \cdot \sqrt{2 \cdot \ln 8} \quad \text{where } \sigma^2 = \frac{1}{N_c - 1} \cdot \sum_{i=p(k)-w}^{p(k)+w} (i - \bar{x}_k)^2 \cdot S_{ij} \quad (3.78)$$

and the asymmetry or skewness by:

$$Skew = \frac{1}{N_c} \cdot \sum_{i=p(k)-w}^{p(k)+w} \left( \frac{i - \bar{x}_k}{\sigma} \right)^3 \cdot S_{ij} \quad (3.79)$$

In the equations above, the central line position  $p(k)$  is taken as the pixel with maximum intensity in the window around the position where the line is expected (which is taken for each line from the Keydata file), and the window halfwidth  $w$  is a parameter ('*line\_width*') on the initialisation file.

Lines where pixels surrounding the centre pixel are not decreasing monotonously to the outside of this window are rejected (these are noisy or double lines).

Lines which do not fulfil certain thresholds are rejected; a line must have a minimum intensity  $N_c$ , and shall not exceed a maximum in FWHM or Skewness. The thresholds are on the initialisation file (preliminary values for intensity '*LineInt\_min*' > 200 BU, for FWHM '*Linefwhm\_max*' < 5 pixels, for skewness '*LineSkew\_max*' < 6). In addition there are similar thresholds for lines which are not good but still acceptable ('*LineInt\_accep*' and '*Linefwhm\_accep*'); these acceptable lines are given a lower weight in the polynomial fit (see below)

During on-ground calibration it appeared that the SLS light is partly blocked internally in the instrument resulting in asymmetric line shapes [43]; therefore this constraint on minimum skewness will have to be relaxed. This blocking also shifts the centre of gravity; this is corrected in the polynomial fitting step.

Once the positions of all lines  $k$  in a channel  $j$  have been determined, a polynomial of order  $order_j$  (initialisation file parameter) is fitted to the line positions:

$$\text{SVD - fit : } \lambda(k) \approx \sum_{m=0}^{order_j} a_m \cdot \bar{x}_k^m \quad (3.80)$$

where the  $a_m$  are the sought polynomial coefficients, and  $\lambda(k)$  are the vacuum wavelengths of the lines, corrected for the shift due to blocking of the SLS light path (each line may have its own shift), and with the 'basis spectrum' subtracted:

$$\lambda(k) = \lambda_0(k) + sh(k) - \Lambda(k)$$

where  $\lambda_0(k)$  and  $sh(k)$  are the true line wavelengths and their blocking shift, respectively (both on the Keydata file under parameter name SPEC\_LINE), and  $\Lambda(k)$  are the wavelengths of the basis spectrum interpolated to the line positions  $\bar{x}_k$ .

In order to prevent run-away of the wavelength fit towards the edges of the channel, two artificial lines are added near the overlap regions in the channel; their exact pixel position is specified on the initialisation file ('*Add\_ovl\_pix*'). They are assigned the same wavelength difference w.r.t. the basis spectrum as their nearest SLS line.

The SVD fit uses weights which are taken as 1 over “standard deviation” specified on the initialisation file. Good lines get the standard deviation ‘*Sigma\_good*’, acceptable lines (see above), ‘*Sigma\_accep*’, artificial lines ‘*Sigma\_artif*’ (all parameters specified per channel). Artificial lines can be effectively removed from the fit by setting ‘*Sigma\_artif*’ to a large number.

A quality check is made on the fitted coefficients. This includes:

- If lines deviate more than a preset value ‘*Wv\_line\_tol*’ times ‘*standard deviation*’ (see above) from the polynomial, the line with the largest deviation shall be discarded and the fitting step shall be repeated.
- If the number of remaining lines is smaller than  $1 + order_j$ , reduce the  $order_j$  by 1. The number of lines used,  $n_j$ , is written as quality parameter to the level 1b product.
- Check whether the wavelengths at the start and at the end of each channel are within a predefined range. Otherwise, the calibration is discarded (on the Level 1b product, the ADS will contain spectral parameters which are zero with a wavelength calibration error set to  $-1$  for the channel).

The mean wavelength calibration error for channel  $j$  is calculated as:

$$\epsilon_j = \frac{1}{n_j \cdot \sqrt{n_j - order_j}} \cdot \sum_{k=1}^{n_j} \left| \lambda(k) - \sum_{m=0}^{order_j} a_m \cdot \bar{x}_k^m \right| \quad (3.81)$$

For monitoring purposes, the line positions  $\bar{x}_k$  of the first, centre, and last line in the channel (excluding the artificial lines) will be written to the level 1b product as diagnostics.

### 3.8.1. Using Fraunhofer lines

Spectral calibration parameters will not be calculated from the SLS only, but also from the solar calibration spectrum using the Fraunhofer lines in the spectrum.

The default will be to use for calibration the SLS results, and to use the results from the solar spectrum only as diagnostics or as backup for failing SLS. The choice for using SLS or solar data is governed by a flag in the initialisation file ‘*Do\_Fraunhofer*’. The flag is used to select the parameters for spectral calibration. Note that spectral in-flight calibration parameters from the solar spectrum can be calculated only once per orbit, and these results are to be applied to all orbit regions.

The algorithms when using the SMR are in principle very similar to those used for the SLS; differences are:

- for the SMR, which contains absorption instead of emission lines, we invert the spectrum i.e. instead of (spectrum – continuum) we take (continuum – spectrum) to obtain “emission” lines.
- The continuum level is not calculated only from the intensities at the start and end points of the window, but from average intensities from a small region of width  $2 \cdot cw + 1$  pixels outside these points;  $cw$  is given on the initialisation file for each channel (‘*ContWid\_Fraun*’).
- doppler shifts and a possible wavelength shift of the line due to convolution of the solar spectrum with the SCIAMACHY slit function have to be taken into account; these pre-calculated shifts are on the initialisation file, and are used like the SLS blocking shifts.

The wavelengths  $\lambda(k)$  to be fitted for the polynomial are then given by:

$$\lambda(k) = \lambda_{F,0}(k) + sh_F(k) - \Lambda(k) + D_{500} \cdot \lambda_{F,0}(k)/500$$

where  $\lambda_{F,0}(k)$  and  $sh_F(k)$  are the true centre wavelengths of the Fraunhofer lines and their shifts, respectively (both on the Keydata file under parameter name FRAUNH\_LINE), and  $D_{500}$  is the doppler shift at 500 nm as calculated from Equation (3.30) on page 43.

### 3.8.2. Additional quality control parameters

It is foreseen in a later update of the software to check the spectral calibration parameters for each measurement State by correlating the measurement spectrum (average over state, or last 'largest groundpixel' of a state) to a theoretical spectrum. The residues will not be used for correcting the spectral calibration coefficients on the level 1 product, but room has been left on the product for a maximum of 20 spectral residues ('errors') per channel. These could be used e.g. in level 2 processing as pre-calculated DOAS shift. The calculation method is still TBD.

### 3.8.3. Doppler shifts

The limb spectra and solar spectra will be doppler shifted due to the motion of the spacecraft in the direction of the light source. For Limb spectra, these shifts vary from minimally 0.0053 nm in channel 1 ( $\approx 0.05$  detector pixel) to maximally 0.053 nm in channel 8 ( $\approx 0.5$  detector pixel). For solar spectra, the maximum doppler shift in channel 8 is 0.047 nm (for the average solar azimuth angle of  $30^\circ$ , there is an annual variation of up to  $\pm 9\%$ ).

This does not in any way influence the wavelength calibration of the instrument as such; the wavelength of each pixel for calibration parameters such as Mueller matrix elements or Radiance Response function is given in the instrument reference frame, not in the moving atmospheric (solar) reference frame.

Therefore, the wavelength calibration on the level 1b product is in the instrument rest frame only.

It may be considered to give users an option in the application of the calibration, during level 1b to 1c processing, to apply the doppler shift to their spectra. For the limb spectra, the variation in viewing direction is insignificant (maximum difference 0.001 nm shift at 2400 nm); one doppler shift can be used for all measurements. For the solar observations, the doppler shift is calculated from the average viewing angles in the State; the variation in angles over the State yields a negligible variation ( $< 2\%$ ).

### 3.9. Apply Spectral Calibration Parameters

The application of the spectral calibration coefficients consists of creating an array with wavelengths, indexed to pixel number. This is in fact the only calibration which does not apply to the measured signals.

Wavelength calibration is required for the final presentation of the calibrated measurements on the level 1c product, and for other calibration steps which involve wavelength-dependent calibration data; notably Straylight, Radiance Response, Polarisation sensitivity, and BSDF calibration.

The spectral calibration parameters are sensitive to the temperature (-gradients) of the optical bench. Therefore they have been derived for several intervals in the orbit, as function of the orbit phase after eclipse,  $\phi_{orb}$ .

Since the shifts in wavelength calibration are expected to be very small, no interpolation of wavelength calibration parameters to orbit phase is made; the same values are taken within one orbit region for which a set of spectral parameters is derived. If a State crosses an orbit region, the orbit region of the middle of the State is taken.

The wavelength of each detector pixel  $i$  in channel  $j$  is given by:

$$\lambda_i(j) = \Lambda_{ij} + \sum_{m=0}^{order_j} a_m(j) \cdot i^m \quad (3.82)$$

where the  $a_m$  are the polynomial coefficients, and  $\Lambda_{ij}$  are the wavelengths of the basis spectrum.

It may be considered to give users an option during level 1b to 1c processing, to apply a doppler shift to the spectra (limb, solar modes). This is not foreseen in the present version of the software.

## 3.10. Determine Spectral Straylight

When light of a particular wavelength is offered to SCIAMACHY, this light will not only be sensed by those detector pixels representing this particular wavelength, but also to some degree by other surrounding pixels. The light measured by these other pixels is called spectral stray light.

Two main classes of stray light may be discerned. Specular reflections off optical components yield so-called ghost images when they are more or less focused on the detector array. Diffuse scatter inside the instrument yields a slowly varying or nearly uniform stray light across a detector array. In principle, transfer of light is also possible between different channels in the instrument. In SCIAMACHY, this is observed in channel 8 which carries a ghost from channel 7 (although this seems to be electrical cross-talk, not optical), and in channel 1 which receives a small amount of light from all other channels - since the detector in channel 1 is insensitive to infrared light only stray light from channels 2-5 needs to be taken into account here.

The stray light is partially dependent on the polarisation of the light, especially ghosts which are reflected from polarising optics. The algorithm proposed by the calibration plan requires the knowledge of the fractional polarisation values  $Q$  (see Section 3.13, note the comments on the iteration between spectral stray light and polarisation determination algorithm).

Note that in order to calculate the stray light spectrum, we need at least one complete channel (several complete channels in case of inter-channel stray light/crosstalk). However, at times only one cluster may be available. If no complete spectrum is available in the readout being processed ( $IT_{current}$ ), use the next available complete spectrum - which at least is present after each period of time covering the longest integration time in the channel(s). Then obtain an estimate of the missing detector readouts for  $IT_{current}$  by scaling the measured intensity from this complete spectrum. The scaling factor is calculated from the integrated intensity (integral over detector pixels in the channel and co-adding of readouts over integration time) in the clusters available at  $IT_{current}$ .

In the processing we discern three cases of stray light which each have their own Calibration Keydata. For channels 2-8 we have:

- uniform stray light (key data is one stray light matrix per channel)
- ghost stray light (key data are for each ghost its intensity, parent/ghost pixel positions, ghost width)

Straylight is calculated per channel, by adding up the uniform component plus all ghosts in the channel.

In addition there is:

- channel 1 stray light (key data are, for 2 polarisation directions, stray light coefficients for several wavelength intervals originating from channels 1-5).

### 3.10.1. Uniform stray light

The stray light component for pixel  $i$  in channel  $j$  is in principle calculated by multiplying the measured spectrum (complete range!) with a  $8192 \times 1024$  stray light matrix. Since processing of the full matrix is inhibitive slow, this matrix multiplication is performed only for a subset of pixels (typically every third pixel, depending on key data input) and the stray light spectrum is then interpolated from the subset pixel grid to the full pixel grid. Calculation on a subset of pixels has the drawback that sharply focussed ghosts cannot be accounted for. For this reason, the stray light calculation is split in a slowly varying uniform component, and an additional ghost component. For more information, see [29].

Following the definition of the key data, the matrix multiplication is performed by multiplying and summing the columns of the matrix with the pixel vector: this is equivalent to the usual definition of matrix multiplication using the transpose of the stray light matrix. The pixel numbers which define the pixel subset are given under the '\_LIST' keyword in the uniform stray light key data.

The key data contain one matrix for the whole spectral range. Before processing the measurements, this matrix is split into 7 submatrices for each channel (3-8). The matrix size is reduced by removing unnecessary zeros from the submatrices. For computational simplicity, all submatrices have the same dimension. All leading zeros

are removed, but trailing zeros may be present for channels with the lesser number of non-zero elements. The first dimension (nr. of columns = nr. of output pixels  $n_{out}(j)$ ) is split according to which pixels from  $list\_samp\_1$  lie in channel  $j$ . The second dimension (nr. of rows = nr. of input pixels  $n\_samp(j)$ ) is determined by the range where the matrix elements for this channel are nonzero:

- For each of the  $out\_dim(j)$  output pixels find the minimum and maximum pixel number where  $M\_kd\_all$  is larger than 1.e-15.
- The smallest minimum and the largest maximum define the range of  $n\_samp(j)$  input pixels.

Let  $l$  and  $m$  denote the row and column indices of the stray light matrix  $M$ , then the stray light vector on the output grid, for channel  $j$ , is given by:

$$S_{unif\_samp_m}(j) = M^T \cdot s = \sum_{l=0}^{n_{out}(j)} M_{lm} \cdot s_l \quad (3.83)$$

where  $M$  is shorthand for  $M_{unif}(j)$  and  $s_l$  are the elements of the vector with input signals on the input grid, where each element  $l$  is the signal integrated (binned) between  $list\_inpix\_start(j)_1$  and  $list\_inpix\_end(j)_l$ . Index  $m$  ( $m = 0 - n_{out}(j) - 1$ ) denotes number in the output pixel subset.

The stray light vector is then divided by the output bin size and linearly interpolated from the subset grid to the full pixel grid:

$$S_{unif_{ij}} = \text{interpolate(array)} S_{unif\_samp_m}(j) / \text{DERIV}(list\_outpix(j)_m) \text{ to pixel } i$$

where the DERIV function denotes the pixel spacing between the elements of  $list\_outpix(j)$ .

### 3.10.2. Ghost stray light

The ghost stray light is calculated for a number of ghosts (< 20) specified on the key data file. In the following, we use the terminology 'ghost' to indicate a more or less focused beam of stray light on the detector, which originates from light of a certain wavelength or wavelength interval. The location on the detector corresponding to the direct beam of this light (i.e. the pixel positions given by the spectral calibration of the corresponding wavelengths) is called the 'parent' of this ghost.

For each ghost  $n$  the following information is present on the key data file (note: for pixels related to the ghost we use indices  $i$ , for pixels related to its parent we use indices  $k$ ; all pixel positions here are counted from 1 to 8192):

- an identification number. An integer number  $n$  denotes an unpolarised ghost, a number  $n.1$  a s-polarised ghost and a number  $n.2$  a p-polarised ghost
- the start- and end pixels of the ghost,  $ig1(n)$  and  $ig2(n)$
- the start- and end pixels of the parent,  $kp1(n)$  and  $kp2(n)$ . In the current algorithm this information is not necessary, but it may be used to check if the ghost needs the parent spectrum in its own channel, or that it needs the signal from another channel (i.c. the ghost in channel 8 which needs the signal in channel 7)
- the pixel position of the ghost as polynomial function (order 2) of the parent pixel, with polynomial coefficients  $CP(n, m)$ ,  $m = 0 - 2$
- the ratio of ghost intensity  $S_{ghost_{ij}}(n, ig)$  at pixel  $ig$  to parent signal  $S_{kj}(n, ip)$ , given as polynomial function (order 3) of the parent pixel  $kp$  by polynomial coefficients  $CI(n, m)$ ,  $m = 0 - 3$
- the width of the ghost  $w(n)$

Note that the key data give the ghost position as function of the parent position. However, we wish to calculate the stray light for each (ghost) pixel in the channel, and therefore we must invert this relation to find the position of the parent as function of the position of the ghost, i.e. we must find for each pixel  $ig$  the value of  $kp$  by finding the root of the 2nd-order polynomial function

$$\left\{ \sum CP(n, m) \cdot kp^m \right\} - ig = 0$$

The root of this equation, denoted by a fractional pixel value  $x_p$ , can be analytically solved as:

$$x_p = \frac{\sqrt{CP(n, 1)^2 - 4 \cdot CP(n, 2) \cdot [CP(n, 0) - ig]} - CP(n, 1)}{2 \cdot CP(n, 2)} \quad (3.84)$$

unless  $CP(n, 2) = 0$ ; in that case we have a linear relationship and

$$x_p = \frac{ig - CP(n, 0)}{CP(n, 1)} \quad (3.85)$$

and this relation is also used in case the argument in the root becomes negative (for border pixels).

The ghost stray light can then be calculated as:

$$S_{ghost_{ij}}(n, ig) = F_{pol, kj} \cdot S_{kj}(n, kp) \cdot \sum_{m=0}^3 CI(n, m) \cdot x_p^m \quad (3.86)$$

where a correction factor for polarisation is included, given by:

$$F_{pol, kj} = \begin{cases} 1.0 & \text{for unpolarised ghosts} \\ 0.5 \cdot (1 + Q_{kj}) & \text{for p - polarised ghosts} \\ 0.5 \cdot (1 - Q_{kj}) & \text{for s - polarised ghosts} \end{cases}$$

where  $Q_{kj}$  is the fractional polarisation calculated for the parent pixel  $kp$ .

The fractional polarisations above are only be significant for Nadir and Limb/Occultation observations; for all other measuring modes one can set  $Q_{kj} = 0$ . For the accuracy required in the stray light application is considered sufficient to take  $Q_{kj}$  as one value per channel. For this we use the value of the PMD located in that channel:

$$Q_{kj} = Q_{X, t}$$

where  $X$  denotes PMD- A, B, C, D, E, F, F for channels 2, 3, 4, 5, 6, 7, 8, respectively.

If a polarisation point is invalid,  $\epsilon_{-}Q_{X, t} = -1$ , then set  $Q_{kj} = 0$ .

For each ghost, the ghost intensity in the channel in which it is located is set to 0 outside the region where  $ig \in [ig1(n), ig2(n)]$ .

The ghost intensity spectrum  $S_{ghost_{ij}}(n, ig)$  is lowered in spectral resolution if  $w(n) > 1.0$ . In this case the ghost intensity spectrum is convolved with a triangular kernel with a FWHM of  $w(n)$  pixels; this kernel has the form  $K = [1, 2, \dots, w(n) - 1, w(n), w(n) - 1, \dots, 1]/T$  where  $T$  is the total (the sum over all  $2 \cdot w(n) - 1$  elements) of the kernel (when during the convolution elements of the kernel extend beyond the edges of the interval  $[ig1(n), ig2(n)]$  those elements of the convolution kernel are (temporarily) set to 0).

As last step in the calculation, the (convolved) ghost intensities are added for each channel.

### 3.10.3. Channel 1 stray light

The stray light spectrum in channel 1 is calculated as the sum of a set of filter constants multiplied with the total parent signal in a wavelength range corresponding to the filter.

On the key data file, the filter coefficients  $FC(i, f)$  are given as 1026 numbers per filter, corresponding to 1024 filter coefficients for each ghost pixel  $i$  (from 0-1023) plus the start- and end pixel numbers of the wavelength region covered by the parent (all filters except the last are located in channel 1 itself; only the last one covers channels 2-5). The filters are given alternating for s and p (there is always approximately, but not exactly, the same wavelength range for each s,p filter).

As the parent signal can be transferred to several filters, and no filter is preferred over the other, we divide the parent signal by the number of filters to which it is associated. This is done separately for the filters belonging to each polarisation.

The number of times a parent signal on pixel  $kj$  is used is, for p polarised light, given by

$$Np_{kj} = \sum_{f=0}^{n_{filter}-1} \begin{cases} 0 & \text{if } kj < kpp1 \text{ or } kj > kpp2 \\ 1 & \text{if } kpp1 \leq kj \leq kpp2 \end{cases}$$

and for s polarised light given by

$$Ns_{kj} = \sum_{f=0}^{n_{filter}-1} \begin{cases} 0 & \text{if } kj < kps1 \text{ or } kj > kps2 \\ 1 & \text{if } kps1 \leq kj \leq kps2 \end{cases}$$

The stray light spectrum in channel 1 is then calculated as:

$$S_{ch1_{ij}} = \sum_{f=0}^{n_{filter}-1} \left( \left\{ FC(i, fp) \cdot \sum_{k=kpp1}^{kpp2} \frac{S_{kj}}{Np_{kj}} \cdot \frac{1+Q_{kj}}{2} \right\} + \left\{ FC(i, fs) \cdot \sum_{k=kps1}^{kps2} \frac{S_{kj}}{Ns_{kj}} \cdot \frac{1-Q_{kj}}{2} \right\} \right) \quad (3.87)$$

where:

$$\begin{aligned} fp &= 2 \cdot f & , & & fs &= 2 \cdot f + 1 \\ kpp1 &= FC(1024, fp) & , & & kpp2 &= FC(1025, fp) \\ kps1 &= FC(1024, fs) & , & & kps2 &= FC(1025, fs) \end{aligned}$$

### 3.10.4. Straylight parameters on the Level 1b product

In order to save space on the Level 1b product, the amount of stray light for each pixel is coded into an 8-bit integer. This implies that the values can range from 0 to 255. Units of this stray light spectrum are 1/10 BU. Straylight levels larger than 25.5 BU are accounted for by an 8-bit scaling factor so that all intensities between 1/10 and 6202.5 BU can be accommodated. To save storage space, this factor is given as one value per channel for each State; the factor is written into an ADS ('States of the Product').

For each channel and for each State the scaling factor is derived so that

$$\text{stray light}_{calculated} [\text{BU}] = \text{stray light}_{coded} [\text{BU}/10] \times \text{scaling\_factor}.$$

The minimum scaling factor is 1 which can accommodate stray light levels up to 25.5 BU with an accuracy of  $\pm 0.05$  BU. For higher stray light levels up to 51 BU the accuracy is reduced to  $\pm 0.01$  BU and so forth. This reduced accuracy is not considered a problem since the accuracy on the stray light calibration Key Data is expected to be not significantly better than 5-10%.

### 3.11. Apply Straylight Correction

This comprises simply subtracting the calculated amount of stray light per pixel from the measurement.

In level 1b to 1c processing also an un-coding of the 8-bit integers on the level 1b product for (coded) stray light and stray light scaling has to be made according to

$$S_{stray}[BU] = \text{straylight\_coded}/10 \times \text{scaling\_factor}$$

The error on the signal due to stray light subtraction is a precision error. This error is added to the precision error  $\epsilon_{S_{DP,ij}}$  which has been calculated in the dark signal correction and PPG correction steps:

$$\epsilon_{S_{DPS,ij}} = \sqrt{\epsilon_{S_{DP,ij}}^2 + (\delta_{stray} \cdot S_{stray})^2} \quad (3.88)$$

where  $\delta_{stray}$  is a general error estimate from the initialisation file, based on the errors on the stray light calibration Key data, the expected errors on polarisation, and the expected errors due to incomplete channel availability.

## 3.12. Apply BSDF and calculate SMR

This section describes the processing of solar calibration spectra, the application of diffuser BSDF to obtain the SMR, and the calculation of out-of-band PMD signal.

### 3.12.1. Introduction

SCIAMACHY takes at regular intervals solar calibration spectra, in the sunrise part of the orbit. An on-board diffuser can be switched into the light path during sun calibration, to scatter the collimated solar light (irradiance) into a diffuse (radiance) beam. Obviously, the solar spectrum thus recorded must be corrected for the characteristics of this diffuser. That correction is made by dividing the detector signals of the measured solar spectrum by the BSDF function of the diffuser (more precisely, what we calculate as 'BSDF' is actually the reflectivity of the azimuth mirror/diffuser unit, which corresponds to one viewing direction out of the BSDF's 2-dim 'reflectivity space').

The diffuser is mounted on the back side of the elevation scan mirror, and is illuminated via the azimuth mirror (as in Limb mode, but with different scan mirror angles). The calibrated BSDF of the diffuser is a (smooth) function of azimuth and elevation of the incoming and outgoing light beam, and of wavelength. The BSDF depends not only on scan mirror angles but there is also a strong dependence on the solar elevation angle. The BSDF has been calibrated only for one elevation mirror angle (this is the default angle to be used in operations), so that in practice it depends on two angles: the ASM angle and the solar elevation angle.

As additional complication, polarisation introduced by the azimuth scan mirror brings the polarisation sensitivity of the optical bench into the equation. For this reason we cannot cleanly separate the BSDF and optical bench response functions, as is often possible in other spectrometers (e.g. GOME, SBUV); this interrelationship is expressed by Equations 3.3 and 3.12. This module therefore also includes application of the Absolute Radiance Response to the solar calibration spectra, even though a similar function for the scanning measurements is implemented elsewhere.

Also corrected for BSDF are the average PMD integrals on the Sun Reference Spectrum ADS, as their purpose is to be used for normalisation of Nadir/Limb PMD measurements.

A function which is also not directly related to application of the BSDF, but which is implemented here because it needs the solar calibration spectrum, is determination of the so-called out-of-band signal of the PMDs. Background of this is the following: the polarisation correction algorithm needs the ratio of PMD- to channel signals. This implies that the wavelength coverage of the PMDs must be contained in the wavelength coverage of the array detectors. This is certainly not the case for PMD-F which has  $\approx 15\%$  of its bandwidth beyond the channel 8 wavelengths. The missing part is, for a solar input spectrum, calculated here using the expected PMD signal based on PMD/channel sensitivities. This missing part implicitly also accounts for any PMD out-of-band stray light, and for inconsistencies in PMD/channel calibration.

#### Additional measurements and calibrations:

Since the calibration has shown that there are several problems with the standard diffuser calibration (in particular the occurrence of high spectral frequency oscillations [48], a Sun Reference will also be calculated for other Sun measurement modes; particular relevant are measurements using the new (but uncalibrated) diffuser on the backside of the ASM. Sun reference spectra are also generated for direct solar observations using the small aperture and NDF, although these may be of limited scientific value and are more intended for instrument monitoring: these use the solar occultation and subsolar modes. For each solar measurement State which is processed, an ADS with Sun Reference is generated on the Level 1b product. Note that only the standard diffuser can be absolutely calibrated; other measurements modes will receive an approximated irradiance calibration and can only be used as relative references.

As of IPF version 6, for each ADS with (approximative) irradiance calibration, a second ADS is generated which contains the solar mean reference spectrum without irradiance calibration (the factor  $M_1$  in Eq. 3.89 and 3.92).

The various measurement modes are identified by a single character on the ADS (field 3). The following table applies:

	Fully Calibrated	No Radiometric Calibration
<i>Diffuser (ESM)</i>	D	E
<i>Diffuser (ASM)</i>	D	A
<i>Occultation</i>	O	U
<i>Sub-solar</i>	S	V

**Table 3.2.:** *Solar spectrum Identifiers on the ADS.*

Calibration has also indicated that for the Sun diffuser mode channels 3 and 4 go partly into saturation. For this reason the default Sun diffuser mode will use a neutral density filter, while the mode without NDF is only carried out monthly.

The on-ground calibration has also shown that a different Etalon is likely to exist for Nadir/Limb measurements and for measurements using the small aperture (Occultation, Subsolar) or the Sun diffuser. For this reason an Etalon will also be calculated (after the correction for the regular Etalon function which is valid for Nadir/Limb), see Section 3.6.

In the processing, the first and last spectrum are discarded, because of anomalies (unknown memory effect and moving scan mirror, respectively).

The various Sun Reference spectra which are calculated will be written to an SMR calibration file (one record for each Sun Reference). The first record will contain the SMR of the standard diffuser, as this is the only one with an absolutely calibrated irradiance. All calibrations in level 0 to 1b processing needing the SMR will use this first record (the others may be used for e.g. DOAS applications in level 1b>2 processing or for instrument monitoring).

### 3.12.2. Solar Mean Reference spectrum from Sun diffuser measurements

The Solar Mean Reference spectrum (SMR) is calculated as the average of all spectra in the solar calibration State, corrected for the instrument's irradiance response - a combination of the radiance response function and BSDF, as calculated in Equation 3.3, 3.12 and 3.13.

The various spectra of this sequence differ from each other because they are measured with slightly different azimuth scan mirror angle and solar elevation angle. As there is a strong dependence on solar elevation angle, the spectra should first be corrected for irradiance response and then averaged.

The spectra are corrected for dark signal, PPG, Etalon, Straylight in the usual way. To obtain the SMR the spectra should be divided by the irradiance response and then averaged. Since there is a large number of readouts in this State we limit the number of calculations by making a pre-averaging of spectra over a time  $T_{Ave}$  (this is a parameter on the initialisation file; the value is currently 5 seconds).

Since the dependence of the irradiance response on ASM angle is small, we calculate irradiance response values for the average ASM angle in the State, and for the average of the Solar Elevation Angle at each pre-averaged measurement.

The Solar Mean Reference spectrum (in units photons/(m<sup>2</sup>.nm.s) is then given by:

$$SMR_{ij} = \frac{1}{N_{pre}} \cdot \sum_{m=1}^{N_{pre}} \frac{\langle SD_{ij} \rangle_{pre}(m)}{M_{1,ij}^{irrad}(\alpha_{SEL}(m))} \quad (3.89)$$

where  $\langle SD_{ij} \rangle_{pre}(m)$  are the pre-averaged spectra, corrected for Dark Signal, PPG, Etalon, Straylight, and normalised to an integration time of 1 second.

The relative precision error on the SMR is calculated as the RMS sum of shot noise (reduced by the averaging of spectra) and the precision errors after stray light correction:

$$\epsilon_{\_SMR,ij} = \sqrt{\left\langle \frac{\epsilon_{\_SDPS,ij}}{t_{PET} \cdot f_{Coadd}} \cdot \frac{1}{SD_{ij}} \right\rangle^2 + \frac{1}{N_p} \cdot \left\langle \frac{\epsilon_{\_shot_{ij}}}{t_{PET} \cdot f_{Coadd}} \cdot \frac{1}{SD_{ij}} \right\rangle^2} \quad (3.90)$$

where  $N_p$  is the number of spectra ; the errors in the righthand-side of this equation are averages over the individual measurements of the absolute errors calculated in Equations 3.76, 3.65 respectively, divided by the measured signals (to convert from absolute to relative errors).

The accuracy error on the irradiance response is calculated from the precision and from the calibration Key Data error  $\epsilon_{\_M_{1,ij}^{irrad}}$  :

$$\Delta_{SMR,ij} = \sqrt{\epsilon_{SMR,ij}^2 + \left( \frac{\epsilon_{\_M_{1,ij}^{irrad}}}{\frac{1}{N_{pre}} \cdot \sum_{m=1}^{N_{pre}} M_{1,ij}^{irrad}(\alpha_{SEL}(m))} \right)^2} \quad (3.91)$$

### 3.12.3. Solar Mean Reference spectrum from other measurements

An average spectrum  $SD_{ij}$  is built, which is corrected for dark signal, PPG, Etalon, Straylight in the usual way, and which is normalised to an integration time of 1 second. For Sun Occultation measurements, only the last spectra in the state are used, starting with the first measurement above a tangent height of 105 km (note that, as the measurements are scanning over the sun, this implies that also a few measurements may be used where the sun is sampled below 105 km). For Sub-solar measurements, all spectra are used.

The SMR with rough intensity calibration is then calculated by dividing this spectrum by an 'appropriate' radiance response function:

$$SMR_{ij} = \frac{\langle SD_{ij} \rangle}{M_{1,ij}} \quad (3.92)$$

For Occultation mode, the radiance response is taken as the radiance response for Limb measurements for the average ASM and ESM angles in the State. For Subsolar mode, the radiance response for Nadir at the null angle  $\alpha_0$  is taken.

The precision of the SMR is calculated as described above for Sun Diffuser measurements. The accuracy on the level 1b product is set to  $-1$  as no absolute calibration is made.

### 3.12.4. Calculation of average PMD signals

For solar measurement modes which do not use the diffuser, average PMD signals for the Level 1b product are simply calculated as the average of the PMD integrals in the State, multiplied by 32/40.

For Sun Diffuser measurements, the PMD signals must first be corrected for BSDF. A problem in correcting the PMDs for BSDF, is that in the PMD measurement the BSDF is integrated over the PMD's spectral bandwidth, weighted with the solar spectrum intensity.

This intensity-weighted integrated BSDF is calculated using the calibrated PMD-to-channel response of the 'PMD virtual pixels'; one time with and one time without BSDF function.

This BSDF calculation uses an auxiliary quantity, which we refer to as the 'PMD in-band signal'. This quantity is also used to calculate the 'out-of-band signal of the PMDs' on the Level 1b product.

The PMD-equivalent signal is calculated from the channel signals (after memory correction) using the 'PMD virtual sum' expression from Equation 3.103 in Section 3.13.2. Since the Sun is unpolarised, we can set  $Q = U = 0$  in this equation, and obtain for each pre-averaged spectrum without BSDF correction:

$$IB_j = \sum_{i=i\_start(j)}^{i\_end(j)} \langle SD_{ij} \rangle \cdot RM_{1,OBM}^{P,D} \cdot \frac{mf_{OBM}^P \cdot M_{1,j}^P}{mf_{OBM}^D \cdot M_{1,j}^D}$$

For PMD45 the key data  $RM_{1,OBM}^{P,D}$  must be replaced with  $RM_{1,OBM}^{P45}$ . We refer to this quantity as the PMD in-band signal.

The average PMD signals [BU] on the level 1b product are calculated from the time series of (synchronised) PMD integrals, which have been pre-averaged like the corresponding solar measurements which passed the pair-wise intensity test:

$$\langle S_{PMD,j} \rangle = \frac{32}{40 \cdot N_{pre}} \cdot \langle I_{PMD,j} \rangle (m) \quad (3.93)$$

### 3.12.5. Calculation of out-of-band PMD signal

The out-of-band signal accounts for light measured by the PMD in spectral regions outside the corresponding channel (e.g. the response of PMD-F above 2383 nm, or stray light contamination in the PMDs), but it also accounts for e.g. degradation in the (PMD or channel) optics not corrected by the M-factors.

The out-of-band signal of the PMDs is calculated as the relative difference between the measured PMD signal and the PMD signal expected on the basis of the channel signals:

$$OB_j = 1 - \frac{IB_j}{40 \cdot \langle S_{PMD,j} \rangle} \quad (3.94)$$

where the factor 40 converts from BU to BU/s.

### 3.12.6. Calculation of the Doppler-shift at 500 nm

For Subsolar measurements, the Doppler-shift is 0.

For Solar occultation measurements, the Doppler-shift is calculated from the average azimuth and elevation scan angles in the State, as described by Equation (3.30) in Section 3.2.

For Sun diffuser measurements, it is calculated similarly, but replace the scan angles by the solar angles on the diffuser, as described below Equation (3.30) in Section 3.2 .

## 3.13. Determine Fractional Polarisation Values

### 3.13.1. Introduction to polarisation measurements

The signals measured by SCIAMACHY are not only dependent on the intensity of the incoming light, but also on its polarisation, due to the polarisation-sensitive transmission of the optics. The light reflected by the Earth and its atmosphere may be linearly polarised; its amount of circular polarisation is negligible. Polarisation is especially strong in the UV below 300nm, where the light originates from pure Rayleigh scattering at heights above  $\approx 20$  km in the atmosphere: ozone absorption prevents a deeper penetration of the sunlight through the atmosphere at these wavelengths. Above 300 nm light can reach the ground; the longer the wavelength, the larger the fraction of (unpolarised) sunlight reflected by the Earth's surface or by clouds can be. The degree of polarisation shows a steep decline from 300 nm to the end of the strongest O3 Huggins absorption band at around 320-330 nm [34, 33, 27]. At longer wavelengths the polarisation properties are increasingly determined by aerosol scattering and surface (cloud) reflection properties.

The polarisation correction algorithms described in this ATBD make use of these facts: below  $\approx 300$  nm a Rayleigh scattering model is used, and in the transition region around 300-330 nm SCIAMACHY polarisation measurements are fitted to a functional form describing the steep decline in degree of polarisation. This is an useful adjunct to the polarisation values derived from SCIAMACHY measurements, since the first available measurement point is the first overlap (around 312 nm) and the next measurement point (PMD-A) has an effective wavelength near 350 nm.

For purposes of radiative transfer calculations it is common to take a representation in terms of Stokes parameters, which describe the light as a vector  $(I, Q, U, V)$ . This representation depends on a definition of co-ordinate frame, but is the most convenient one to use for describing the polarisation properties of the SCIAMACHY instrument. For details see the introduction in Section 3.1 on page 25.

In our algorithms we use, instead of the Stokes parameters themselves, the parameters normalised to intensity  $I$ ; these normalised parameters we denote 'Stokes fractions' and as shorthand we will from here onwards write  $Q$  for  $Q/I$  and  $U$  for  $U/I$ .

Another widely used representation of polarisation is in terms of a degree of polarisation,  $P$ , and a polarisation angle,  $\chi$ . The advantage of this representation is that  $P$  is a quantity which is independent of any co-ordinate frame used.

The conversion between  $P, \chi$  and the Stokes fractions (i.e. the Stokes parameters normalised to intensity)  $Q, U$  is given by:

$$P = \sqrt{Q^2 + U^2}$$

and

$$\chi = \arctan\left(\frac{U}{Q}\right)$$

Since the application of the radiance sensitivity parameters of the radiometric calibration assumes an unpolarised input (atmospheric spectrum), a Polarisation Correction Algorithm (PCA) has to transform the measured signal, which depends on a fractional polarisation of  $Q(\lambda)$  and  $U(\lambda)$ , to the signal which would have been measured for unpolarised light (for which  $Q = U = 0$ ) of the same intensity.

For SCIAMACHY, there are 11 wavelength regions which are covered by at least two detectors having different polarisation sensitivities - thereby allowing for a determination of the input polarisation. These are

- (a) the six general Polarisation Measurement Devices (PMDs) which cover part of the wavelength ranges of channels 2 (PMD-A), 3 (PMD-B), 4 (PMD-C), 5 (PMD-D), 6 (PMD-E) and 8 (PMD-F), and
- (b) the five overlapping regions of the six continuous channels 1-6. These PMDs and overlaps measure  $Q$ .

There is also an additional 45° PMD sensor which overlaps PMD-D. This special PMD is required to determine  $U$ . For channel 7, interpolation between channel 6 and channel 8 has to be used. For channel 1, a theoretical model calculation is used for the wavelength range below 300 nm.

Since we measure the polarisation only at a limited number of wavelengths, interpolating the polarisation parameters to all the wavelengths measured is a significant part of the PCA. Especially elaborate is the interpolation of the  $U(\lambda)$  where only one measurement at  $\approx 850$  nm is available (in addition, the theoretical model is used in the UV). Whereby it should be noted that the instrument efficiency is only weakly dependent on  $U$ , so that even large errors in  $U$  may result in small errors on the calibrated radiance.

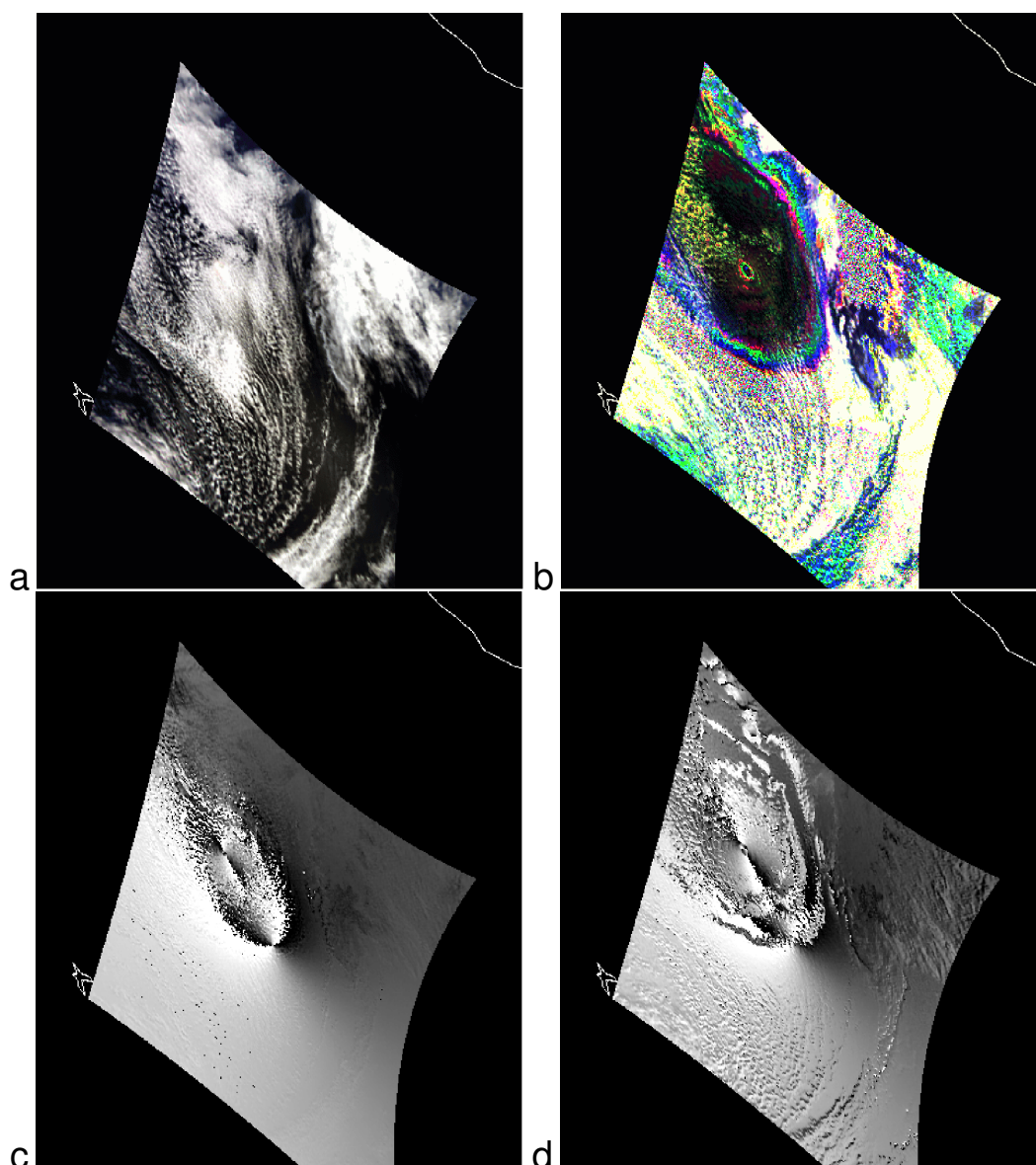


**Figure 3.9.:** POLDER image showing polarisation parameters over a partially clouded scene:  
 a) RGB image of total reflectance (Red= 865 nm, Green= 670 nm, Blue= 443 nm)  
 b) RGB image of Degree of Polarisation  
 c) Polarisation angle  $\chi$  at 443 nm  
 d) Polarisation angle  $\chi$  at 670 nm  
 The FOV of this scene is  $\sim 102^\circ \times 86^\circ$  (compare with SCIAMACHY  $15^\circ \times 2^\circ$  for 1 second exposure time at nominal swath width); West on top. Panel b) clearly shows a rainbow phenomenon. Outside the rainbow, polarisation is low over thick clouds, where the residual polarisation is predominantly in the blue.  
 POLDER data courtesy CNES/NASDA

Interpolation is not only necessary for wavelength but also for time, because of the clustered readout not all polarisation points are available at all times. Thus the PCA requires that the atmospheric polarisation behaves as a smooth function both of wavelength and of time (or equivalently: ground scene). That this requirement is not always met can be inferred from Figure 3.9.

Figure 3.9 shows a somewhat un-typical, but illustrative example of the problems that may be encountered. The images [12] are derived from data of the POLDER instrument on ADEOS, and show a partially clouded scene above the Southern Atlantic (coastline of South-Africa shown in the upper right corner), where the viewing geometry is such that a rainbow may occur. Figure 3.9a shows the intensity image, Fig. 3.9b the image for the degree of polarisation.

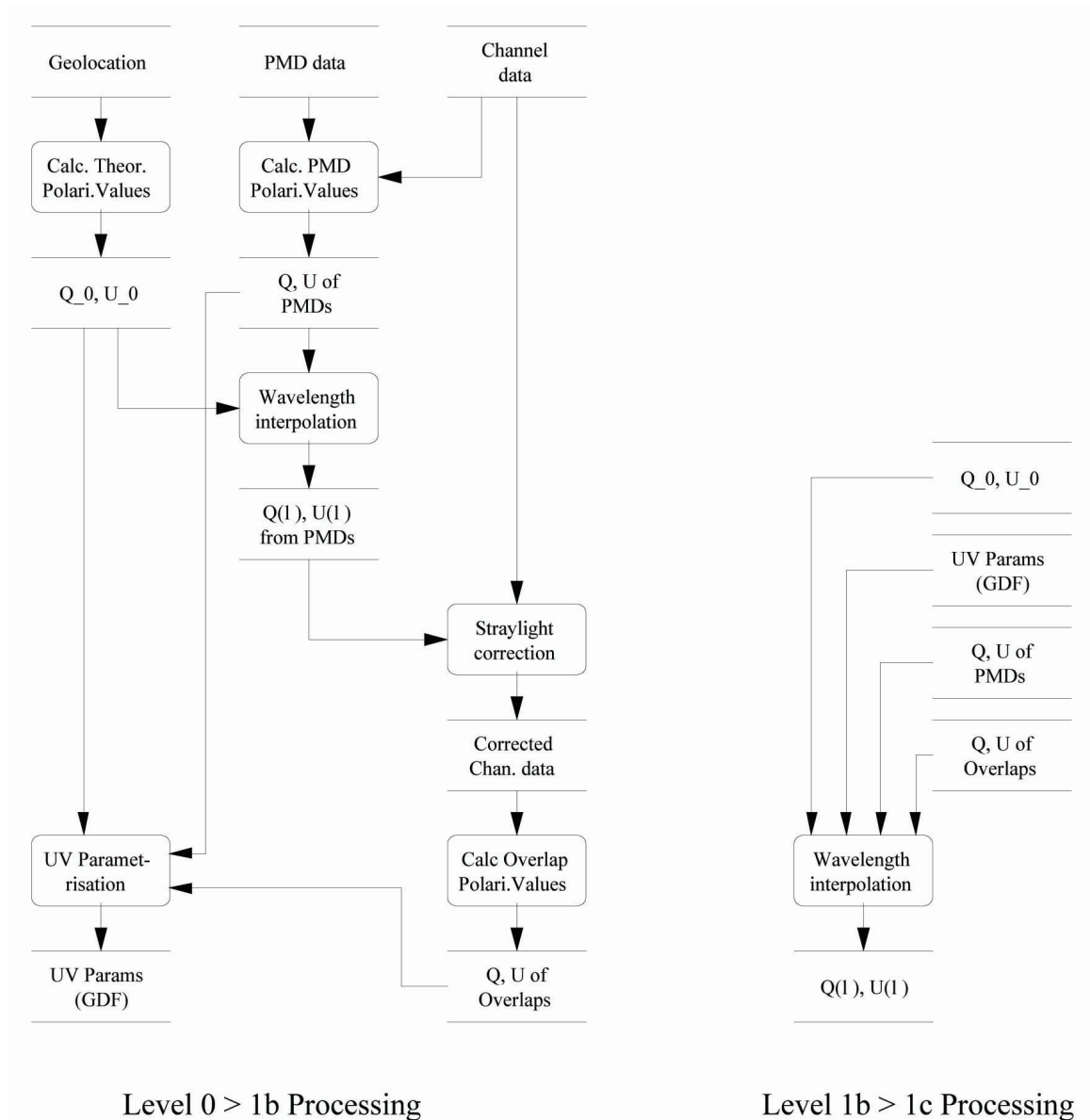
Clearly visible in the upper left quarter of the polarisation image is the rainbow, which has a slightly different size for the different wavelengths. In this case the interpolation in wavelength would obviously be inaccurate if interpolation is made between clusters with different ground pixel size (=different weighting of the polarised intensity). Also the connection to the theoretically calculated far-UV single scattering polarisation (from the stratosphere, hence not influenced by clouds) will be inaccurate here. For this particular rainbow problem, the SCIAMACHY level 1b data are flagged if the geometry is favourable for the occurrence of a rainbow (see Section 3.16).

Figure 3.9c and 3.9d show the same scene for the polarisation angle  $\chi$ . The 443 nm image shows a smooth geometrical distribution of  $\chi$  (outside the rainbow) as expected for Rayleigh scattering. The 670 nm image however shows clear structure associated with clouds. The assumption made in the PCA that  $\chi$  and thus the ratio  $U/Q$  is constant in wavelength, or can be (linearly) interpolated between the 300 nm and the 850 nm point, is not quite valid there. On the other hand, clouds are usually associated with low polarisation (due to the multiple scattering) and therefore even a relatively large error in  $\chi$  (in combination with the low sensitivity of SCIAMACHY for  $U = P \cdot \sin(2\chi)$ ) may be relatively harmless for the final polarisation correction.

Also the requirement that the atmospheric polarisation behaves as a smooth function of wavelength is not strictly fulfilled. Fine-structure in polarisation can be observed in Fraunhofer lines in connection to the Ring effect [25, 9]. Very strong atmospheric absorption lines (e.g. O<sub>2</sub> A-band or, to a lesser extend, O<sub>3</sub> Huggins bands) may show a significantly different polarisation than their surrounding continuum, probably caused by a different effective absorption depth in connection to different aerosol layers [8]. To take account of these effects, a degree of atmospheric modelling would be required which goes beyond Level 1 (defined as using own sensor data only for instrument calibration). However, the Level 1b product contains all measurement signals and polarisation information present in the data, so that a recalibration in Level 2 is in principle possible if such a level of accuracy would be required.

## Processing Overview

The determination of polarisation fractions and their wavelength interpolation is a complex and time consuming part of the level 0 to 1c processing.



**Figure 3.10.:** Data flow of the polarisation correction algorithm (simplified).

In order to keep a clear picture of this processing, we divide the algorithm specification into four self standing parts:

1. Calculation of theoretical polarisation fractions (below 300 nm);
2. Calculation of polarisation fractions from PMD measurements;
3. Calculation of polarisation fractions using channel overlap regions;
4. Wavelength interpolation of polarisation fractions.

Each part has its own requirements with respect to the amount of preprocessing required. The theoretical calculations only require the geolocation information. The use of PMDs requires a wavelength-calibrated spec-

trum with dark signal subtracted. The channel overlap intensities are sensitive to stray light, and therefore the third part of the algorithm additionally needs stray light to be subtracted from the spectrum.

These modules only calculate  $Q$  and  $U$  at  $\leq 12$  specific wavelengths. To obtain the values for all spectral wavelengths, a dedicated interpolation scheme has to be applied, see Section 3.14.

Note that the stray light correction algorithm needs the  $Q$  and  $U$  to be known. We will therefore first determine these fractions using the first two parts of the polarisation algorithm, then go into the stray light correction module, and finally calculate the polarisation fractions in the overlap regions. The implicit assumption here is that  $Q$  and  $U$  as function of wavelength can be determined with sufficient accuracy (for the stray light correction purpose) from theory and PMDs only. This is expected to be the case, with the possible exception of the overlap between channels 1 and 2 (near 312 nm). For the latter eventuality, a closed-loop between the stray light module and the overlap-polarisation module should be held optional.

The dedicated wavelength interpolation scheme of Section 3.14 is currently only implemented for the Level 1b to 1c processing; the wavelength interpolation for the purpose of stray light correction uses currently a simplified scheme, see Section 3.10. However, to speed up the Level 1b to 1c processing, the part of this algorithm which calculates the UV parameterisation (the GDF parameters, see Section 3.14) is performed in Level 0 to 1b processing and the parameters are written to the Level 1b product, to be directly available for the Level 1b to 1c processing.

The dataflow of the polarisation processing is shown in Figure 3.10. This picture is simplified in the sense that the theoretical polarisation values  $Q_0, U_0$  are in fact used in all processing steps.

The polarisation parameters (and Mueller matrices) are calculated in a coordinate frame used for the calibration of the instrument. However, before writing to the level 1b product, we convert  $Q$  and  $U$  to a coordinate frame commonly used in atmospheric science. For details see Part I of the PCA (Section 3.13.2).

### Complications due to clustered readout

Special problems occur if interpolation has to take place over clusters with different integration time (IT). A straightforward interpolation over all these clusters would imply that polarisations averaged over one ground pixel size are compared to polarisations averaged over a much smaller or larger ground pixel size. This is certainly not correct (especially when polarisation changes considerably over the ground scene as e.g. in case of fractional cloud cover). A simple approximation would be to calculate for the larger ground pixels an intensity-weighted mean from the smaller ground pixels contained therein. This approximation may be valid for the polarisation from overlap regions, but not for the polarisation of the PMDs, because these polarisation fractions are derived using a convolution of spectral shape of the input spectrum with the PMD response. Especially in critical ground scenes, like fractional cloud cover, this spectral shape of the input spectrum may change drastically; and simple averaging of polarisation fractions is no longer allowed. A further complication is that single clusters with small IT may not cover the whole PMD spectral range, in which case an extrapolation from the larger ground pixels to the smaller ground pixels is necessary - which implies that the smaller ground pixels are not giving the most accurate information available.

For this reason, we calculate the polarisation fractions not only for each cluster available, but we do this for all ground pixel sizes contained in the groundpixel of the cluster with largest IT. This information is also needed on the level 1b product, if later one wants to extract accurate level 1c data for user-defined (averaged) ground pixel sizes.

As example, consider the simplified readout scheme of Figure 3.11 (horizontal lines indicate the wavelengths which are read out at the time plotted on the lefthand side of the graph). Suppose that there are 3 different wavelength regions, each with their own integration time. Region A has a finished integration every 1.0 seconds, region B every 0.25 seconds and region C every 0.5 seconds.

On the Level 1b product, all polarisation fractions  $Q, U$  are calculated over the whole spectrum for each of the 3 different integration times (0.25, 0.5, 1.0 second). If this were one State, there would be  $4 + 2 + 1 = 7$  sets of polarisation values on the product for this State.

Suppose that PMD-A is in region A, and PMD-B in region B, then a GDF (see Section 3.14) is only calculated for  $t=1.0$ . The polarisation curve in region B will only be correctly connected to the GDF for a spectrum in region B averaged over the readouts at 0.25, 0.5, 0.75 and 1.0 seconds.

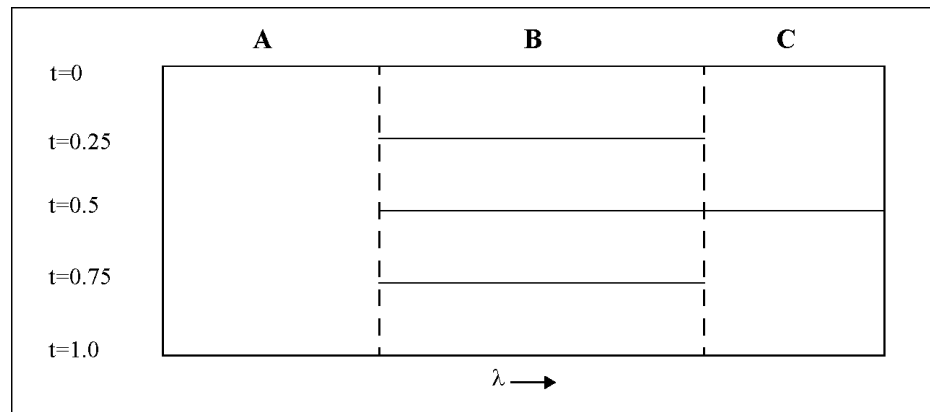


**Figure 3.11.:** Example of clustered readout (see text).

For the readouts with the short integration time, some interpolation errors will occur when the polarisation points are connected to the theoretical value using Akima interpolation (for these readouts, the theoretical value is the only polarisation point in region A). This is still true for the readout in region B at  $t=1.0$  (without averaging of previous readouts), because once cannot connect a GDF averaged over 1 second to a measurement which covers only the last 0.25 second. In this example, the GDF may only be fitted to measurements averaged over 1 second integration time.

### 3.13.2. The theoretical point near 300 nm

For the UV part of the spectrum a fractional polarisation value may be derived from a model calculation. Below  $\approx 300$  nm, polarisation is dominated by Rayleigh scattering, and a simple calculation based on a Rayleigh single-scattering model, yields a wavelength-independent value depending only on the illumination geometry (see [34], a somewhat improved description is given in [59] and, mathematically equivalent, in [57] which is used here).

The algorithm calculates the polarisation fractions  $Q$  and  $U$  from the degree of polarisation  $P$  and from the angle of the polarisation plane  $\chi$  (angle with respect to the local meridian plane - the plane through satellite, zenith, and centre-of-FOV).  $P$  and  $\chi$  can be calculated readily, once the geolocation is known. Orbit simulations show that the value of  $Q$  follows the solar zenith curve quite closely, and there are some variations across the swath (east versus west pixels) - this is especially true for the large swath width (960 km) measurement mode.

In the current implementation of the algorithm, the polarisation quantities are only calculated at the centre geolocation of the ground pixels with the smallest IT (more sophisticated schemes might involve calculation on sub-pixel level, and averaging using weights derived from PMD measurements but the scientific improvement seems questionable). The solar and viewing angles in the geolocation are calculated for top-of-atmosphere (TOA). For the best accuracy, one should use the angles at the scattering height, which has the complication that this height is dependent on wavelength and on ozone profile. In general, the errors due to taking TOA angles are small. Only for large solar zenith angles significant errors may be expected. However, here we have the general problem that the angles vary significantly over the ground pixel and for the usual case of inhomogeneous ground scenes it becomes very difficult anyway to determine from which direction within the pixel the average radiation comes from.

For the same reason, theoretical values for ground pixels with a larger IT are calculated as simple averages of the values obtained for the smallest IT (this applies to the values  $Q_0, U_0, \lambda_0$  described below, and to the value  $\lambda_m$  described in Section 3.14 but in the processing calculated here because it also uses as only input the geolocation).

*Note on coordinate frames:*

When using the keydata, we follow the convention from [22] which defines  $Q$  as the fractional polarisation parallel to the spectrograph's slit, at the location of the slit, i.e. behind the scan unit.  $U$

is defined at this location as 45 degree clockwise when looking into the instrument; this we call the “calibration co-ordinate frame”. The original formulation in [34] specified  $Q$  for the parallel direction in front of the instrument, which corresponds to the conventional definition of Stokes parameters in a geophysical co-ordinate frame.

We first calculate the relations between  $Q$  (or  $U$ ) and  $P$ , using the geophysical co-ordinate frame from [34]. To indicate in this co-ordinate frame the theoretical values for the single-scattering model, we write  $P, \chi$  with subscript  $ss$ . In this co-ordinate frame we denote the Stokes fractions as  $Q_{ss}, U_{ss}$ . Note that the orientation of  $U$  (or the sign of  $\chi$ ) was not explicitly defined in the original formulation of the geophysical co-ordinate frame; for our definition of the orientation of  $U_{ss}$  refer to fig. 3.1.

Then  $Q_{ss}, U_{ss}$  are converted to the corresponding quantities  $Q_0, U_0$  in the calibration co-ordinate frame and these are used further down in the PCA. When writing the fractional polarisation parameters to the level 1b product, a reverse transformation back to the geophysical co-ordinate frame is made.

The degree of polarisation due to single scattering by molecules is

$$P = \frac{1 - \cos^2 \Theta}{1 + \Delta + \cos^2 \Theta} \quad (3.95)$$

where  $\Delta$  is a term which accounts for anisotropic scattering (specified on the initialisation file), and  $\Theta$  is the scattering angle in the atmosphere.  $\Theta$  is defined in the interval  $[0^\circ, 180^\circ]$  and is given by:

$$\cos \Theta = \sin \theta \cdot \sin \theta_0 \cdot \cos(\phi_0 - \phi) - \cos \theta \cdot \cos \theta_0 \quad (3.96)$$

where  $\theta, \theta_0$  and  $\phi - \phi_0$  are the local geometrical angles at the scattering height (here taken as TOA): line-of-sight zenith, solar zenith and relative azimuth respectively.

The term  $1 + \Delta$  equals  $(1 + \rho)/(1 - \rho)$  where  $\rho$  is the depolarisation factor of air. This factor is slightly wavelength-dependent; we will use the value from [11] at 280 nm as a representative value for the UV ( $\Delta \approx 0.0068$ ).

The angle of the polarisation plane (with respect to the local meridian plane, defined in the interval  $[0^\circ, 180^\circ]$ ) is given by:

$$\chi_{ss} = \arccos \left( \pm \frac{\sin \theta_0 \cdot \sin(\phi_0 - \phi)}{\sqrt{1 - \cos^2 \Theta}} \right) \quad (3.97)$$

where the + sign applies if:  $\sin \theta \cdot \cos \theta_0 + \cos \theta \cdot \sin \theta_0 \cdot \cos(\phi_0 - \phi) > 0$ .

The fractional polarisation values  $Q_{ss}, U_{ss}$  are calculated from:

$$\begin{aligned} Q_{ss} &= P_{ss} \cdot \cos(2 \cdot \chi_{ss}) \\ U_{ss} &= P_{ss} \cdot \sin(2 \cdot \chi_{ss}) \end{aligned} \quad (3.98)$$

For the effective wavelength  $\lambda_0$  [nm] of this theoretical polarisation point, we take the maximum wavelength of single scattering near 300 nm. The current implementation of the algorithm uses a functional form taken from [26], where  $\lambda_0$  is expressed as a function of  $\cos \theta_0$  (note: recently a more sophisticated parameterisation has been found, see [27]):

$$\lambda_0 = \lambda_{ss}(\cos \theta_0) \quad (3.99)$$

where the  $\lambda_{ss}(\cos \theta_0)$  are specified on the initialisation file for certain values of the cosine of the solar zenith angle; these values are linearly interpolated to the  $\cos \theta_0$  of the measurement (these initialisation file data will be derived from [26] for the US-standard atmosphere).

The conversion to the calibration co-ordinate frame is given by (assuming that alignment errors are negligible):

$$\begin{aligned} Q_0 &= -Q_{ss} \\ U_0 &= -U_{ss} \end{aligned} \quad (3.100)$$

These values are used further down in the PCA. When writing the fractional polarisation parameters to the level 1b product, a reverse transformation back to the geophysical coordinate frame is made. Since we only change signs here, the back transformation is equal to the transformation above, i.e.  $Q$  changes sign.

The error on the Stokes fractions is a combination of the error in  $\chi$  and the error in  $P$ :

$$\begin{aligned} \epsilon_{Q_0} &= 2 \cdot \epsilon_{\chi} \cdot |\sin(2 \cdot \chi_{ss})| + \epsilon_{P} \cdot (1 + P_{ss}) \cdot \cos(2 \cdot \chi_{ss}) \\ \epsilon_{U_0} &= 2 \cdot \epsilon_{\chi} \cdot |\cos(2 \cdot \chi_{ss})| + \epsilon_{P} \cdot (1 + P_{ss}) \cdot \sin(2 \cdot \chi_{ss}) \end{aligned} \quad (3.101)$$

where we take for the relative error  $\epsilon_{\chi}$  an error estimate from the initialisation file (preliminary value 0.02 based on [33]); for the error  $\epsilon_{P}$  we assume that the error in  $P$  is due to an error in the depolarisation term; we set  $\epsilon_{P} = 0.0045$  as the difference in  $P$  due to the wavelength dependence of  $\Delta$  amounts to 0.009 over the range 240-300 nm.

The above algorithm is only used for Nadir and for Limb States, where we measure scattered light. For Occultation States, polarisation fractions are not calculated and set to 0, because there are no polarisation calibration data available for the measurements with the small aperture. In any case are the expected polarisation values for occultation very low. At this point it should be mentioned that, on the Level 1b product, *all invalid determinations of  $Q$  and  $U$  are characterised by having as error  $-1$ .*

The reason for doing this instead of setting the values of  $Q, U$  themselves to some invalid number, is that so the (derived but wrong) values of  $Q, U$  still may give clues to why the algorithm failed (especially for polarisation from PMDs and overlaps).

### 3.13.3. Polarisation fractions from PMDs

The PMDs measure the intensity in one specific polarisation direction. The PMDs A, B, C, D, E, F (overlapping with channels 2,3,4,5,6,8 respectively) measure the polarisation in the direction parallel to the spectrometer slit (in the 'length' of the IFOV). The PMD-45 (overlapping with PMD-D) measures the polarisation in a direction at 45° to the spectrometer slit.

By comparison with the intensity measured by the array detector channels, which is a (calibrated) mixture of polarised intensities, it is possible to derive the fraction of intensity having the polarisation measured by the PMDs. A problem in this comparison is that the PMD bandwidth is much larger (factor  $\geq 100$ ) than the array detector bandwidth.

To solve this, we think of the PMD detector as a 'virtual array detector' with 'virtual pixels' which have exactly the same spectral bandwidth as the pixels of the corresponding channel array detector (e.g. the virtual pixels of PMD-A correspond to the pixels of channel 2).

We can then write the PMD signal (or intensity) as the sum over all virtual pixels of the spectral signal (intensity). For the PMDs, the basic equation for the instrument response, Equation 3.2 on page 26, then takes the form

$$S_{PMD} = \sum_{i=i_{start}}^{i_{end}} M_{1,i}^P \cdot I_i \cdot \{1 + \mu 2_i^P \cdot Q_i + \mu 3_i^P \cdot U_i\}$$

$$\text{using } \mu X = \frac{M_X}{M_1}$$

where index  $i$  denotes the virtual pixel number from the start of the PMD band to the end of the PMD band, which has the same properties as the corresponding channel pixel (corresponding in wavelength). All other notation is as in Section 3.1.

Since a PMD measures either  $Q$  or  $U$ , with the other being zero, this equation can be solved for the Stokes fraction  $Q$  or  $U$  (but only averaged over the PMD's wavelength band) once the intensity  $I_i$  is known. The latter can be solved via Equation 3.2 for the channel signals, which however still contains  $Q$  and  $U$ .

Substituting for  $I_i$  in the equation above, the channel signals  $S_i$  via Equation 3.2, we obtain the following expression, which we refer to as the '**PMD virtual sum**':

$$S_{PMD} = \sum_{i=i_{start}}^{i_{end}} \left( \frac{c_i \cdot S_i}{M_{1,i}} \right)^D \cdot M_{1,i}^P \cdot \{1 + \mu 2_i^P \cdot Q + \mu 3_i^P \cdot U\}$$

where  $c_i$  is the polarisation correction factor for the channels (using the polarisation averaged over the PMD band):

$$c_i = \{1 + \mu 2_i^D \cdot Q + \mu 3_i^D \cdot U\}^{-1} \quad (3.102)$$

For PMDs which extend over a channel boundary, care must be taken that the summation over signals is not counted double in the overlap. Channel pixels which lie beyond a wavelength  $PMD\_ovl\_wv$  (specified on the initialisation file for each overlap) are not taken into account for the PMD virtual sum.

There are three further refinements which we need to take before the PMD virtual sum can be used:

- it must be ensured that PMDs and channels measure the same intensity, hence the PMD measurements need to be integrated over the detector pixel IT - this can be easily done as summation over the PMD integrals calculated in Equation 3.22 on page 37 ;
- if the edge of a PMD band lies in a cluster which is not read out at the time where the polarisation is to be determined, we have to apply a correction factor which accounts for the (estimated) missing signal.
- signals of bad pixels in the channel signal are replaced by linearly interpolated values from neighbouring good pixels.

The PMD virtual sum equation as used in the processor becomes then for each PMD  $j$ :

$$B_j \cdot \sum_{IT} I_{PMD,j}(t) = \sum_{i=i\_start(j)}^{i\_end(j)} \left( \frac{RM_{1,OBM}^{P,D} \cdot c_i \cdot S_i^D}{M_{1,i}^D \cdot mf_{OBM}^D} \right) \cdot M_{1,i}^P \cdot mf_{OBM}^P \cdot \{1 + \mu 2_i^P \cdot Q_j + \mu 3_i^P \cdot U_j\} \quad (3.103)$$

where the factor  $B_j$  accounts for light measured by the PMD for which no corresponding detector-array measurements exist.  $RM_{1,OBM}^{P,D}$  and  $mf_{OBM}^P$  are taken from the key data (see Table 3.1). This contains not only light contained in clusters which are missing in the current ISP, but also the 'PMD out-of-band signal', which has been derived from Sun calibration measurements (see Section 3.12).

This out-of-band signal can be derived from the Sun since we know that the solar light is unpolarised ( $Q = U = 0$ ), and hence the PMD virtual sum can be evaluated directly to obtain  $B_j$  for the Sun - the deviation of  $B_j$  from 1.0 is the out-of-band signal denoted as  $OB_j$  (see Section 3.12).

For the Earthshine measurements we use (in case all clusters covering the PMD spectral region are available):

$$B_j = (1 - G_j \cdot OB_j) \quad (3.104)$$

where  $G_j$  is for each PMD a weighting factor (on the initialisation file) which grosso-modo takes account of the differences in spectral shape of the Solar spectra and of the Earth-shine spectra. The values for  $OB_j$  are taken from the SMR GADS. This contains values obtained from NDF-in and NDF-out solar measurements. Although the Earthshine measurements have NDF-out, we use the SMR NDF-in values: these are measured daily instead of monthly, and the NDF-out values for PMD-C,D (channel 4,5) show saturation effects (note that the ND filter is only in the light path of channels 3-6).

### Complications due to clustered readout

A complication for calculating the virtual sum arises when the clusters on an ISP do not completely contain the required PMD spectral coverage (we name this the 'incomplete' readout). In this case the missing part of the virtual sum must be estimated.

This missing part is calculated from the next, 'complete', readout which contains all the clusters covering the PMD bandwidth.

To this end we have to add the spectra of all relevant clusters in the 'incomplete' readouts(s) to the spectra in the 'complete' readout, to obtain one 'averaged' spectrum over the ground pixel size of the relevant cluster with the longest IT ('relevant' means here: within the PMD bandwidth).

The virtual sum equation for the 'averaged' ground pixel can now be solved to yield the polarisation fractions  $Q^{Ave}$  and  $U^{Ave}$ .

Using these polarisation fractions, we calculate the right hand side quantities in the virtual sum equations, one time for the complete spectral PMD bandwidth and one time for the bandwidth available in the incomplete readout:

$$\begin{aligned} Sum\_all(t^{Ave}) &= \sum_{i=i\_start(j)}^{i\_end(j)} \left( \frac{c_i^{Ave} \cdot S_i^{Ave}}{M_{1,i}} \right)^D \cdot M_{1,i}^P \cdot \{1 + \mu 2_i^P \cdot Q_j^{Ave} + \mu 3_i^P \cdot U_j^{Ave}\} \\ Sum\_part(t^{Ave}) &= \sum_{i=i\_first(j)}^{i\_last(j)} \left( \frac{c_i^{Ave} \cdot S_i^{Ave}}{M_{1,i}} \right)^D \cdot M_{1,i}^P \cdot \{1 + \mu 2_i^P \cdot Q_j^{Ave} + \mu 3_i^P \cdot U_j^{Ave}\} \end{aligned}$$

where  $i\_first$  and  $i\_last$  are the first and last pixel of the cluster with the incomplete coverage; the superscripts  $Ave$  refer to averages of the quantities over the smaller ground pixels contained in the averaged ground pixel; note that the ratios of Mueller matrix elements have to be averaged as well.

The general expression for  $B_j$  then becomes:

$$B_j = \frac{Sum\_part(t^{Ave})}{Sum\_all(t^{Ave})} \cdot (1 - G_j \cdot OB_j) \quad (3.105)$$

## Solving the virtual sum

Having established the PMD virtual sum equation, one has to solve it to obtain the values of  $Q$  and  $U$ . The PMDs A-F measure mainly  $Q$ , but due to a small amount of polarisation mixing in the optics they also measure a small part of the  $U$  component (i.e.  $\mu_3$  is non-zero but small). PMD-45 measures mainly  $U$ , but also a small part of the  $Q$  component (i.e.  $\mu_2$  is non-zero but small). To simultaneously solve  $Q$  and  $U$  at  $\approx 850$  nm from PMDs D and  $45^\circ$ , we first solve  $Q$  from PMD-D under the assumption  $U = 0$ , then use this value of  $Q$  to solve  $U$  from PMD-45 and iterate between the two PMDs until a stable solution is found.

For the other PMDs, we solve  $Q$ , using for  $U$  a pre-defined relationship between  $Q$  and  $U$ . To this end we divide the SCIAMACHY wavelength range in 3 parts:

- Below a pre-defined wavelength  $\lambda_{Ray}$  (preliminary value: 400 nm) we assume that Rayleigh scattering dominates and that the scattering angle  $\chi$  is independent of wavelength; the ratio  $U/Q$  is then given by the ratio for the theoretical point at 300 nm  $U_0/Q_0$  [method 1].
- For wavelength above a pre-defined wavelength  $\lambda_{Aer}$  we assume that aerosol scattering/cloud reflection dominates and that the scattering angle  $\chi$  is independent of wavelength; the ratio  $U/Q$  is then given by the ratio for the measured point at 850 nm  $U_{45}/Q_D$  [method 2].
- In-between  $\lambda_{Ray}$  and  $\lambda_{Aer}$  we use a linear interpolation of the of the points  $(\lambda_{Ray}, U[method1])$  and  $(\lambda_{Aer}, U[method2])$  to the central wavelength of the PMD-band, given by the average of  $\lambda_{i\_start(j)}$  and  $\lambda_{i\_end(j)}$ . Note that this interpolation is in fact equivalent to taking a weighted mean of the  $U$  values calculated by both methods.

The calculations are performed in such a way that the sign of  $U$  is conserved, irrespective of a change of sign in  $Q$  - this is because near  $\chi = \pm 45^\circ$  the sign of  $Q$  may change (when it changes quadrant) while the sign of  $U$  does not.

The computation scheme above must be adapted for two eventualities:

1. If  $U_{45}$  would be invalid (see below) for a ground pixel with an integration time smaller than  $IT_L$ , the largest IT in the State, but a valid value (say  $U_{45}(L)$ ) exists for a larger ground pixel with  $IT < IT_L$  in which this one is contained, then the interpolation is performed using:  
 $U_{45} = U_{45}(L)$   
else this interpolation is performed using  $U_{45} = 0$ .
2. If the  $Q_{45}$  or  $Q_0$  values in the ratio  $U/Q$  are close to 0, then the calculated  $U(\lambda)$  may explode in case of measurement errors on  $Q$  (or in case the underlying assumption of a constant polarisation angle is not quite correct) - this is due to a basic lack of information in the SCIAMACHY instrument: the PMDs A-F contain no information on the degree of polarisation when the polarisation angle is near  $45^\circ$  (unfortunately this is exactly where  $U$  is largest).

To prevent the latter, we adopt the following scheme to 'limit the damage'. This scheme is applied when theoretical  $|Q|$  is very small or measured  $|Q|$  falls below a pre-defined limit  $Pol\_Q\_min$  (initialisation file parameter, the preliminary value is 0.1 which corresponds to 2 times the expected measurement error); in this case the value of  $U$  is limited by the statistical amount of depolarisation we expect from the atmosphere,  $DPstat$  (initialisation file parameter for each polarisation point; separate value for Nadir and for Limb):

$$U_j = \begin{cases} U_0 \cdot DPstat_j & \text{for } |Q_0| < 0.01 \text{ and } \lambda_j \leq \lambda_{Ray} \\ U_{45} \cdot \frac{DPstat_j}{DPstat_{45}} & \text{for } |Q_{45}| < Pol\_Q\_min \text{ and } \lambda_j \geq \lambda_{Aer} \end{cases}$$

For wavelengths in-between  $\lambda_{Ray}$  and  $\lambda_{Aer}$  an interpolation of  $U$  in wavelength is made.

A further limit is set on  $U$  by requiring that it does not exceed the maximum theoretical degree of polarisation for rayleigh single-scattering:

$$U_{SS-MAX}^2 = Q_0^2 + U_0^2 - Q_j \\ \forall (U_{SS-MAX}^2 < 0) : U_{SS-MAX}^2 = 0$$

If this maximum limit is exceeded, we set the value of  $U$  to the maximum value, retaining the sign of  $U$ :

$$\forall (U_j^2 > U_{SS-MAX}^2) : U_j = \pm \sqrt{U_{SS-MAX}^2}$$

*Note: for the polarisation-correction of the radiance this 'limit the damage' should keep errors below an acceptable level; for the scientific study of polarisation the results of the interpolation are worthless - signalled by a large error on the  $U$  values.*

The virtual sum is solved numerically, using a root-finding algorithm. The iterations between PMD-D and PMD-45, to obtain consistent values of  $U$  and  $Q$ , are terminated if the difference in parameter value between two consecutive iterations is less than  $PCA\_conver$  (initialisation file parameter) or if a maximum number of iterations  $PCA\_maxiter$  (initialisation file parameter) is reached.

There are 3 ways to obtain 'invalid' polarisation values (error on  $Q, U$  set to  $-1$ , see Sect. 3.13.2):

- If for a given PMD no corresponding cluster data are available, i.e. the cluster which contains the PMD's central pixel number is missing on the ISP.
- If  $Q_\lambda^2 + U_\lambda^2 > 1$  after the calculation of  $Q$  and  $U$  is terminated, this shall always be checked.
- If the maximum number of iterations was reached (PMD-D and PMD-45 only).

### Disabling PMD-45

In-flight, it has been found that PMD-45 may have a stray light problem, as the calculated  $U_{45}$  values are systematically off. From IPF version 6, a workaround has been implemented to neglect the PMD-45 measurement until this problem is solved. The value of  $\lambda_{Ray}$  on the initialisation file is set above the central wavelength of PMD-45. If this is the case, then the iteration between PMD-D and PMD-45 is not performed. PMD-D is in this case treated like all other PMDs A-F using method [1] (i.e. the ratio  $U/Q$  is then for all PMDs given by the ratio for the theoretical point at 300 nm,  $U_0/Q_0$ ). The effective wavelength of PMD-45 (see below) is set to  $-1$ .

### Q and U for high-altitude Limb

Spatial stray light in Limb measurements poses a problem for main-channel and for PMD measurements; especially at high altitudes where Limb radiances are very low. The  $Q$  and  $U$  values above a certain tangent height  $h\_scattering$  (value from the initialisation file, currently 30 km) are not calculated from the virtual sum equation, but are obtained by scaling the  $Q$  and  $U$  values from a lower altitude with a factor obtained from single-scattering theory.

The expected polarisation is given by the theoretical single-scattering polarisation calculated in section 3.13.2, multiplied by a factor which accounts for depolarisation by multiple scattering, which mainly depends on ground albedo and tropospheric properties. This factor may vary during one scan mirror movement in the azimuth direction, but it is about constant within each vertical column.

Therefore, this factor is calculated for each of the ground pixel sizes and for each vertical column, and the polarisation value for tangent height  $h$  and vertical column  $icol$  is then given by:

$$Q_j(h, icol) = Q_j(h\_scattering, icol) \cdot \frac{Q_0(h, icol)}{Q_0(h\_scattering, icol)}$$

where  $Q_j(h\_scattering, icol)$  is the polarisation of PMD  $j$  of the last measurement below  $h\_scattering$ . The lowest height in a 1.5 sec. horizontal scan is decisive here (use same height for all columns).

If  $Q_0(h\_scattering, icol) < 0.01$  then set

$$\frac{Q_0(h, icol)}{Q_0(h\_scattering, icol)} = 1$$

The errors are likewise scaled:

$$\epsilon_{_Q_j}(h, icol) = \epsilon_{_Q_j}(h_{_scattering}, icol) \cdot \frac{Q_o(h, icol)}{Q_o(h_{_scattering}, icol)}$$

The values of  $U_j$  are calculated similarly (replace every  $Q$  by  $U$  in the above equation)

The number of vertical columns is given by  $n_{_col} = 1.5/IT$ . Note that during the limb scanning, the direction of column counting is reversed in every new azimuth scan: e.g. for  $IT = 0.375$  seconds we have the following column numbers for the series of measurements in the state (counting from 0): 0, 1, 2, 3, 3, 2, 1, 0, 0,1, 2, 3, 3, 2... etc.

### Calculate effective wavelengths of PMDs

The effective wavelengths of the PMDs,  $\lambda_j$  are calculated from the centre of gravity found by weighting the virtual PMD signals over the PMD wavelength band:

$$\lambda_j = \frac{\sum_{i=i_{_first}(j)}^{i_{_last}(j)} \lambda_i \cdot \left(\frac{c_i^{Ave} \cdot S_i^{Ave}}{M_{1,i}}\right)^D \cdot M_{1,i}^P \cdot \{1 + \mu_2^P \cdot Q_j^{Ave} + \mu_3^P \cdot U_j^{Ave}\}}{\sum_{i=i_{_first}(j)}^{i_{_last}(j)} \left(\frac{c_i^{Ave} \cdot S_i^{Ave}}{M_{1,i}}\right)^D \cdot M_{1,i}^P \cdot \{1 + \mu_2^P \cdot Q_j^{Ave} + \mu_3^P \cdot U_j^{Ave}\}} \quad (3.106)$$

where  $i_{_first}(j)$  and  $i_{_last}(j)$  are equal to  $i_{_start}(j)$  and  $i_{_end}(j)$  in case we have complete wavelength coverage of the PMDs, and are the first and last pixel of the available cluster(s) in case of incomplete coverage (analogue to the situation in the virtual sum expression).

For high-altitude limb, the effective wavelengths are taken as the wavelengths of the last measurement below  $h_{_scattering}$  in vertical column  $icol$  (see previous subsection):

$$\lambda_j(h, icol) = \lambda_j(h_{_scattering}, icol)$$

### Calculate errors on polarisation fractions

For a more elaborate discussion of the calculation of the errors, see document [56]. It is noted here that the PMD virtual sum can be analytically evaluated under the simplifying assumption that both the ratios of Mueller matrix elements and the input spectrum are constant in wavelength. For the purpose of error estimation this simplification is legal. The relevant quantities are evaluated at the centre of the bandwidth for each PMD.

As shorthand notation, define (using notation of Section 3.1 ):

$$\begin{aligned} I^P &:= B_j \cdot \sum_{IT} I_{PMDj}(t) \\ I^D &:= \sum_{i=i_{_start}}^{i_{_end}} S_i^D \\ I^{P/D} &:= \frac{I^P}{I^D} \\ \mu_1^{P/D} &:= \frac{M_1^P}{M_1^D} \\ A &:= \mu_2^D \cdot I^{P/D} - \mu_1^{P/D} \cdot \mu_2^P \\ B &:= \mu_1^{P/D} \cdot \mu_3^P - I^{P/D} \cdot \mu_3^D \\ C &:= \left(\mu_1^{P/D} - I^{P/D}\right) + U \cdot \left(\mu_1^{P/D} \cdot \mu_3^P - I^{P/D} \cdot \mu_3^D\right) = \left(\mu_1^{P/D} - I^{P/D}\right) + U \cdot B \\ D &:= \left(\mu_1^{P/D} - I^{P/D}\right) + Q \cdot \left(\mu_2^D \cdot I^{P/D} - \mu_1^{P/D} \cdot \mu_2^P\right) = \left(\mu_1^{P/D} - I^{P/D}\right) - Q \cdot A \end{aligned}$$

where all quantities are calculated for [virtual] pixel  $i$  in the centre of the bandwidth of PMD  $j$ . Superscript  $P$  refers to PMD  $j$  ( $j = A, \dots, F$ ).

The partial derivatives are (neglecting small terms for  $\mu_1^{P/D}, I^{P/D}$ ):

$$\begin{aligned}\frac{\partial Q}{\partial \mu_1^{P/D}} &= \frac{A + \mu 2^P \cdot C}{A^2} \\ \frac{\partial Q}{\partial I^{P/D}} &= \frac{A + \mu 2^D \cdot C}{A^2} \\ \frac{\partial Q}{\partial U} &= \frac{B}{A} \\ \frac{\partial Q}{\partial \mu 3^P} &= \frac{\mu_1^{P/D} \cdot U}{A} \\ \frac{\partial Q}{\partial \mu 3^D} &= -\frac{I^{P/D} \cdot U}{A} \\ \frac{\partial Q}{\partial \mu 2^P} &= \frac{\mu_1^{P/D} \cdot C}{A^2} \\ \frac{\partial Q}{\partial \mu 2^D} &= -\frac{I^{P/D} \cdot C}{A^2}\end{aligned}$$

The partial derivatives shall be evaluated for all centre pixels in the PMD bandwidth, and then averaged over pixel. Since the expressions rely on an often subtle cancellation of terms, it is not allowed to first calculate the averages and then use these averages in the expressions.

Assuming quasi-random errors on the ratios of Mueller matrix elements, the absolute error on  $Q$ ,  $\epsilon_{-Q}$ , is given by RMS sum of partial errors:

$$\epsilon_{-Q}^2 = \left[ \frac{\partial Q}{\partial U} \cdot \epsilon_{-U} \right]^2 + \left[ \frac{\partial Q}{\partial I^{P/D}} \cdot \epsilon_{-I^{P/D}} \right]^2 + \sum_Z \left[ \frac{\partial Q}{\partial \mu_Z} \cdot \epsilon_{-Z} \right]^2 \quad (3.107)$$

where the  $\epsilon_{-Z}$  are the absolute errors on the matrix elements  $\mu_Z$  above (with  $Z=2P, 2D$  etc. ) as calculated in Section 3.1; the errors  $\epsilon_{-U}$  and  $\epsilon_{-I^{P/D}}$  are calculated below.

For the error on  $U$  from PMD-45 the partial derivatives are (neglecting small terms for  $\mu_1^{P/D}, I^{P/D}$ ):

$$\begin{aligned}\frac{\partial U}{\partial \mu_1^{P/D}} &= \frac{\mu 3^P \cdot D - B}{B^2} \\ \frac{\partial U}{\partial I^{P/D}} &= \frac{B - \mu 3^D \cdot D}{B^2} \\ \frac{\partial U}{\partial Q} &= \frac{A}{B} \\ \frac{\partial U}{\partial \mu 3^P} &= \frac{\mu_1^{P/D} \cdot D}{B^2} \\ \frac{\partial U}{\partial \mu 3^D} &= -\frac{I^{P/D} \cdot D}{B^2} \\ \frac{\partial U}{\partial \mu 2^P} &= -\frac{\mu_1^{P/D} \cdot Q}{B} \\ \frac{\partial U}{\partial \mu 2^D} &= \frac{I^{P/D} \cdot Q}{B}\end{aligned}$$

where superscript  $P$  refers here to PMD-45 (compares to superscript P45 referring to PMD-45 in Section 3.1).

The absolute error on U from PMD-45 is then given by:

$$\epsilon_{-U^2} = \left[ \frac{\partial U}{\partial Q} \cdot \epsilon_{-Q} \right]^2 + \left[ \frac{\partial U}{\partial I^{P/D}} \cdot \epsilon_{-I^{P/D}} \right]^2 + \sum_Z \left[ \frac{\partial U}{\partial \mu_Z} \cdot \epsilon_{-Z} \right]^2 \quad (3.108)$$

Note that above error is not taken if PMD-45 is disabled, i.e. if  $\lambda_{Ray} > \lambda_D$ ; in this case use  $\epsilon_{-U_X}$  as calculated below (for X=D).

The error on  $I^{P/D}$  is assumed to be dominated by the accuracy of the PMD measurements w.r.t. the out-of-band signal and, for very low illumination conditions, the PMD signal-to-noise (using the signal-to-noise on PMD integrals derived in Section 3.5,  $SN_{PMD,j}(IT)$ , where IT refers to the integration time of the cluster corresponding to PMD  $j$ ):

$$\epsilon_{-I^{P/D}} = I^{P/D} \cdot \sqrt{[\delta B \cdot (1 - |B_j|)]^2 + \left[ \frac{1}{SN_{PMD,j}(IT)} \right]^2}$$

where  $\delta B$  is an error estimate from the initialisation file.

The error on the interpolated  $U_X$  for PMD X=A-F, is a combination of the error  $\epsilon_{-U_{45}}$  and an error on the interpolation from wavelength region of PMD-45 to PMD X. The interpolation is done via (see above, conserving the sign of U)  $U_X = Q_X \cdot U_Y / Q_Y$  where Y denotes the theoretical value (Rayleigh single scattering) or the PMD-45 c.q. PMD-D value or a linear interpolation (w.r.t. PMD wavelength between the two. The error propagation rule yields:

$$\epsilon_{-U_x^2} = \frac{1}{Q_Y^2} \cdot \left( [U_Y \cdot \epsilon_{-Q_X}]^2 + [Q_X \cdot \epsilon_{-U_Y}]^2 + \left[ \frac{Q_X \cdot U_Y}{Q_Y} \cdot \epsilon_{-Q_Y} \right]^2 \right) \quad (3.109)$$

but this is not quite correct for the theoretical value because the calculated Stokes parameters are not independent. In fact for the theoretical point the total error is related to the error in polarisation angle  $\chi$ . Using  $Q_Y \approx \cos \chi$  in the derivative of  $\tan \chi$  we obtain for  $\lambda \leq \lambda_{Ray}$ :

$$\epsilon_{-U_X^2} = \frac{1}{Q_0^2} \cdot \left( [U_0 \cdot \epsilon_{-Q_X}]^2 + \left[ \frac{Q_X}{Q_0} \cdot \epsilon_{-\chi} \right]^2 \right) \quad (3.110)$$

Note that  $\epsilon_{-U_X}$  needs to be limited, similar as we limited  $U_\lambda$  for small  $Q_Y$  (see page 90):

$$\forall (|Q_Y| < Q_{min}) : \epsilon_{-U_X} = \delta U_{max} \quad (3.111)$$

where  $\delta U_{max}$  is an error estimate from the initialisation file, and where  $Q_{min} = 0.01$  for  $\lambda_j \leq \lambda_{Ray}$  and  $Q_{min} = Pol\_Q\_min$  for  $\lambda_j > \lambda_{Aer}$ .

### 3.13.4. Polarisation fractions from channel overlaps

Due to issues with the accuracy of these polarisation fractions, which are described in the text below, calculations of polarisation from channel overlaps is currently switched off in the L0-1b processor. However, the software still has the capability to perform these calculations, and therefore we retain the algorithm description here.

The channels 1-6 in SCIAMACHY do not measure completely different spectral bands, but have at their extremes an overlap of a few nm wide with their neighbouring channels.

In these so-called 'overlap regions' we have the same spectral intensity and polarisation incident in the neighbouring channels (at the identical wavelengths in the channels), but we measure different signals due to differences in the instrument's sensitivity and polarisation response for these channels. Knowing that the incident intensity/polarisation should be identical, we can reconstruct the incident polarisation from comparison of signals in the overlap regions of two channels.

In the algorithm we do not compare the signals from 2 channels directly, but we compare the reflectivity, i.e. the (calibrated) Earth signal divided by the Sun Mean Reference (SMR). This is done to divide out errors in etalon function and channel-dependent errors in instrument response function. The SMR is taken from an auxiliary input file (which is copied to the Sun Reference GADS on the Level 1b product, see [4]). Note that there are several records with different SMRs on this file. Level 0-1b processing always uses the first record, which shall contain the SMR with the best broad-band irradiance calibration.

Combining Equation with the calculation of  $U$  using the ratio  $U/Q$  as in the calculation of the PMD virtual sum in the previous subsection, we obtain after division by the solar SMR spectrum the following relation between measured signals  $S$  and Earth-shine intensity  $I$ :

$$\frac{S_{ij}}{S_{SMR,ij}} = \frac{I_{ij}}{I_{SMR,ij}} \cdot \frac{M_{1,ij}}{M_{1,ij}^{irrad}} \cdot \left\{ 1 + \left[ \mu_{2ij} + \mu_{3ij} \cdot \left( \frac{U}{Q} \right)_X \right] \cdot Q \right\}$$

where  $ij$  denotes pixel  $i$  in channel  $j$ , and where the ratio  $(U/Q)_X$  stands for the  $U_0/Q_0$  ratio for overlaps of channels 1/2 and 2/3, and for the ratio  $U_{45}/Q_D$  for overlaps of channels 3/4, 4/5, 5/6.

This relation is valid for both channels on either side of the overlap, assuming identity for  $I$  and for  $Q$  the polarisation can be derived as:

$$Q_{ij} = \frac{\mathfrak{R}_{ij} - 1}{ma_{ij} - mb_{ij} \cdot \mathfrak{R}_{ij}} \quad (3.112)$$

where the auxiliary quantities  $ma, mb, \mathfrak{R}$  are defined as:

$$\begin{aligned} ma_{ij} &= \left[ \mu_{2ij} + \mu_{3ij} \cdot \left( \frac{U}{Q} \right)_X \right] \\ mb_{ij} &= \left[ \mu_{2i(j+1)} + \mu_{3i(j+1)} \cdot \left( \frac{U}{Q} \right)_X \right] \\ \mathfrak{R}_{ij} &= \left( \frac{S_{ij}}{M_{1,ij}} \right) / \left( \frac{S_{i(j+1)}}{M_{1,i(j+1)}} \right) \end{aligned}$$

and the ratios of Mueller matrix elements for channel  $(j + 1)$  are to be interpolated to the wavelengths corresponding to the detector pixels  $i$  in the shorter-wavelength channel  $j$ .

If the  $Q_X$  values in the ratio  $U/Q$  are close to 0, then this ratio may explode in case of measurement errors on  $Q$ , this is the same problem as encountered for the PMDs, see previous subsection:

*if  $|Q_0| < Pol\_Q\_min$  then: calculate  $U_X$  as in the corresponding case for the PMDs,*

*and use this value of  $U$  to calculate  $Q$  from:*

$$Q_{ij} = \frac{\mathfrak{R}_{ij} - 1 + (\mu_{3i(j+1)} \cdot \mathfrak{R}_{ij} - \mu_{3ij}) \cdot U_X}{\mu_{2ij} - \mu_{2i(j+1)} \cdot \mathfrak{R}_{ij}} \quad (3.113)$$

The pixel widths of the overlap regions (2 per overlap) are pre-defined by initialisation file parameters  $ovl\_bound\_min(j,2)$  and  $ovl\_bound\_max(j,2)$ . In addition,  $Q_{ij}$  is only calculated for signals which are sufficiently high (signal-to-noise issue); as minimum signal limit is taken a pre-defined fraction  $ovl\_min\_signal(j)$  of the maximum signal in the overlap region. The resulting effective overlap boundaries are denoted  $p\_min(j)$  and  $p\_max(j)$  (detector pixels in the shorter-wavelength channel  $j$  to which all quantities are interpolated) in the equations below.

The final value for the overlap polarisation is calculated as the average of the polarisation value for each pixel; the 'noise' on this quantity may be used as one of the quality control criteria (see below):

$$Q_j = \frac{1}{N(Q)} \cdot \sum_{i=p\_min(j)}^{p\_max(j)} Q_{ij} \quad (3.114)$$

where  $N(Q)$  is the number of points in the summation. For a number of reasons, it appears in practice that individual pixels may have an outlier value of  $Q_{ij}$ . To remove these outliers from the average, the above calculation is performed twice. In the first iteration, all values are used which are close to physical, defined here as:

$$|Q_{ij}| < 1.1$$

In the second iteration, only those values are used which deviate no more than 2 times the distance from the average found in the first iteration, i.e. using those  $Q_{ij}$  for which:

$$|Q_{ij} - Q_j| \leq 2 \cdot \sigma_{Q_j}$$

where the average distance is calculated using the points in the first iteration as:

$$\sigma_{Q_j} = \frac{1}{N(Q)} \cdot \sum_{i=p\_min(j)}^{p\_max(j)} |Q_{ij} - Q_j|$$

## Errors and quality check

Unfortunately, the required identity for  $I$  and for  $Q$  in the overlapping parts of the detector arrays is not always valid. This is due to the combination of serial read-out of the detector pixels and the moving instantaneous field of view (IFOV) which induces a spatial aliasing (effect of different effective FOV aliased in the measured intensities) between the end of a channel  $j$  and the beginning of a channel  $(j + 1)$ . To counteract this, it was decided to implement in SCIAMACHY a reverse read-out of channel 2 to secure overlaps 1/2 and 2/3 (considered the most important ones because the largest gradients of the polarisation are expected in this wavelength range).

For the GOME instrument it has been suggested to use PMD measurements to map the measured intensity over the FOV, and use this to unalias the spectra. However, with the detector read-out delay of  $\approx 1/30$  second and SCIAMACHY's PMD filter response of  $\approx 1/10$  second, this possibility looks rather dim, and will not be attempted for the time being.

Another potential hazard is shifting of the instrument response function in orbit. This changes the Mueller matrix elements in the equation above. To minimise the effects of a possible shift, the normalisation with the solar spectrum is made. Else the instrument response would enter the equation, and this has especially in the overlap regions a strong dependence on wavelength, making it very sensitive to shifts. However, the overlaps between channels 3-6 are implemented using dichroic filters, and these have a strongly wavelength-dependent polarisation response. For these channels a shift in instrument response would still have large impact on the possibility to retrieve a reliable polarisation from overlaps.

The channel split between channel-1/ channel-2 and channel-2/channel-3 is done mechanically by a partially reflective prism, located in an intermediate focal plane. There are indications that the splitting itself depends on polarisation, and/or on how homogeneously the beam is polarised.

Due to these hazards, the polarisation retrieved from overlaps must be considered suspect, unless diagnostics are passed which indicate that the hazards have not occurred.

In the GOME instrument it appears that unreliable overlap polarisations are characterised by a retrieved value of  $Q_{ij}$  which fluctuates strongly over the detector pixels in the overlap. It further appears that the uncertainty on retrieved  $Q$  is mainly due to instrument calibration problems and to problems with synchronisation of the detector readout (the latter problem will probably be smaller for SCIAMACHY).

We therefore calculate the error on  $Q$  as the square root of the variance of  $Q_{ij}$  over the overlap:

$$\epsilon_{-Q_j} = \sqrt{\frac{1}{N(Q)} \cdot \sum_{i=p_{min}(j)}^{p_{max}(j)} (Q_{ij} - Q_j)^2} \quad (3.115)$$

The test for quality control is passed when

$$\epsilon_{-Q_j} \leq NQ_{max} \quad (3.116)$$

where  $NQ_{max}$  is a noise error estimate from the initialisation file.

The polarisation from an overlap will be flagged as 'invalid' for an ISP if this test fails, or if  $Q_\lambda^2 + U_\lambda^2 > 1$ , or if one of the clusters in the overlap is missing.

As for the PMDs, polarisation values are marked invalid by setting the error on their  $Q$  and  $U$  values to  $-1$ . The values themselves are written to the level 1b product for diagnostic purposes (however wrong) except for the last case where they do not exist, and where they are to be set to 0.

### Averaging over IT

The polarisation values are calculated for all ITs contained in the largest IT in the State. In contrast to the PMDs where all PMD virtual sums are separately evaluated for each IT, the polarisation values from overlaps are only calculated for the smallest IT where they are available, and then averaged to obtain values for the larger ITs. This averaging is done weighted with the Sun-normalised intensity (i.e. we average the Stokes intensities not the Stokes fractions).

For each IT define an 'albedo' averaged over the overlap detector pixels:

$$A_j(t) = \frac{1}{N(Q)} \cdot \sum_{i=p_{min}(j)}^{p_{max}(j)} \frac{S_{ij}}{M_{1,ij} I_{SMR,ij}} \quad (3.117)$$

where the sum is taken over the same pixels as used for the final calculation of  $Q_j$ .

The average polarisation fraction over the larger ground pixel,  $\langle Q_j \rangle$ , is calculated using this albedo as weight:

$$\langle Q_j \rangle = \frac{\sum_{t=t_{start}}^{t_{end}} A_j \cdot \langle Q_{ij} \rangle(t)}{\sum_{t=t_{start}}^{t_{end}} A_j(t)} \quad (3.118)$$

and similar for the error  $\epsilon_{-Q_j}$ .

### Effective wavelengths of overlap polarisations

We simply take the wavelength of the SMR evaluated at the centre of the overlap pixels:

$$\lambda_j = \lambda_{SMR,n_j}, n = 0.5 \cdot (p_{min}(j) + p_{max}(j)) \quad (3.119)$$

## Calculation of polarisation fractions U

$U$  is calculated from the values of  $Q$  derived here from the overlaps, and from the ratios of Stokes parameters from the theoretical calculation  $U_0/Q_0$  and from the PMDs  $U_{45}/Q_D$ . This is done using the interpolation scheme described in Section 88 under 'Solving the PMD virtual sum'.

The errors are calculated as:

$$\epsilon_{-U_j} = \left(\frac{U}{Q}\right)_X \cdot \epsilon_{-Q} + \frac{Q_j}{Q_X} \cdot \epsilon_{-U_X} + \frac{Q_j}{Q_X} \cdot \left(\frac{U}{Q}\right)_X \cdot \epsilon_{-Q_x} \quad (3.120)$$

but for invalid overlap points (see above) the error is set to  $-1$ .

Also here  $\epsilon_{-U_j}$  needs to be limited for small  $Q_X$ , similar as done for the PMDs (Eq. 3.111):

$$\forall (|Q_X| < Q_{min}) : \epsilon_{-U_j} = \delta U_{max}$$

where  $Q_{min} = 0.01$  for  $\lambda_j \leq \lambda_{Ray}$  and  $Q_{min} = Pol\_Q_{min}$  for  $\lambda_j > \lambda_{Aer}$ .

## 3.14. Wavelength interpolation of polarisation values

### 3.14.1. Introduction

The Polarisation Correction Algorithm (PCA), as described in Section 3.13, generates a small array of fractional polarisation values at certain well-spaced wavelengths across the SCIAMACHY spectral range. Up to 12 points can be specified.

Six points come from the comparison of channel array signals with broad-band PMD signals (in Figure 3.12 these are the filled circles at points  $P$  with index  $A, B, \dots, F$ ; the corresponding wavelengths  $\lambda_A, \lambda_B, \dots, \lambda_F$  are approximately 370 nm, 500 nm and 700 nm, 900 nm, 1400 nm, 2400 nm depending on the exact spectral shape of the input spectrum). Five more points come from the channel overlap regions (in Figure 3.12 these are the open circles at points  $P$  with index 1, 2,  $\dots$ , 5 for overlaps between channels 1/2, 2/3,  $\dots$  5/6; the corresponding wavelengths  $\lambda_1, \lambda_2, \dots, \lambda_5$  are at 312.5, 400, 600, 800 and 1030 nm approximately). The last ("theoretical") point (labelled  $[\lambda_0, P_0]$  in the figure) comes from the Rayleigh single-scatter model simulation of polarisation in the Ultra Violet.

Before these polarisation values can be used for polarisation correction of the measured intensity, they must be interpolated to the wavelengths of all detector pixels. For reasons described below, our interpolation scheme should be performed on the Degree of Polarisation,  $P$ , rather than on the polarisation fractions. The degree of polarisation is defined in terms of Stokes fractions as:

$$P = \sqrt{Q_\lambda^2 + U_\lambda^2} = |Q_\lambda| \cdot \sqrt{1 + \frac{U_\lambda^2}{Q_\lambda^2}} = |U_\lambda| \cdot \sqrt{1 + \frac{Q_\lambda^2}{U_\lambda^2}}$$

As mentioned in the PCA description in Section 3.13.3, we take the ratio  $U/Q$  constant (except in a relatively small transition region between  $\lambda_{Ray}$  and  $\lambda_{Aer}$ ), in which case we may as well interpolate over  $Q$  as over  $P$ , because the difference is then only a fixed scaling factor. Since the ratio of  $U/Q$  as derived from the measurement is very uncertain if  $Q$  is small (comparable to its error), and m.m. for  $U$ , it is in fact safer to perform the interpolations over  $Q$  and  $U$  separately - at least for the purpose of polarisation correction, which basically depends on the value of  $Q(\lambda)$ . This is not quite legal in the transition region between  $\lambda_{Ray}$  and  $\lambda_{Aer}$  (see Section 3.13.3) where the polarisation angle (i.e. the ratio  $U/Q$ ) may change, but there we use an unconstrained Akima interpolation instead of a theoretical parameterisation in  $P$  (see below) and the necessity for interpolation in  $P$  is absent there.

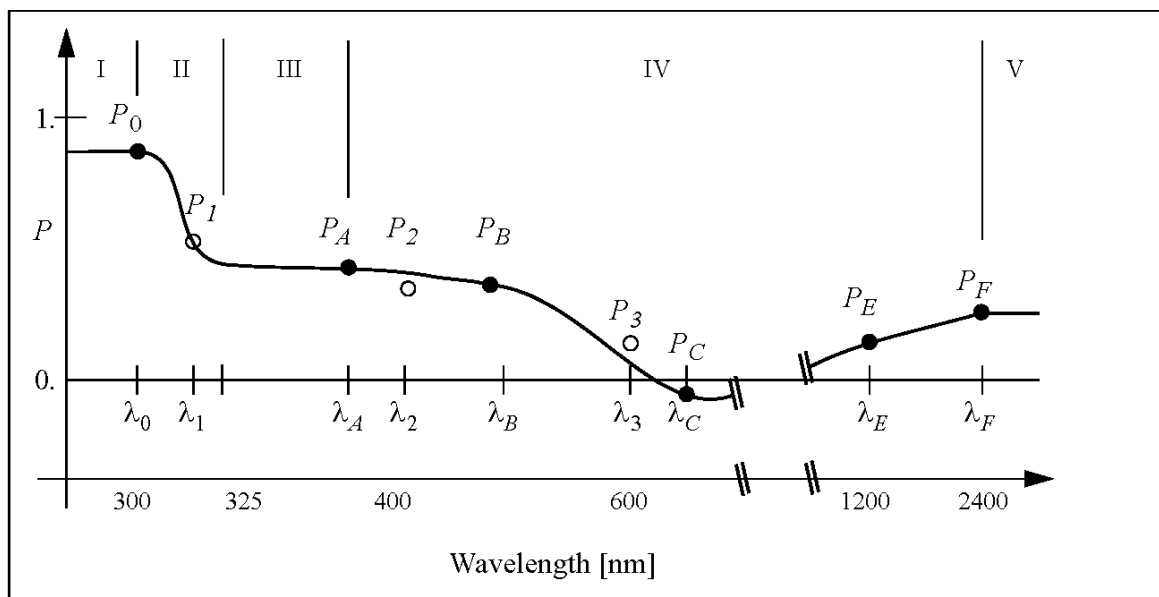


Figure 3.12.: Wavelength interpolation of polarisation values.

In the following we will keep the description general and always refer to an interpolation in  $P$ . This shall be read as: 2 interpolations, one in  $Q$  and one in  $U$ .

The SCIAMACHY wavelength range is for the interpolation purpose subdivided into 5 regions, which each have their own interpolation scheme. These regions are bounded by the following wavelengths, see Figure 3.12:

- Region I:* shortward of wavelength  $\lambda_0 (\approx 300\text{nm})$ .
- Region II:* between  $\lambda_0$  and  $\lambda_0 + \Delta\lambda_{\text{end-GDF}}$  (a pre-defined wavelength interval  $\approx 15\text{ nm}$  wide).
- Region III:* between  $(\lambda_0 + \Delta\lambda_{\text{end-GDF}})$  and  $\lambda_A$ , the effective wavelength of PMD-A.
- Region IV:* between  $\lambda_A$  and  $\lambda_F$ , the effective wavelength of PMD-F.
- Region V:* longward of  $\lambda_F$ .

In the following, we first consider the case where all measurement points are available. This should at least be the case for the Measurement States where all clusters have the same Integration Time. Subsequently we discuss the case where only single clusters out of the spectrum are available.

### 3.14.2. Interpolation - default case with all points available

For the critical region in the UV, where the polarisation may be a steep function of wavelength, (Region II), a parameterisation of the polarisation curve is assumed (analytic functions described by a small number of parameters which must be fitted according to the available information in that region).

For Regions III and IV, a suitable common interpolation routine is sufficient (Akima interpolation has been selected because of its capability to avoid oscillations as in common splines) - this applies to PMDs A to F, and to channel overlaps 2 to 5. However, the polarisation values of the overlaps may be expected to have low accuracy, in which case we do not want to use them for the interpolation. Two 'guards' are implemented again using dubious values:

- In the initialisation file a switch *do\_pol\_point* is present which for each of the 12 points indicates whether it shall be used for interpolation or not. This includes the theoretical point. It is not expected that this point will be invalid during in-flight processing, but it is useful to retain this contingency, as the validation of the polarisation correction algorithm will require testing with SCIAMACHY pre-flight FM measurements (hence no atmospheric polarisation point). The setting of switches for the measured polarisation values has to be tuned during in-orbit commissioning of the instrument. Default will be to exclude the overlaps unless they prove to contain useful information (for this reason they are indicated with open circles in Figure 3.12; the figure depicts a situation where overlaps 2 and 3 are not used in the interpolation).
- Each measured polarisation point carries a quality flag from the PCA algorithm. If this flag is set (implementation: error = -1), the point is neglected for interpolation.

Interpolation routines are not reliable for extrapolation beyond  $\lambda_F$  to the end of the wavelength range. Instead, a constant has been assumed for Region V, with value equal to  $P_F$  (the Akima interpolation in region IV is forced to approach this point with zero gradient)

Radiative transfer model calculations, including polarisation, have been performed by P. Stammes (KNMI) to study the polarisation behaviour in the UV for application to the GOME instrument [33]. These simulations show that up to wavelength  $\lambda_0$  (300 nm), the degree of polarisation  $P(\lambda)$  is virtually a constant, so there we set fractional polarisation equal to the theoretical single-scatter value at  $\lambda_0$ .  $P(\lambda)$  then changes rapidly between  $\lambda_0$  and a value  $\bar{\lambda} (\approx 325\text{nm})$ , then shows smooth behaviour into the visible (ca. 325-400 nm). Thereafter,  $P(\lambda)$  is a smooth slowly-varying function of wavelength.

The critical region is Region II (ca. 300-325 nm). An analytic function is required that mirrors the shape of simulated polarisation for all atmospheric scenarios. This function must have a turning point at the theoretical point  $\lambda_0$ , with parabolic fall-off behaviour near this point. The function must also show exponential tail behaviour as  $\lambda$  tends towards  $\bar{\lambda}$ . This role is fulfilled by the Generalised Distribution Function (GDF) constructed by R.

Spurr for the GOME calibration [61]:

$$P(\lambda) = \bar{P}(\bar{\lambda}) + \frac{w_0 \cdot e^{-(\lambda-\lambda_0)\cdot\beta}}{(1 + e^{-(\lambda-\lambda_0)\cdot\beta})^2} \quad (3.121)$$

where  $\bar{P}$ ,  $w_0$ ,  $\beta$  are parameters that characterise the GDF; they must be found to fit the given interpolation points.

The actually simulated polarisation shows a bit more complex behaviour, e.g. some residual structure of the O<sub>3</sub> Huggins bands is visible in the polarisation (due to different airmasses in- and outside the absorption peaks with different depolarisation by aerosols), but the approximation above was found accurate to better than 3% compared to the simulated polarisation values.

A practical problem with this theoretical approach is that we need to solve the GDF function for 3 parameters  $\bar{P}$ ,  $w_0$ ,  $\beta$ , while only two independent constraints ( $P_0, P_1$ ) are available in the region between  $\lambda_0$  and  $\bar{\lambda}$ . We briefly discuss 3 possible solutions of this problem:

1. Extrapolate the polarisation curve from region IV into region III. Join the GDF at  $\bar{\lambda}$  to this curve, requiring continuity in  $P$ -value and in gradient.  
This was the approach taken for GOME, but it has the disadvantage that, in Nadir, the (surface/boundary layer -) polarisation determined at visible wavelengths is largely prescribing the shape of the (stratospheric -) polarisation curve in the UV.
2. Extend the GDF curve to  $\lambda_A$  and use  $P_A$  as the third independent parameter.  
This has the advantage that only UV polarisation points are used for the GDF calculation, but the disadvantage that one prescribes a rather flat polarisation curve between  $\bar{P}$  and  $P_A$  which, according to theoretical models, is not always appropriate. We adopt a somewhat less strict approach and use the point  $(\lambda_A, P_A)$  to determine the GDF parameters, but terminate the GDF parameterisation at a point  $\lambda_0 + \Delta\lambda_{end-GDF}$ , chosen to be in-between  $\lambda_1$  and  $\bar{\lambda}$ , and extend the Akima interpolation from region IV to include region III as well (but only if  $P_2$  is present, see discussion below), with the constraint on the Akima interpolation that the curve joins the GDF smoothly in value and in gradient. This does not solve the fundamental problem that  $P_A$  may not be quite representative for the polarisation at  $\bar{\lambda}$ , but it gives the algorithm more freedom to shape the curve according to measurements around  $\lambda_A$ .
3. Find from theory an independent 3rd parameter.  
It seems that this is in fact possible. Examination of the aforementioned model data by R. Spurr for GOME, suggests that the wavelength at which the gradient of polarisation is steepest is more or less independent of the atmospheric composition, and depends only on the scattering geometry - or equivalently the value of  $P_0$ . This implies we can pre-calculate from models a data set  $\lambda_m, P_0$  of this maximum-gradient wavelength  $\lambda_m$  against  $P_0$ .

For the baseline algorithm of SCIAMACHY, we reject solution (1) because of the disadvantage mentioned. Solution (3) is also less preferred, because it leans more on theory than on actual measurements. However, if  $P_1$  is not available, we will use this additional piece of theoretical information.

As baseline we adopt solution (2).

The method to determine the 3 GDF parameters is as follows. Define the auxiliary functions

$$\begin{aligned} g_A(\beta) &= 4 \cdot \frac{e^{-(\lambda_A-\lambda_0)\cdot\beta}}{(1 + e^{-(\lambda_A-\lambda_0)\cdot\beta})^2} \\ g_1(\beta) &= 4 \cdot \frac{e^{-(\lambda_1-\lambda_0)\cdot\beta}}{(1 + e^{-(\lambda_1-\lambda_0)\cdot\beta})^2} \end{aligned} \quad (3.122)$$

then the parameters are successively solved from the following equations:

1. Solve  $\beta$  numerically using a root-finding algorithm from the equation

$$g_1(\beta) \cdot (P_A - P_0) + g_A(\beta) \cdot (P_0 - P_1) + (P_1 - P_A) = 0$$

2. Use this value of  $\beta$  to obtain

$$\bar{P}(\bar{\lambda}) = \frac{P_A - P_0 \cdot g_A(\beta)}{1 - g_A(\beta)}$$

3. and then

$$w_0 = 4 \cdot (P_0 - \bar{P}(\bar{\lambda}))$$

If the point  $P_1$  would not be available, we use the boundary condition of the wavelength of the steepest gradient,  $\lambda_m$ , and replace the first step (1) by:

$$1. \beta = \frac{\ln(2 + \sqrt{3})}{\lambda_m - \lambda_0}$$

The current calculation of  $\lambda_m$  uses a functional form taken from [26], and is similar to the calculation of the theoretical point. Here  $\lambda_m$  is expressed as a function of  $\cos \theta_0$  (note: recently a more sophisticated parameterisation has been found, see [27]):

$$\lambda_m = \lambda_{sg}(\cos \theta_0) \quad (3.123)$$

where the  $\lambda_{sg}(\cos \theta_0)$  are specified on the initialisation file for certain values of the cosine of the solar zenith angle; these values are linearly interpolated to the  $\cos \theta_0$  of the measurement (these initialisation file data will be derived from [26] for the US-standard atmosphere).

The GDF can only be constructed if a number of conditions apply. It requires that:

- $P_0$  and  $P_A$  are available
- $|P_0| > |P_A|$  or, if  $P_1$  is available,  $|P_0| > |P_1| > |P_A|$
- $P_0 \cdot P_A > 0$

If these conditions are not all true then the physical model is not applicable and the GDF shall not be calculated; on the Level 1b product the GDF parameter values are set to -99.

Once the GDF parameterisation has been calculated, the remaining issue is how to connect it optimally to the polarisation points at longer wavelengths. As a matter of principle, we make all connections continuous in value as well as in gradient. Although the GDF is constructed for wavelengths up to  $\bar{\lambda}$ , its nearly horizontal gradient at that point constraints the interpolation in Region III too much. Therefore, the connecting point is made at a wavelength  $\lambda_0 + \Delta\lambda_{end-GDF}$  where the second term is pre-defined on the initialisation file - the idea is to choose a wavelength which is shortly after the steepest gradient, in order to give the Akima interpolation in Region III a maximum of flexibility. At the same time this can correct to some extent for the situation where the measured polarisation at  $\lambda_A$  is different from the polarisation at  $\bar{\lambda}$  which ideally should be used to calculate the GDF.

However, the Akima interpolation in Region III should only be allowed this degree of freedom if it contains sufficient information from the UV region. Its gradient is mainly determined by the value at  $\lambda_A$  and the next polarisation point. If the next point is not at  $\lambda_2$  (i.e. if this polarisation point is missing), the Akima interpolation would be strongly influenced by wavelengths totally decoupled from the UV. To avoid that situation, the GDF parameterisation will be extended to  $\lambda_A$  if the point at  $\lambda_2$  is missing.

The GDF parameterisation shall only be used if the measured polarisation points behave more or less as expected; the minimum requirement is that the polarisation decreases with wavelength and that the Stokes intensities do not change sign in this region between  $\lambda_0$  and  $\lambda_A$ . If these conditions are not fulfilled, Akima interpolation shall be used in the whole region between  $\lambda_0$  and  $\lambda_F$ .

In general, whenever an Akima interpolation is joined to a parameterisation (either a GDF or a constant), the Akima interpolation is forced to join the parameterisation with continuity in gradient. This is achieved by extending the array of polarisation points with two artificial points located in the parameterisation region. These points have a value given by the parameterisation, and a wavelength corresponding to the last (first) wavelength of the parameterisation region minus (plus) 1 and 2 pixels.

The GDF parameters on the Level 1b product are calculated for Stokes fraction  $Q$ . The corresponding GDF parameters for the wavelength interpolation of  $U$  are then derived using the fact that the polarisation angle is assumed to be constant in this region, which can be translated into:

$$U(\lambda) = Q(\lambda) \cdot \left| \frac{U_0}{Q_0} \right|$$

### 3.14.3. Interpolation - only few points available

In case only measurements from a limited number of cluster are available, the procedure is a bit different. Note that, just like geolocation, the polarisation information has been calculated on the time scale of the cluster with shortest IT, for all 12 Fractional Polarisation points - but several points will be marked 'invalid' because no actual measurement is available.

Two schemes are envisaged:

1. *Using only information from the current datapacket:*

(note that the first polarisation points missing will be those in Regions I and II since low light levels there ask for longer integration times than in other spectral regions. We therefore are always in regions where we would use Akima polarisation anyway). If two or more valid polarisation measurements are available, interpolation in-between these points is performed using the Akima routine. Extrapolation outside the wavelength region covered by these points is done using a constant polarisation (c.f. Region V above) - adding two points with constant polarisation outside the measurement points will let Akima do this automatically, with a smooth transition (see above). If one polarisation point is available, the whole wavelength range attains this polarisation. If no polarisation point is available, the polarisation points  $P_{Ave}$  from the average ground pixel are used (see below) with the interpolation just mentioned.

2. *Using averaged information of the largest ground pixel:*

(as above, the UV region is again not taken into account). First the value  $P_{Ave}$  of the average over the ground pixel with the largest IT is calculated; here we always have a complete spectrum available hence information from all polarisation points. Using for the current (smaller) ground pixel the points where a polarisation measurement  $P_{cur}$  is available, a 'depolarisation ratio' is calculated (one for each point). This ratio is defined as:

$$\Delta = \frac{P_{cur}}{P_{Ave}}$$

The depolarisation ratio is interpolated to all polarisation points using the same interpolation scheme as under (1). All polarisation points between  $\lambda_A$  and  $\lambda_F$  are then updated using the formula  $P_{cur} = \Delta \cdot P_{Ave}$  and subsequently Akima interpolation (with constant extrapolation at the edges) is used to calculate the polarisation at all detector pixel wavelengths.

Scheme (2) retains more of the shape of the polarisation curve. This is advantageous if this shape does not vary too much from ground pixel to ground pixel; but else the simpler interpolation scheme (1) may be better. Scheme (1) is currently implemented; if this simple scheme is sufficient will have to be determined.

In any case the polarisation correction and hence the absolute radiance calibration of the clusters with a higher read-out rate will be compromised a bit - exactly for this reason we have calculated in Section 3.13 the polarisation values for all ground pixel sizes contained in the largest IT of a State, so that at least for this largest ground pixel an optimum polarisation correction is available.

### 3.15. Apply Radiance Response

The application of the radiance response is simply a division of the observational signals (after dark current, PPG, Etalon and stray light correction) by the radiance response function as calculated in Section 3.1 for the various observing modes.

The calibrated radiance of detector pixel  $i$  in units of  $photons/(s \cdot cm^2 \cdot sr \cdot nm)$  is calculated as:

$$S_{cal,i} = \frac{c_i \cdot S_{DPS,i}}{(M_1)_{i,\alpha} \cdot IT} \quad (3.124)$$

where  $c_i$  is the polarisation correction factor according to Equation (3.102) in Section 3.13.3, which is calculated using the Stokes fractions interpolated to wavelength (see Section 3.14).

Note that the angles for the Mueller matrix elements are instrument scan angles, but that the angles specified in the geolocation record of the Level 1b product are viewing angles. These are converted back to instrument scan angles by inversion of Equations (3.23) and (3.24), making sure that the angles lie in the interval  $[-180^\circ, +180^\circ]$ . The necessary zero offset angles are in the GADS 'Static Instrument Parameters' on the Level 1b product.

The precision error on the spectrum is calculated as the RMS sum of shot noise and the precision errors after PPG and stray light correction:

$$\epsilon_{-S_i} = \sqrt{\epsilon_{-S_{DPS,i}}^2 + \epsilon_{-shot_i}^2 + 0.25} \quad (3.125)$$

where the shot noise is used as calculated from Equation (3.65), and where the last term accounts for a digitalisation error of 0.5 BU. Note that this precision error is an absolute error in [BU]; to obtain a relative error the value has to be divided by the signal value  $S_{DPS,i}$  in [BU].

The accuracy is calculated as RMS sum of the accuracies from the previous calibration steps, including the radiance response accuracy as calculated by Equation 3.14 in Section 3.1.6, and the polarisation correction accuracy (consisting of accuracy on Stokes parameters and on ratios of Mueller matrix elements).

The accuracy on polarisation correction can be written as:

$$\Delta_{pol_i} = \sqrt{(\mu_2^D \cdot \epsilon_{-Q_i})^2 + (\mu_3^D \cdot \epsilon_{-U_i})^2} \quad (3.126)$$

where it is assumed that the error on the Mueller matrix elements is already implicitly included in the error on the Stokes fractions.

The total relative accuracy is then given as:

$$\Delta_{-S_i} = \sqrt{\left(\frac{\epsilon_{-S_i}}{S_{DPS,i}}\right)^2 + \epsilon_{-M_{1,i}}^2 + \left(\frac{\Delta_{pol_i}}{c_i}\right)^2} \quad (3.127)$$

#### 3.15.1. Sun-normalised radiance

The Sun-normalised radiance or Reflectivity can be calculated as:

$$R_i = \pi \cdot \frac{S_{cal,i}}{SMR_i} \quad (3.128)$$

where the factor  $\pi$  arises from the integration over half space, assuming a Lambertian reflecting ground surface.

Before the division by the SMR is made, the SMR is interpolated to the wavelength grid of the Earth-shine spectrum. The reason why the SMR is regridded and not the radiance spectrum, is that the latter contains more (atmospheric) structure and is thus more sensitive to undersampling effects.

The relative precision error is calculated as RMS sum of relative precision errors on the calibrated radiance and on the SMR. Interpolation errors due to undersampling effects are not accounted for.

The accuracy is calculated similar as for the calibrated radiance, except that in Equation (3.127) the error  $\epsilon_{M_1}$  is replaced by the relative accuracy on BSDF calculated from Equation 3.15 on page 33 . This is because the radiance response function divides out, but the BSDF does not.

The total relative accuracy on Sun-normalised radiance is given by:

$$\Delta_{R_i} = \sqrt{\left(\frac{\epsilon_{S_i}}{S_{DPS,i}}\right)^2 + \epsilon_{S_{SMR,i}}^2 + \epsilon_{BSDF_i}^2 + \left(\frac{\Delta_{pol_i}}{c_i}\right)^2} \quad (3.129)$$

Note that this accuracy on Sun-normalised radiance is not only relevant to users who work with the Reflectivity directly, but also to users who in their trace gas retrieval match the calibrated radiance spectrum with a SMR (e.g. O<sub>3</sub> profile retrieval applications). See also Section 5.

## 3.16. Quality Flagging

There are several data quality flags written to the Level 1b product. These may apply to the whole orbit, or only to a State, or only to a (cluster) readout in a State. These are summary flags; in level 1b to 1c processing a more detailed flagging (e.g. saturation check per pixel) may be triggered using these summary flags.

### 3.16.1. Dead or bad pixel mask

A mask with 'good' and 'Bad Pixels' is included as global (whole orbit) information. Bad pixel identification is based upon WLS measurements, as described in Section 3.6 'Calculate PPG and Etalon Parameters'.

### 3.16.2. Dark signal quality assessment

For each Limb state a check on the quality of the dark signal subtraction is made. This is done using the last measurement in the Limb State which is an exposure into 'deep space' at the highest tangent height of 150 km or 250 km. The average signal of this measurement after dark signal subtraction is determined. Ideally this should be zero. The calculation is described in Section 3.4 on page 50.

### 3.16.3. Wavelength calibration check

A quality check on the wavelength calibration could be made once per State. In the current processing, this is not done, but a placeholder exists on the Level 1 product. The method envisaged for future implementation could be the following. For this purpose a mean spectrum is calculated from all spectra obtained in this state after every longest integration time (when a full spectrum, albeit with different exposure times per cluster, is available). For a maximum of 20 positions per channel, the centre of gravity of Fraunhofer lines in the spectrum is calculated and the theoretical wavelengths are compared to the calibrated instrument wavelengths. Details of this calculation have still to be worked out. This calculation shall include Doppler shifts and line blend effects in accordance with SCIA's resolution; also we wish to use wavelengths where the centre of gravity is not influenced by strong atmospheric absorptions.

### 3.16.4. Sun glint and Rainbow flag

Sun glint is a phenomenon which does not invalidate the level 1b data per se, but it invalidates the calculation of air mass factors in the level 1b to 2 processing and therefore is flagged here using two thresholds for medium and high sun-glint danger.

Rainbow is a phenomenon which, above water clouds, yields high polarisation which may invalidate some of the assumptions made in the interpolation of fractional polarisation parameters.

Sun glint and rainbow are (strongly) dependent on the observing geometry. For small ground pixels, it is sufficient to evaluate the check only in the middle of the pixel (position F in the footprint, see Figure 3.6 on page 41); for larger ground pixels, the check is also evaluated at the ground pixel edges (footprint positions E,F,G). The flag is only calculated for the clusters with the shortest integration time. For clusters with longer integration time, the highest danger level flag is taken from the shorter exposures which are contained in this long integration time. For rainbow it is furthermore ascertained that the rainbow does not lie between centre and border of the (larger) ground pixels. The present flags only indicate a geometrical possibility. The actual presence of reflecting surface (water or clouds) is not checked. This would be a level 2 activity.

For sun glint a flag is set if both the viewing zenith angle and the viewing azimuth angle are within a limit  $\gamma$  equal to the corresponding solar zenith/azimuth angle. Preliminary limits are  $\gamma_1 = 15^\circ$  for low sun glint danger and  $\gamma_2 = 5^\circ$  for high sun glint danger. The flag is calculated for footprint position F only (and not for E,G) if the

ground pixel size is smaller than the sunglint angle:

$$IT_{smallest} \leq \gamma_1/60^\circ$$

where the maximum swath width angle is taken as  $60^\circ$ .

The rainbow occurs when the scattering angle  $\Theta$ , as calculated by Equation (3.96) in Section 3.13.2, is within an angular limit  $\rho_2$  around an angle  $\rho_1$ :

$$|\Theta_X - \rho_1| \leq \rho_2$$

for  $X=F$  if the ground pixel size is smaller than the angular rainbow width  $IT_{smallest} \leq \rho_2/60^\circ$  and else for  $X=E,F,G$ .

Preliminary values are  $\rho_1 = 140^\circ$  and  $\rho_2 = 3^\circ$ . Because of the small width  $\rho_2$  of the rainbow we also need to check if it doesn't lie in-between the points E-F or F-G. If

$$IT_{smallest} > 2 \cdot \rho_2/60^\circ$$

then the rainbow flag is set if not

$$\forall X : \Theta_X \leq \rho_1 - \rho_2 \text{ OR } \forall X : \Theta_X \geq \rho_1 + \rho_2$$

The sun glint/rainbow flag is set to a value of 1 for medium sun glint danger; to a value of 2 for high sun glint danger, and to a value of 4 for rainbow. If the pixel would be so large that rainbow and sunglint occur in the same pixel, the flag is the sum of sun glint and rainbow flags (i.e. 5 or 6).

### 3.16.5. Saturation

If a detector pixel read-out exceeds a certain limit it is regarded to be saturated. For each readout, the total number of saturated pixels in the data packet is written to the Level 1b product. In the level 1b to 1c processing, only the flagged readouts then need to be checked for saturation.

### 3.16.6. Hot pixels

Hot pixels as defined here are caused by impact of cosmic particles on the detector array; they can only be reliably detected on smooth spectra. Hot pixel checks are therefore only performed on dark and on WLS measurements, see the description of dark signal Health check in Section 3.4.2 on page 50 and of WLS pre-processing in Section 3.6.3 on page 60. The hot pixel thresholds used are different for dark and for WLS measurements: for WLS measurements they have been increased to prevent triggering on WLS signal noise. For the PMDs, only dark measurements are checked for hot pixels, as the PMDs are not used in WLS processing. Note that the chance of having hot pixels is large in the SAA; although hot pixels are not flagged on science (atmospheric) measurements, these measurements are flagged by a SAA flag, when the geolocation of the State indicates an overpass through the SAA (see Section 3.2 on page 34).

### 3.16.7. Red Grass

Red Grass is an artefact of SCIAMACHY's Reticon detector readout electronics (channel 1-5). It appears as a pixel-to-pixel oscillation with a frequency of 2 pixels (odd pixel value high - even pixel value low) around the true value. The oscillation seems to be toggled by certain signal levels, but not systematically enough that it can be predicted. Red Grass may occur in part of a channel, and even over several separate regions within a channel. In each region the pixel-to-pixel amplitude is constant. Based on the latter fact, a Red Grass flagging algorithm is implemented in the Level 0 to 1b processing. The algorithm is taken from [49] and is not further described here.

For each cluster which is read out, the flag is written to the Level 1b product. In the level 1b to 1c processing, only the flagged clusters need to be checked or corrected for Red Grass. A correction algorithm for Red Grass has been proposed [50], but is currently not implemented in the operational processing.

### 3.16.8. Decontamination flag

Decontamination is an infrequently used instrument mode where the detectors are heated to remove ice. As this causes an instable dark signal, the user is warned by a decontamination flag on the level 1b product.

The decontamination mode is detected via the "Detector Temperature" field in the Channel Data Header of each instrument data packet. If the nominal temperature threshold for one data packet in a state is exceeded, the flag is set for the whole orbit (the flag, y or n for each channel, is written in Field 11 of the SPH, which previously contained 50 blank (spare) characters. It now contains, besides the decontamination flag, also the version of the initialisation file).

The lower and upper limits for nominal operation (temperature sensor binary units) are given by (one value for each channel):

```
min_binary_limit_ch = [ 19923, 20033, 21505, 21315, 21421, 19328, 14624, 14527]  
max_binary_limit_ch = [ 20433, 20547, 21990, 21452, 21528, 19918, 15648, 15223]
```

### 3.17. Notes on algorithm description

In the algorithm description of the preceding sections, several remarks must be taken into account. These are either clarifications, or later additions to the algorithms which are generally applicable.

- Note 1: the term 'channel' used in the algorithm description refers to whole detectors, i.e. channel 1a and 1b (for example) are not to be taken as 2 individual channels as in the SCIAMACHY instrument terminology, but have to be combined into one 'channel 1'. An exception occurs in channels 6 and 8 whenever key data are to be interpolated in wavelength. The interpolation here shall be done separately for the first and second part of these channels, designated as 'channel 6 (8)' and 'channel 6+ (8+)' respectively. The boundaries between these sub-channels are specified on the initialisation file.
- Note 2: whenever a summation, average, or median value is taken in the processing of calibration measurements, pixel values which are flagged as "bad" in the Bad Pixel Mask have to be omitted from this summation, average, or median value. The same holds for 'hot' pixels detected in Dark or WLS calibration measurements.
- Note 3: There may be a difference between the integration time (IT) of a (pixel in a) cluster and the readout time (RT) of the corresponding data packet. This occurs if the IT is shorter than 1 BCPS. In that case, only the last on-board readout of the detector during the RT is kept and transmitted to ground; other detector readouts are discarded. The following equations hold (times in seconds):

$$\begin{aligned} IT[s] &= t_{PET}[s] \cdot f_{Coadd} \\ RT[s] &= MAX(t_{PET}[s], 1/16) \cdot f_{Coadd} \end{aligned}$$

For historic reasons, this document may use the term integration time where readout time would be more appropriate. Generally we define that in dealing with issues of packet lengths, integration time means  $RT$ , while with issues of signal strengths integration time means  $IT$ . In the latter case we will mostly write  $t_{PET} \cdot f_{Coadd}$  instead of  $IT$ .

A special case exists for the Epitax detectors in channels 6-8. Here the end of integration time is triggered on the leading edge of the BCPS (as with the Reticons), but the next integration starts on the trailing edge of the BCPS. Therefore, the true exposure time  $t_{PET}$  for  $IT$  is slightly smaller than the data packet separation time  $t_{PET}$  for  $RT$ . This readout scheme is only for 'normal' readouts, not for the hot mode. For channel 6-8 we then have:

If

$$t_{PET}[s] > 0.031$$

then

$$IT[s] = (t_{PET}[s] - 0.00118125) \cdot f_{Coadd}$$

This difference of ca. 1 ms is only significant for States with very short integration times. We apply this correction only in the calculation of Dark Signal and in the application of the (ir)radiance response, e.g. for the calculation of the Sun Mean Reference. This effect has been neglected in e.g. the integration of the PMD signals to the exposure time of the corresponding channel signals, or in the calculation of stray light.

## 4. Limitations of the Algorithms

This Section describes, in no particular order, limitations which apply to the algorithms. Some of these limitations are inherent to the algorithm itself, whilst others are due to unforeseen behaviour of the instrument (the latter points are taken from discussions within the SCIAMACHY Calibration Group).

### **NIR channels 6,7,8**

The detectors in these channels suffer from non-linearity effects which are currently under study. This may lead to signal errors of up to a few 100 BU. Furthermore there is severe icing on the detectors in channel 7 and 8 which influences, on orbital basis, the transmission and also the thermal background. The icing also invalidates the polarisation values of PMD-F. In addition, there seems to be a light leak in channel 7. Spectral calibration may be problematic, especially in channel 7 and 8, due to unavailability of sufficient good lines (lines partly spoiled by 'bad' pixels).

At present, Level 1b radiances from these channels shall be regarded as experimental and not suitable for operational use.

### **UV/VIS channels 1-5: first and last readout in a state**

The memory effect of each first readout in a state is not reliable - by absence of measurement information, the algorithm assumes that during the state set-up time the signal was equal to that of the first measurement.

At the last readout in a state, it may happen that the scan mirror is already moving to its rest position (viewing 'dark' inside the instrument) before all the detector pixels are read out. This may cause a slight drop-off of intensity which increases with pixel number.

### **Spatial stray light in Limb**

Although the scan mirrors of SCIAMACHY have been specially manufactured to be ultra-smooth, there is still a residual scattering of light on the mirror surface. In limb observations, this is noticeable as stray light. The effect is particularly observable at high altitude measurements, where the backscattered signal at that altitude is very low. The stray light shows a tropospheric signature; around sunrise there is also an amount of stray light from the Sun. Currently, the bi-directional properties of the scattering are not characterised and no correction algorithm exists.

### **Stray light in PMD-45**

PMD-45 measures a signal which is about 13% higher than expected on the basis of the on-ground calibration data. There are strong indications for stray light to this PMD, but also a problem with the on-ground calibration data cannot be ruled out. As a consequence, the polarisation values  $Q$  and especially  $U$  from the combination PMD-D + PMD-45 are unreliable.

To minimise influence on the other PMDs, the value of  $\lambda_{Ray}$  in the polarisation algorithm has been set to cover the whole SCIAMACHY wavelength range, so that at all wavelengths except 850 nm the theoretical polarisation angle is used to calculate  $U$  from  $Q$ .

## Polarisation in Occultation mode

The algorithm to calculate polarisation values for solar Occultation Measurements neglects the influence of the small aperture (as calibration data do not exist for the small aperture mode). In practice it appears that the small aperture has a large effect on polarisation. Therefore, in version 8 the polarisation values are no longer calculated for occultation measurements.

## PMD crosstalk

For historical reasons, the PMD crosstalk algorithm works on dark-signal corrected PMD signals, instead of on raw signals. In a restricted signal range where the cross-talk is non-linear, this yields the following errors. Signal values from 3880 to  $\approx 4500$  BU (i.e. 3880 + dark) suffer from 0 to 0.6% error; signal values from 50600 to  $\approx 51200$  also show this effect but these signals are considered saturated anyway. The cross-talk is only present for amplifier B (the default, high-gain choice) of PMDs A-F, not for PMD-45.

## PMD synchronisation

The synchronisation of the PMDs to the corresponding channel measurements uses the PMD analogue filter delay from the initialisation file. Currently this is one number for all PMDs, which includes a correction term for the sequential readout of the Reticon detectors (see Section 3.2.2 on page 36). In fact, each PMD should have its own delay time. At the time of writing, the filter delay value of 24 ms, which optimises the UV/VIS PMDs, cause the synchronisation of PMDs E and F to be in front by  $\approx 10$  ms.

## Geolocation

The geolocation on the Level 1b product is given for the readout time of the BCPS. For the Reticon detectors (channel 1-5) this is valid for pixel 0 only; all other detector pixels lag behind by a value of  $0.028 \cdot i$  ms where  $i$  is the detector pixel number ( $i = 0, 1, \dots, 1023$  for consecutive wavelengths in channels 1-5 and  $1023, \dots, 1, 0$  for channel 2 which is reversed). For the Epitaxx detectors (channel 6-8) there is a lag of 1.8 ms for all pixels.

As a consequence, the Nadir scan pattern may be wrapped around the edges for higher pixel numbers. In Limb mode, the azimuth scanner waits at the end of the horizontal scan till all pixels are read out before moving to the next tangent height.

## Tangent height in Limb

The geolocation, and especially the calculation of tangent height in Limb, uses predictions of the pointing of the spacecraft platform. In practice, deviations exist which may cause errors (slowly varying offsets) in tangent height of up to  $\approx 2.5$  km. Starting with IPF version 6.03, this error is reduced via misalignment correction to  $\pm 1$  km in NRT, and to a few 100m in Offline Processing using the AUX\_FRA auxiliary file (this file is unavailable in NRT). See also [36].

## Sun Mean Reference

Absolute calibration is only provided for Sun diffuser spectra using the ESM diffuser. All other solar spectra are semi-calibrated and may contain residual polarisation features. This shall be taken into account when interpreting the SMR auxiliary data.

(Note: at the time of writing also the absolute calibration of the ESM diffuser shows a large offset - it is currently under re-calibration)

## BSDF

The approach for the BSDF calibration of the ESM diffuser assumes a smooth function of wavelength. On-ground calibration data have shown different high-frequency spectral features for Solar and Earth-shine modes, but it is not known to which extent these features are real or an artefact of the calibration set-up. Based on preliminary analysis by TPD, and based on experience with the GOME instrument, such features on the BSDF may be expected, but they depend on the solar incidence angle on the diffuser.

## Etalon

The algorithm for etalon correction only covers a pixel range given by initialisation parameters *etal\_pix\_min* and *etal\_pix\_max* (values per channel). Outside this region the etalon is set to a value of 1. Applying etalon may cause a radiance jump at these pixels (in the overlap regions, which are normally not used).

The Fourier-filtering algorithm for etalon is intended to correct broad, sine-wave like features. It cannot cope with very sharp features, such as the dichroic shift feature near 480 nm. Applying etalon may cause a spurious feature here from 'algorithm overshoot'.

## PPG

The WLS measurements used for deriving the PPG suffer from noise which in channels 1-5 may dominate the PPG effect. PPG values from a single WLS measurement shall not be used, only averages over a large number of measurements (in other words, neglect the 'newly calculated' PPG values and only use those from the GADS).

## 'Newly Calculated' Calibration parameters

In concordance with what has been said above for PPG, the parameters on the 'newly calculated' ADSs of the Level 1b product are intended for further processing by the processor. They shall be ignored by the general user, as they do have certain limitations which are not further discussed here.

## 5. Measurement Uncertainty Analysis

*This chapter only presents a general overview. More detailed information may be presented in the Product Handbook.*

### 5.1. Introduction

It is important to distinguish between the terms accuracy and precision:

- The accuracy of a measurement is a measure of how close its result is to the true value.
- The precision of a measurement is a measure of how well its result has been determined, without reference to its agreement with the true value. Precision is therefore a measure of the reproducibility of the result, irrespective of e.g. a systematic deviation.

Note: the definitions of precision and accuracy have some grey areas.

For example, the leakage current which is determined around once per month carries noise, and errors due to this noise should be contained in the precision - but one may also argue that for each month the errors are calibrate able, and therefore should only be contained in the accuracy. As other example, pixel-to-pixel noise on the calibrated radiance response  $RR(\lambda_i)$  is a fixed (in principle calibrate able) error which therefore should be contained in the accuracy not precision - but one may also argue that fluctuations in wavelength calibration alias this noise quasi-randomly on the measurements and therefore degrade the precision.

In this document we will stretch the definition of precision to all quantities which are pixel-to-pixel dependent. This facilitates reference to the SIRD requirement which also speaks of a relative (pixel-to-pixel) radiometric accuracy.

On the SCIAMACHY level 1b product only accuracy errors are specified. These comprise the accuracy errors on key data for (ir)radiance sensitivity and on key data for polarisation sensitivity. In addition, accuracy errors are given for the calculated Stokes fractions  $Q, U$ .

Precision errors are calculated in the Level 1b to 1c processing step. On the level 1c product both the precision and the accuracy errors should be specified. At the moment of writing, in the first release of the level 1b-1c software, the level 1c product contains only precision errors (which are the errors relevant for the NRT level 2 processing); users should consult the software documentation for the situation in future software versions.

## 5.2. Overview of errors on Level 1c data

SCIAMACHY level 0 data is converted into ‘calibrated radiance’ (level 1c) by applying calibration algorithms and calibration parameters.

Part of these calibration parameters are determined regularly using in-flight measurement data when SCIAMACHY looks into deep space or takes white light or spectral lamp, or sun diffuser calibration measurements. The in-flight calibration parameters will be collected over the whole lifetime of SCIAMACHY, to be applied to the science observations of the Earth’s atmosphere as well as to those of the Sun.

In addition, data from pre-flight instrument calibration, the so-called ‘Key Data’ are required.

As will be shown below, the errors on the in-flight calibration data are mainly significant for the precision, while the errors on the Key Data are both significant for the precision and for the accuracy.

The important type of error for the ‘calibrated radiance’ is the accuracy.

For Level 2 trace-gas retrieval using absolute radiances in connection with a SCIAMACHY Sun reference spectrum (e.g. for  $O_3$  profile retrieval), the absolute error on calibrated radiance is irrelevant, since this cancels out in the ratio of Earthshine spectrum to Solar spectrum (albedo), which is the usual retrieved quantity. For these data users, the relevant accuracies are the accuracy error on BSDF and the accuracy error on the polarisation correction factor.

The important type of error for the retrieval of trace gases, using differential methods such as DOAS, is the precision, notably the precision on the Earthshine radiance normalised to the Solar irradiance.

In order to retrieve trace gases with small absorption depths, e.g. BrO which has (in channel 2) a relative absorption depth of only  $\approx 10^{-3}$ , the precision requirements on the SCIAMACHY measurements are very high: the SIRD [15] requires a relative precision of  $2 \times 10^{-4}$ . Great care must be taken during the calibration to achieve this goal, as will be shown below.

The accuracy on the calibrated radiance is derived from the noise and the memory-effect correction on the measurements, and from the accuracy on individual calibration measurements through the usual error propagation.

Similar holds for the precision, but here we have a few important notes to make regarding the PPG correction:

- the function  $ABS\_RAD(\lambda_i)$  as determined during the on-ground calibration of the instrument, has been obtained by dividing the measured radiance response for pixel  $i$  by the  $PPG(i)$  calculated with a certain ‘on-ground calibration’ algorithm (after which a spectral calibration assigns a wavelength to each pixel). This is done to separate pixel-dependent sensitivity of the detector from wavelength-dependent sensitivity of the optical bench, since the wavelengths may shift ‘over the detector’ (depending on temperature[gradients]) while the pixel-dependent quantities remain stationary. However, the determination of PPG, which is the ‘relative sensitivity’ of pixel  $i$  compared to its neighbours, is very sensitive to how this ‘relative sensitivity’ is determined in the algorithm (see next section); slightly different algorithms for ‘on-ground calibration’ and for in-flight data processing may lead here to considerable loss of precision.
- similar holds for the calibration Key Data parameters  $ETA(\lambda_i)$  and  $ZETA(\lambda_i)$  (see Section 3.1) which are contained in the polarisation correction term  $C_{pol}(\lambda_i)$ .

The reason why we address only precision here, is that the PPG correction is too small to significantly affect the overall accuracy, which will usually (at sufficient signal level) be determined by the errors on the radiance response and the polarisation correction.

We now give a concise overview of error types carried from the various input calibration data.

### Memory correction

At this moment it is not clear if this is a precision issue or not. Since all pixels of one detector are going through the same electronics, it may be hoped that pixel-to-pixel errors only arise due to the non-linearity of the effect.

For small absorption depths, this non-linearity is negligible. For spectra taken under constant illumination, such as solar calibration spectra, non-linearity errors may be introduced in the Fraunhofer lines but this leads to constant ('calibrateable') errors in time. Therefore we do not include memory correction in the precision error budget. For strong absorptions under changing illumination conditions (e.g. O<sub>2</sub>-A band) precision may be affected though.

Memory effect is not present for signals under  $\approx 10,000$  BU. For larger signals, the uncertainty on memory effect correction is  $\approx 5$  BU.

### **Dark signal subtraction**

The dark signal is calculated for each pixel independently. Errors in dark signal due to noise are included in the precision. Errors in thermal background (channels 6-8) due to temperature (gradients) are currently not considered, but should be included in the accuracy, not in the precision.

### **Stray light signal subtraction**

As far as currently foreseeable (before the calibration), stray light will be a relatively smooth function of wavelength. Errors on stray light subtraction will be included in the accuracy, not in the precision.

In the level 1b to 1c processing a fixed number from the initialisation file (also on Static Instrument Parameter GADS) is used; value t.b.d.

### **Wavelength calibration**

Errors in wavelength calibration result indirectly in radiometric errors because the wrong interpolation of Key Data is made. This is usually not a pixel-to-pixel issue unless there is significant noise on the Key Data (but see also the discussion above on PPG correction). These wavelength calibration errors will be covered in the description of errors on Key Data.

### **Pixel-to-pixel gain**

Errors on PPG affect the precision, as discussed above.

In the level 1b to 1c processing a fixed number from the initialisation file (also on Static Instrument Parameter GADS) is used; value t.b.d.

### **Etalon correction**

Since this is a broad-band phenomenon, it only affects accuracy, not precision. At present no method is available to estimate how well etalon can be corrected. It is expected that errors on the etalon correction are significantly smaller than the errors on the Radiance Response Key Data; therefore etalon correction errors are at present neglected.

### **BSDF correction**

The BSDF of the diffuser is specified in the on-ground calibration data for  $\approx 20$  wavelengths. Errors on these calibration data affect the (broad-band) accuracy only.

## Polarisation correction

Errors due to noise and PPG correction on Key Data parameters  $ETA(\lambda_i)$  and  $ZETA(\lambda_i)$  affect the precision; the other ('greek') Key Data parameters are integrated over broad-band wavelength regions where noise is averaged out; it is no longer a precision issue. Accuracy is further determined by on-ground calibration errors on Key Data, and by level 0 to 1b processing errors in the determination of the atmospheric polarisation parameters.

The accuracy for the determination of  $Q$ ,  $U$  from PMDs is expected to be near 0.1 (this is 5% of the full range from  $[-1, 1]$ ).

For the polarisation fractions from overlaps, no estimate can be given before the results of the commissioning phase arrive; these errors may be dominated by spatial inhomogeneity of the ground scene (t.b.d.) or by certain small-scale features in the on-ground calibration data which require further study.

For the polarisation correction factor, also errors due to wavelength interpolation must be taken into account, although these are probably not the dominant source of error.

## Radiance response

Errors due to noise and PPG correction on radiance response Key Data affect the precision; systematic errors in the calibration measurement set-up, or in radiance standards, affect accuracy only.

See discussion above.

## Summary of errors

The following table summarises the error sources on the calibrated radiance. Wavelength calibration errors are not included here, for reasons discussed above.

Measurement	Accuracy	Precision
<i>Memory correction</i>	$\approx 5$ BU for signals $> 10,000$ BU	-
<i>Dark signal subtraction</i>	calibration data errors: $\sigma_{FPN}, \sigma_{LC}$	readout noise $\sigma_E$ , shot noise on LC
<i>Stray light subtraction</i>	errors in on-ground calibration data (TBD); errors in signal estimate for single clusters (presently ignored)	-
<i>Etalon correction</i>	presently ignored	-
<i>Pixel-to-pixel gain</i>		(preset value, TBD)
<i>Radiance response</i>	errors in on-ground calibration data (TBD)	noise and PPG-correction errors in on-ground calibration data ABS_RAD (TBD)
<i>Polarisation correction</i>	errors in on-ground calibration 'Greek' Key data (TBD); errors on level 1 $U, Q$ errors in interpolation of $U, Q$ to $\lambda$	noise and PPG-correction errors in on-ground calibration data ETA, ZETA (TBC, only if not smoothed)

**Table 5.1.:** Summary of error sources on Level 1c data.

The error on the wavelength registration of the calibrated spectra is given by the quantity  $\epsilon_j$  calculated in Section 3.1. Based on experience from GOME, the magnitude of this error is estimated to be  $\approx 0.05$  of a detector pixel.

## A. Level 1b product structure

Detailed definitions and product formatting can be found in the appropriate documents [4, 42]. Here we shall list the main structure of the product file, which is in accordance with the general ENVISAT PDS formatting rules.

The level 1b product will include headers (MPH, SPH), calibration data sets which are constant for the entire product, the so-called global annotation data sets (GADS), annotation data sets varying over time (ADS), and several measurement data sets (MDS) depending on the viewing modes which are given by the definition of the corresponding instrument state. The level 1b data product will consist of just one file including all sensor modes excepting dark measurements.

The *main product header* (MPH) has a fixed format, as described in [42] and includes information about product identification, data acquisition and processing, time and position of the measurement data, ENVISAT orbit and position, SBT to UTC conversion, product confidence data and sizes of the following data.

A *specific product header* (SPH) will include slicing information, start and stop times and location, references to calibration data, product confidence data, summary of the number of states and the data set description records (DSD).

Directly after the DSD records two general PDS-defined *annotation data sets* (ADSs) follow, containing condensed quality information (SQADS) and a rough geolocation for each measurement State on the product (LADS).

The different *global annotation data sets* (GADS) will include calibration data prepared for the processing: leakage current and noise characteristics, pixel-to-pixel gain and Etalon parameters, spectral and radiometric calibration parameters, sun reference spectra and the polarisation sensitivity parameters and errors on the Key Data are given in those GADSs. In addition there is a GADS 'Static Instrument Parameters' which contains data from the Level 0-1b initialisation file which are relevant for Level 1b-1c processing.

The *measurement data sets* (MDS) may be divided into three observational MDSs and one monitoring MDS. The observational MDSs include the raw signal values of the array detectors, the memory effect correction (channel 1-5 only), the calculated straylight, geolocation information (two different geolocation information types; one for nadir and the other for limb and occultation measurements), the fractional polarisation values, derived quality flags, and header information retained from the detector module data packets. The monitoring MDS includes only the raw signal values of the array detectors, a reduced set of geolocation information, and header information retained from the detector module data packets.

The *annotation data sets* (ADS) include time dependent information about the sequence of states, the PMD and auxiliary data packets of the level 0 data, and optionally a set of newly calculated in-flight calibration parameters if the corresponding measurements are present in the level 0 data.

Using the included calibration data from the GADS, the raw signals in the observational MDSs can be converted by the level 1b to 1c processing program to calibrated (ir)radiance.

Figure A.1, taken from [4], gives a graphical representation of the product structure.

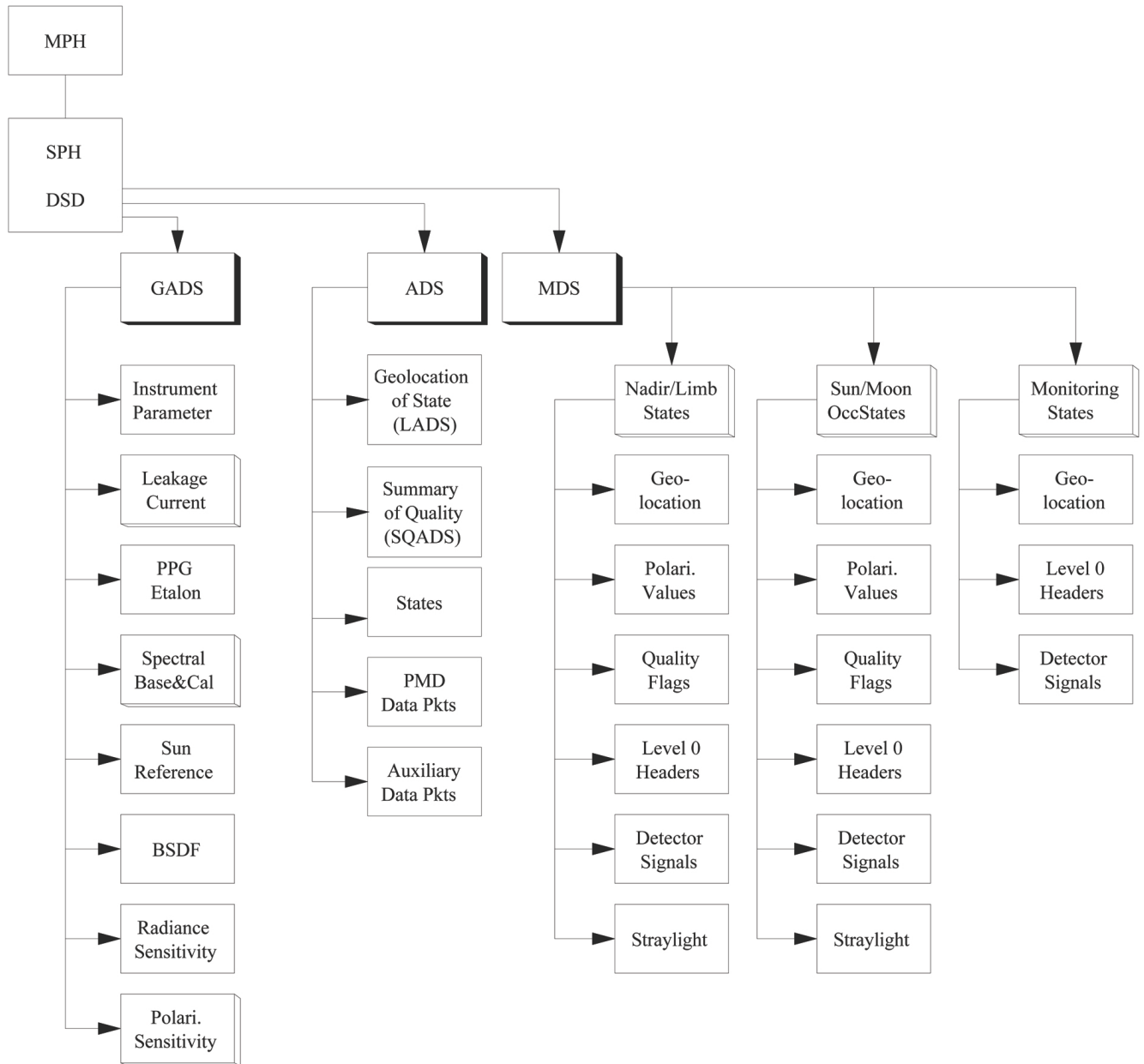


**Figure A.1.:** Schematic structure of the Level 1n Product.

## B. References

### B.1. Applicable Documents

- [1] SCIAMACHY Level 0 to 1b Processing, Ground Processing Performance Requirements, ENV-TN- DLR- SCIA-0004, August 1996. Draft, DLR-IMF.
- [2] SCIAMACHY: Optical Assembly Requirements and Constraints for In-Flight Operation and Calibration, TN-SCIA-1000FO/117, 12.01. 1996. issue 1, Fokker Space.
- [3] SCIAMACHY Operations Concept: III. Instrument States, PO-TN-DLR-SH-0001/3, 30.3. 2001. Issue3/1, DLR-IMF.
- [4] W. Balzer and S. Slijkhuis. SCIAMACHY Level 0 to 1b Processing, Input/Output Data Definition, ENV-TN-DLR- SCIA-0005. Technical Report Issue 5, DLR-IMF, 21.07. 2000.
- [5] SCIAMACHY Algorithm Development and Data Usage Subgroup. Scientific Requirements Document for Data and Algorithm Development, January 1998. issue 2A.
- [6] SCIAMACHY Operations Support Team. SCIAMACHY Instrument Monitoring I. The Concept. Technical report, DLR, 31.3. 1998.

### B.2. Literature References

- [7] ENVISAT-1, Mission & System Summary, March 1998. ESA brochure (also on <http://envisat.esa.int/support-docs>).
- [8] I. Aben, F. Helderma, D. M. Stam, and P. Stammes. Spectral fine-structure in the polarisation of skylight. *Geophys. Res. Letters*, 26:591, 1999.
- [9] I. Aben, D. M. Stam, and F. Helderma. The Ring effect in skylight polarisation. *Geophys. Res. Letters*, 28:519, 2001.
- [10] R. M. Azzam and N. M. Bashara. *Ellipsometry and Polarized Light*. Elsevier Science Pub., 1987.
- [11] D. R. Bates. Rayleigh Scattering by Air. *Planet. Space Sci.*, 32:785, 1984.
- [12] Ute Boettger. Private communication. DLR, 1998.
- [13] M. Born and E Wolf. *Principles of Optics*. Pergamon Press, 1965.
- [14] H. Bovensmann, J. P. Burrows, M. Buchwitz, J. Frerick, S. Noël, V.V. Rozanov, K.V. Chance, and A. H. P. Goede. SCIAMACHY - mission objectives and measurement modes. *J. Atm. Sci.*, 56(2):127 – 150, 1999.
- [15] J. P. Burrows, K. Chance, P. Crutzen, H. van Dop, J. Geary, T. Johnson, G. Harris, I. Isaksen, G. Moortgat, C. Muller, D. Perner, U. Platt, J.-P. Pommereau, H. Rodhe, E. Roeckner, W. Schneider, P. Simon, H. Sundquist, and J. Vercheval. SCIAMACHY A European proposal for atmospheric remote sensing from the ESA polar platform. 55122 Mainz, Germany, 1988. Max-Planck Institut für Chemie.
- [16] J. P. Burrows and K. V. Chance. SCIAMACHY and GOME: The scientific objectives. In *Optical Methods in Atmospheric Chemistry*, volume 1715 of *Proc. SPIE*, 1992.
- [17] J. P. Burrows, E. Hölzle, A. P. H. Goede, H. Visser, and W. Fricke. SCIAMACHY- Scanning Imaging Absorption Spectrometer for Atmospheric Chartography. *Acta Astronautica*, 35(7):445, 1995.

- [18] W. R. Falk. Data Reduction from Experimental Histograms. *Nuclear Instruments and Methods in Physics Research*, 220:473–478, 1984.
- [19] A. P. H. Goede. SCIAMACHY Instrument Concept. In *Proceedings ESAMS 99 - European Symposium on Atmospheric Measurements from Space*, volume 1, pages 147–155. ESA, 1999.
- [20] M. Gottwald, E. Krieg, S. Slijkhuis, C. von Savigny, S. Noël, H. Bovensmann, and K. Bramstedt. Determination of SCIAMACHY line of sight misalignments. In *Proc. ERS-ENVISAT Symposium*, number ESA SP-636, Montreux, 2007. ESA. CDROM.
- [21] R. W. M. Hoogeveen, R. van der A, and A. P. H. Goede. Extended wavelength InGaAs infrared (1.0-2.4  $\mu\text{m}$ ) detector arrays on SCIAMACHY for space-based spectrometry of the earth atmosphere. *Infrared Physics & Technology*, 42:1, 2001.
- [22] J. Krijger, R. Snel, and S. Slijkhuis. Revised polarisation calibration of SCIAMACHY. In *Atmospheric Science Conference Proceedings*, SP-676. ESA, 2009.
- [23] S. Noël, H. Bovensmann, J. P. Burrows, J. Frerick, K. V. Chance, and A. H. P. Goede. Global atmospheric monitoring with SCIAMACHY. *Phys. Chem. Earth (C)*, 24(5):427–434, 1999.
- [24] S. Noël, H. Bovensmann, M. W. Wuttke, J. P. Burrows, M. Gottwald, E. Krieg, A. P. H. Goede, and R. Mager. SCIAMACHY nominal operations and special features. In *Proc. ERS-ENVISAT Symposium*, number ESA SP-461, Gothenburg, 2000. ESA. CDROM, 439noel.pdf.
- [25] S. Salomon, A. L. Schmeltekopf, and R. W. Sanders. On the interpretation of Zenith Sky Absorption Measurements. *J. Geophys. Res.*, 92:8311, 1987.
- [26] N. A. J. Schutgens and P. Stammes. Characterising top-of-atmosphere ultra-violet polarisation from radiative transfer calculations. In *Proc. ERS-ENVISAT Symposium*, number ESA SP-461, Gothenburg, 2000. ESA. CDROM, 422schut.pdf.
- [27] N. A. J. Schutgens and P. Stammes. Parametrisation of Earth s polarisation spectrum from 290 to 330 nm. *JQSRT*, submitted, 2001. KNMI preprint 2001-19.
- [28] S. Slijkhuis and J. Frerick. SCIAMACHY Polarisation Sensitivity. In *Proc. ERS-ENVISAT Symposium*, number ESA SP-461, Gothenburg, 2000. ESA. CDROM, 344slijk.pdf.
- [29] S. Slijkhuis, R. Snel, B. Aberle, G. Lichtenberg, M. Meringer, and A. von Bargaen. Results of a new Straylight Correction for SCIAMACHY. In *Proc. ERS-ENVISAT Symposium*, number ESA SP-636, Montreux, 2007. ESA. CDROM.
- [30] R. Snel. SCIAMACHY On-Ground Performance: Polarisation Phase Shift. In *Proceedings ESAMS 99 - European Symposium on Atmospheric Measurements from Space*, volume 2, page 725. ESA, 1999.
- [31] R. Snel. In-Orbit Optical Path Degradation: GOME Experience and SCIAMACHY Prediction. In *Proc. ERS-ENVISAT Symposium*, number ESA SP-461, Gothenburg, 2000. ESA. CDROM, 316snel.pdf.
- [32] G. L. Squires. *Practical Physics*. McGraw-Hill, London, 1968.
- [33] P. Stammes, I. Aben, R. B. A. Koelemeijer, S. Slijkhuis, and D. M. Stam. Gome polarisation validation study. In *Proceedings of the Third ERS Symposium on "Space at the Service of our Environment"*, volume II, pages 669 – 674, Florence, 1997.
- [34] Piet Stammes. The seventh point polarisation algorithm, Internal Report. (GOME and SCIAMACHY), KNMI De Bilt, 1994.
- [35] Jochen Stutz and Ulrich Platt. Problems in using diode arrays for open path DOAS measurements of atmospheric species. Institut für Umweltphysik, Universität Heidelberg.
- [36] C. von Savigny, A. Rozanov, H. Bovensmann, S. Noël, M. Gottwald, S. Slijkhuis, and J. P. Burrows. Studying Envisat Attitude with SCIAMACHY Limb-scatter Measurements. In *Proc. ERS-ENVISAT Symposium*, number ESA SP-636, Montreux, 2007. ESA. CDROM.
- [37] M. W. Wuttke, S. Noël, H. Bovensmann, J.P. Burrows, M. Gottwald, and E. Krieg. Operational long term monitoring of the SCIAMACHY instrument on ENVISAT. In *Proc. ERS-ENVISAT Symposium*, number ESA SP-461, Gothenburg, 2000. ESA. CDROM, 286wuttk.pdf.

### B.3. Project References

- [38] SCIAMACHY Operations Support homepage, <http://atmos.af.op.dlr.de/projects/scops>.
- [39] SCIAMACHY: Optical and Radiant Cooler Assemblies Design Description, RP-SCIA-1000FO/025, Issue 2, 14.02. 1996. Fokker Space.
- [40] Detector characteristics of the 8 SCIAMACHY array detectors: good/ bad/ dead pixels, SRON-EOS-MD-detectors, Issue 1, 3.9. 1997. SRON.
- [41] ENVISAT-1 Mission CFI Software PPF\_LIB Software User Manual, PO-IS-GMV-GS-0557, Issue 4.1, 15.01. 1997. ESA.
- [42] ENVISAT-1 Products Specification, PO-RS-MDA-GS-2009, Issue 3, 19.6. 1997. ESA.
- [43] SCIAMACHY Internal SLS blocking, RP-SCIA-1000TP/197, Issue 1, 16.3. 1998. TNO-TPD.
- [44] SCIAMACHY Analysis of Measurement Data Datation Accuracy, TN-SCIA-0000DO/19, Issue B, 10.3. 1999. Dornier (now Astrium).
- [45] Klaus Bramstedt. Scan-angle dependent degradation correction with the scanner model approach, Version 1. Technical report, IUP Bremen, 11.12. 2013.
- [46] R. de Beek. Review of SCIAMACHYs algorithm theoretical basis documents, draft revision guide. Technical report, IUP University Bremen, 22.12. 1999. ESTEC contract 13594/99/NL/PR.
- [47] J. de Vries. Optec Cold Tests Instrument Performance Evaluation Report, RP-SCIA-0000FO/191, Issue 1. Technical report, Fokker Space, 18.12. 1997.
- [48] M. Dobber. Spectral oscillations in sun irradiance measurements mode, TN-SCIA-1000TP/219. Technical report, TNO-TPD, 17.02. 2000.
- [49] W. Gurlit. Study of the Red Grass, 1st progress report. Technical report, IUP Uni. Bremen, 10.03. 2000.
- [50] W. Gurlit. Study of the Red Grass, Draft report final result. Technical report, IUP Uni. Bremen, August 2000.
- [51] Q. Kleipool. SCIAMACHY: Recalculation of OPTEC5 Non-Linearity, SRON-SCIA-PhE-RP-13 Issue 1. Technical report, SRON, 7.11. 2003.
- [52] E. Krieg. SCIAMACHY Limb Scan timing. Technical report, DLR-IMF, 28.10. 2003.
- [53] J. M. Krijger. SCIAMACHY degradation model ATBD, SRON-SQWG-TN-2011-001, draft. Technical report, SRON, 7.03. 2011.
- [54] B. Kruizinga and H. G. C. Werij. SCIAMACHY Calibration Plan, PL-SCIA-1000TP/022. Technical Report issue 2, TNO-TPD, 22.1. 1996.
- [55] G. Lichtenberg. SCIAMACHY Channel 1-5 Memory Effect I: Keydata implementation and in-flight measurements, SRON-SCIA-PhE-RP-11 Issue 2. Technical report, SRON, 12.9. 2003.
- [56] S. Slijkhuis. SCIAMACHY Level 0 to 1b Processing Error Analysis: Precision and Accuracy on Level1b Data, ENV-TN-DLR-SCIA-0035, Draft. Technical report, DLR-IMF, 15.12. 1997.
- [57] S. Slijkhuis. Calculation of Polarisation from Rayleigh Single Scattering, ENV-TN-DLR-SCIA-0043. Technical report, DLR, 24.1. 2000.
- [58] SRON SCIAMACHY team. Test Report Detector Module FM#1 - ...FM#8, TR-SCIA-1120SR/37-44. Technical report, SRON, June 1996.
- [59] P. Stammes and C. P. Tanzi. Considerations on Stokes parameters derived from memo "The seventh point polarisation algorithm". SRON Internal Report, 21.9. 1999.

## B.4. GOME project documentation and study reports

- [60] GOME Users Manual, 1996. ESA SP-1182, ESA/ESTEC, Noordwijk, The Netherlands.
- [61] W. Balzer, B. Aberle, D. Loyola, and R. Spurr. GOME Level 0 to 1b Algorithm Description, ER-TN-DLR-GO-0022. Technical Report Issue 4/A, DLR-DFD, August 1996.
- [62] T. D. Guyenne and C. J. Readings, editors. *GOME Interim Science Report*. Number SP-1151. ESA publications Division, ESTEC, Noordwijk, The Netherlands, 1993. ISBN 92-9092-041-6.
- [63] S. Slijkhuis. Study on Algorithm Differences between ERS-2/GOME and GOME-2, MO-TN-DLR-GO-0005. Technical Report Issue 1, DLR-IMF, 8.9. 2000.